ANUL XLIII **1998**

S T U D I A

UNIVERSITATIS BABEŞ-BOLYAI

PHYSICA

2

Editorial Office: 3400 CLUJ-NAPOCA, Gh. Bilaşcu no.24 ♦ Phone: 405300 ex. 167

SUMAR - CONTENTS - SOMMAIRE

Solid State Physics

Spectroscopy

Theoretical Physics

Computational Physics

STUDIA UNIVERSITATIS BABEŞ-BOLYAI, PHYSICA, XLIII, 2, 1998

Cu^{2+} CONTAINING STRONTIUM-BORATE GLASSES STUDIED BY ELECTRON PARAMAGNETIC RESONANCE

I. ARDELEAN*, M. PETEANU, R. CICEO-LUCACEL

ABSTRACT. EPR absorption spectra of Cu^{2+} ions were investigated in $2B_2O_3{\cdot}SrO$ and $2B_2O_3{\cdot}SrF_2$ glasses over a wide concentration range. Octahedral environments axially distorted were detected. A great structural stability of the vitreous matrix when copper accumulate during the doping process, characterises the investigated systems. No clusters of Cu^{2+} ions were detected. Mixed valence states of copper ions were revealed, especially at high CuO content. The influence of composition changes when using SrO or SrF_2 as network-modifier upon the valence state and distribution of copper ions was also revealed.

Introduction

There are several factors such as composition, melting temperature, cooling rate, etc. which determine the local order and consequently the properties of the oxide glasses. For study the ways in which these factors influence the glass structure and properties magnetic resonance methods were often used [1]. Borate glasses were investigated by means of both NMR of the ^{11}B nucleus [2-4] and EPR of paramagnetic ions involved in their composition, one of the most sensitive to the matrix structure being Cu^{2+} [5-7]. The valence state of copper impurities introduced to probe the vitreous matrix depend on glass composition. There are vitreous systems where only the divalent state of copper ions was reported [8] and other containing both Cu^{+} and Cu^{2+} ionic species [9-11].

This paper aims to present our results concerning strontium-borate $2B_2O_3{\cdot}SrX$ glasses, for X = O, F_2, investigated by means of EPR of Cu^{2+} ions introduced by controlled doping as paramagnetic probes. The purpose of research was to see how changes in the matrix composition may

* Babeş-Bolyai University, Faculty of Physics, 3400 Cluj-Napoca, Romania

influence the valence state of impurity ions and their distribution on various structural units building the glass.

Experimental

Structural details of two oxide vitreous matrices, namely $2B_2O_3 \cdot SrO$ and $2B_2O_3 \cdot SrF_2$, were investigated by means of EPR of Cu^{2+} ions introduced by controlled doping within a broad concentration range. Consequently, two series of samples:

(1) $xCuO(100-x)[2B_2O_3 \cdot SrO]$

(2) $xCuO(100-x)[2B_2O_3 \cdot SrF_2]$

both having $0.1 \leq x \leq 30$ mol %, were analysed. Samples were prepared by using reagent grade compounds, i.e. H_3BO_3, $SrCO_3$, SrF_2 and CuO. The melting was performed in sintered corundum crucibles, in an electric furnace, at 1250^oC. After 30 min. the molten material was quenched at room temperature by pouring on a stainless-steel plate.

The samples structure was tested by mean of X-ray diffraction. The diffraction pattern did not reveal crystalline phases up to 30 mol % CuO.

EPR measurement were performed using a JEOL-type spectrometer, in the X frequency band, at room temperature and a field modulation of 100 kHz.

Results and discussion

The recorded EPR spectra evidenced for both series of samples Cu^{2+} ($3d^9$) ions entered the matrix as paramagnetic species. The shape and intensity of the EPR absorption line depend strongly of the Cu^{2+} ions concentration in the sample, that is the reached doping level. The evolution of the absorption spectra when increasing the CuO content of sample may be followed in Fig. 1 showing several representative spectra of the investigated systems. The absorption line is asymmetric, characteristic for Cu^{2+} ions in axially distorted octahedral symmetric sites. For both systems the spectrum keeps its asymmetric character within the entire concentration range proving the great structural stability of the vitreous system in accepting Cu^{2+} ions in units having more or less the same symmetry and configuration.

Within the low concentration range ($0.1 \leq x \leq 5$ mol %) the spectrum shows the hyperfine structure (hfs) due to the interaction of the unpaired electron spin with the nuclear one, $I = 3/2$, characteristic to Cu^{2+} ion. The hfs is well resolved in both parallel and perpendicular band of the spectrum. Its evolution when increasing the CuO content is presented in

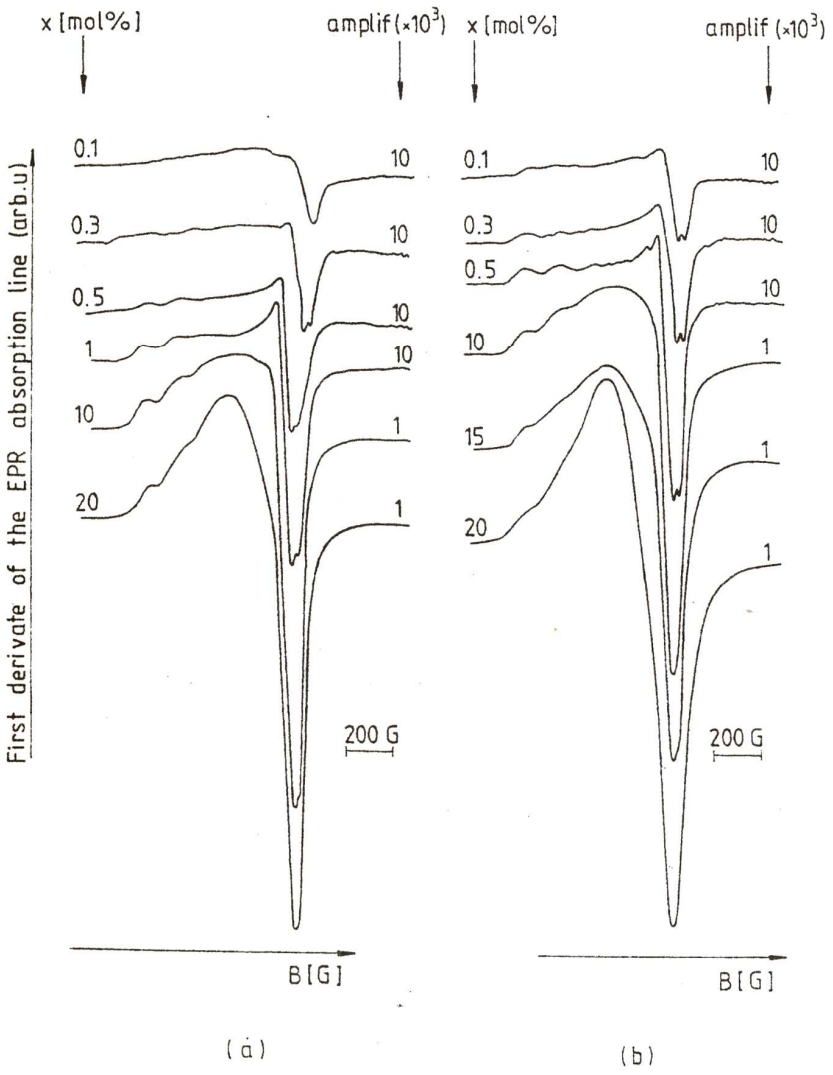

Fig. 1. EPR absorption spectra due to Cu^{2+} ions in glasses of the xCuO(100-x)[$2B_2O_3$·SrO] system (a) and xCuO(100-x)[$2B_2O_3$·SrF_2] system (b).

Figs. 2 and 3 for some representative spectra of the two systems. The best resolution was obtained at the lowest degree of impurification. As rising the concentration of paramagnetic ions the resolution diminishes due to the individual hfs lines broadening, the hyperfine structure smears out,

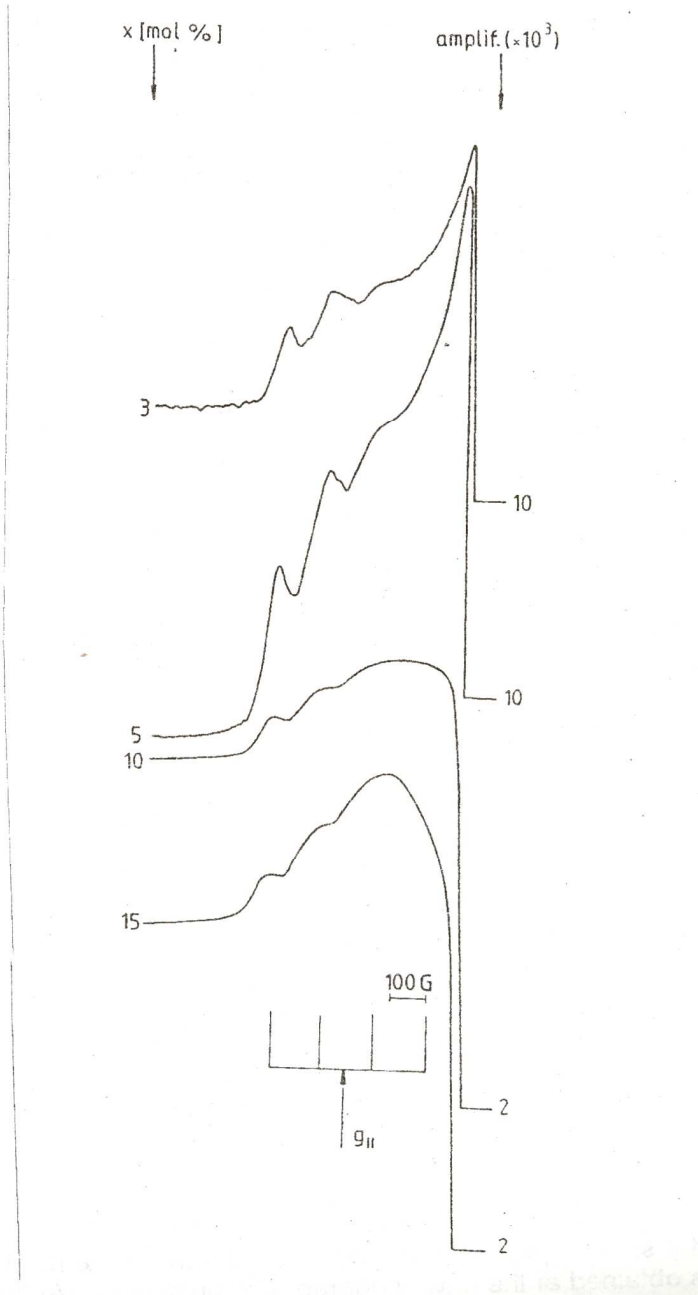

Fig. 2(a). The evolution of hfs in the parallel band when increasing concentration in xCuO(100-x)[$2B_2O_3$·SrO] samples.

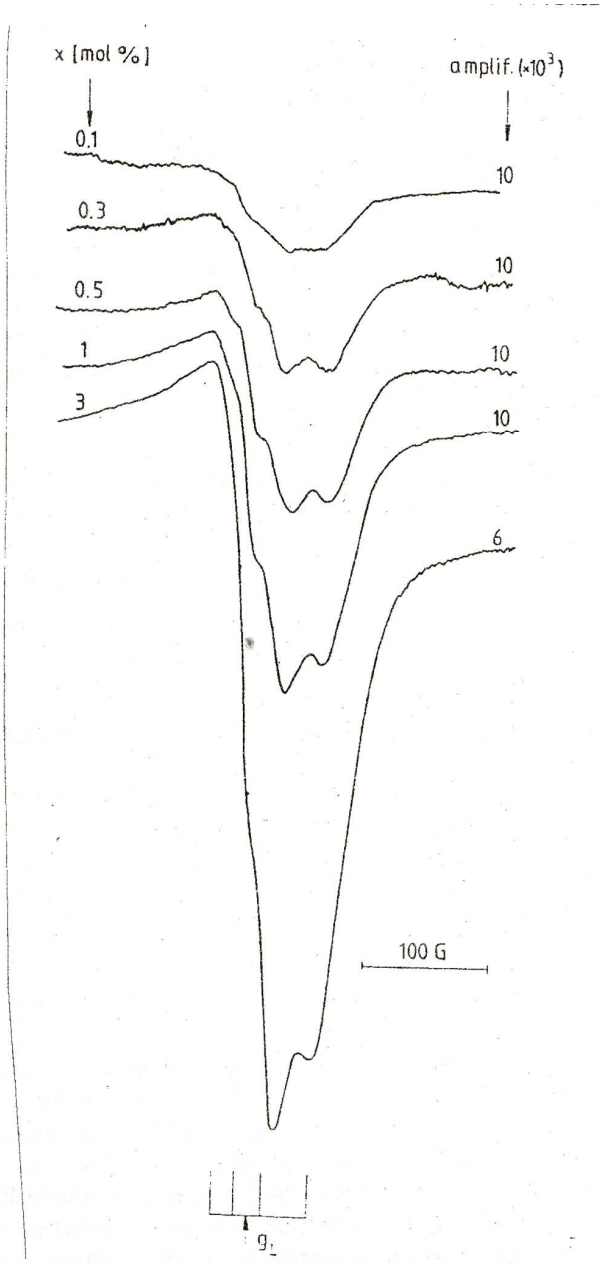

Fig. 2(b). The evolution of hfs in the perpendicular band when increasing concentration in xCuO(100-x)[$2B_2O_3$·SrO] samples.

so that for samples with high paramagnetic ions content the line reduces to the broad envelope of all contributions to the EPR absorption. The relatively broad range in which the spectrum shows a resolved hfs denote an appreciable degree of short range ordering in the vitreous matrix built by approximately identical structural units, involving Cu^{2+} ions.

For spectra with the best resolution, the $A_{||}$ and $A_{\perp}$ hyperfine constants were estimated as separation between the central pair of peaks in the parallel, respectively perpendicular band, and the values of the corresponding g factor were calculated, in the midpoint of this. The values are given in Tables 1 and 2. The accuracy in estimating these parameters was compromised by the progressive broadening of the hfs components.

The obtained $g_{||}$ and $g_{\perp}$ values satisfy the relationship $g_{||} > g_{\perp} > g_e = 2.0023$ characteristic to Cu^{2+} ions coordinated with six ligand atoms in a distorted octahedron, elongated along one axis. The values of the EPR parameters attest the predominantly ionic character of bonding between Cu^{2+} ion and the ligand atoms. Because Cu^{2+} is a network-modifier in our samples [12] there is a competition between Cu^{2+} and the network-forming cations in its neighbourhood (B^{3+} in our case) in attracting the oxygen pairs, available in its vicinity. The covalence of the Cu^{2+} - O bonds increases when the B-O bonds become weaker in structural aggregates involving them.

In the parallel band the hfs lines are almost equidistant whereas in the perpendicular band the separation between them increases with increasing the magnetic field. Another characteristic of the parallel hfs lines is their progressive broadening as following the m values (the magnetic quantum number denoting each hf transition). This is the effect of fluctuations in the ligands field involving Cu^{2+} ion from a structural aggregate to another. For samples containing $x < 5$ mol % CuO the shape and structure of the resonance line is typical to isolated Cu^{2+} ions in sites of axial symmetry. As rising the CuO content of the sample, the poor resonance line resolution is due to the individual line broadening as effect of dipolar interactions increasing and to ligand field fluctuations in the paramagnetic ion neighbourhood. Consequently the hfs peaks width become larger than the separation between them, so finally the line results as a large envelope of all contributions. As effect of inter ionic interactions increasing the $g_{\perp}$ factor values increase for both systems according to the data in Tables 1, 2.

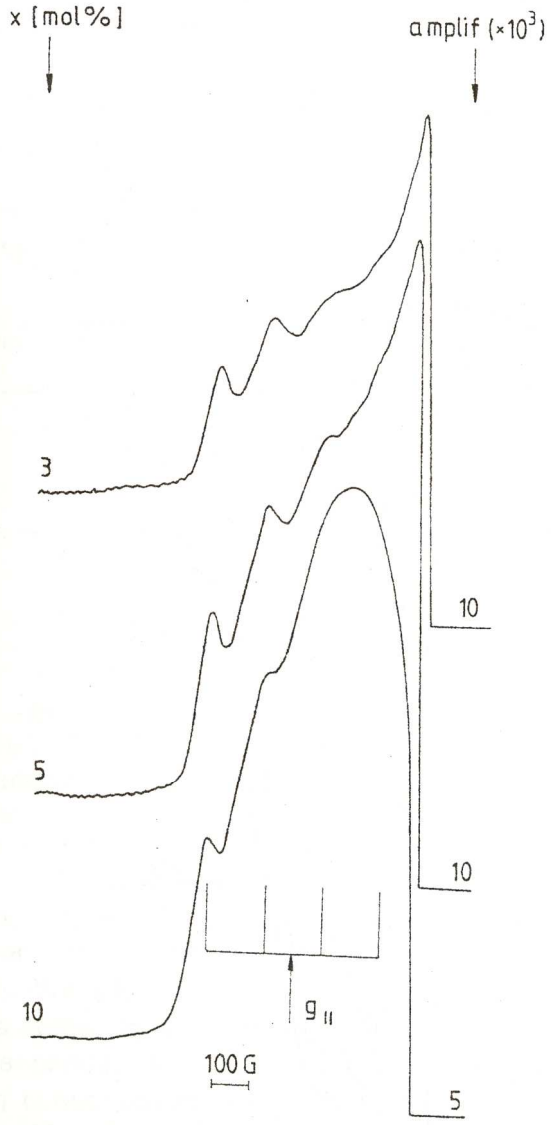

Fig. 3(a) The evolution of hfs in the parallel band when increasing concentration in $xCuO(100-x)[2B_2O_3 \cdot SrF_2]$ samples.

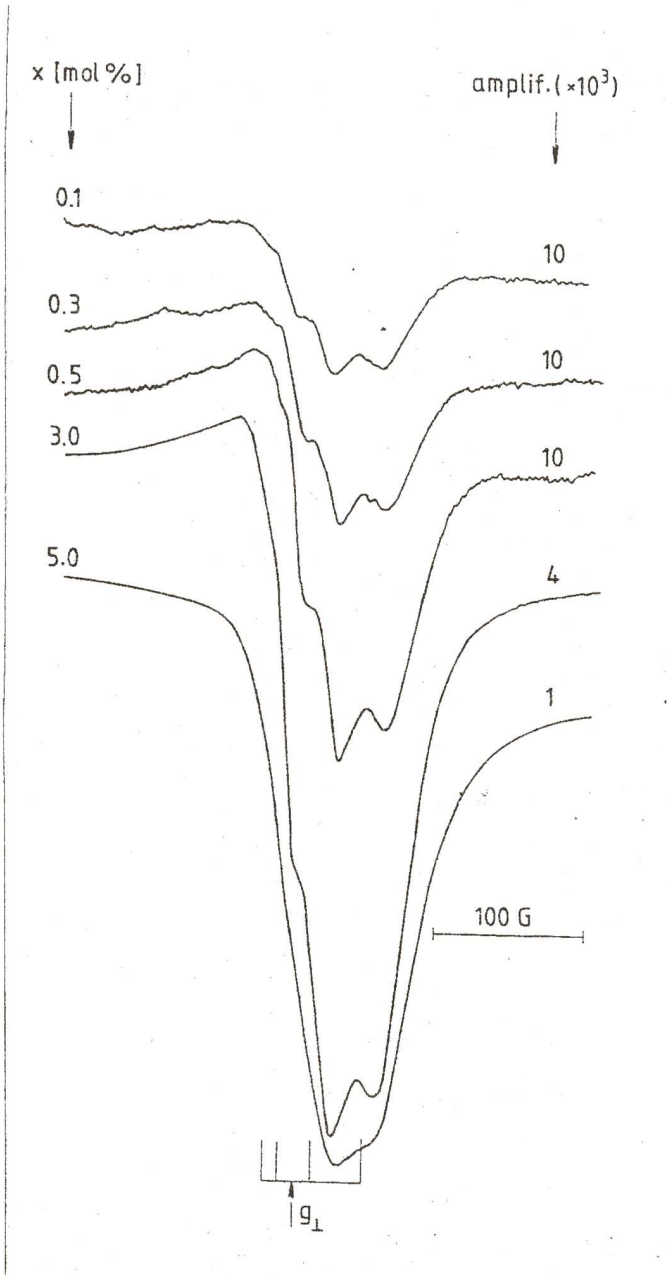

Fig. 3(b) The evolution of hfs in the perpendicular band when increasing concentration in $xCuO(100-x)[2B_2O_3 \cdot SrF_2]$ samples.

Table 1. EPR parameters corresponding to the resolved parallel band of the spectra

System	x [mol %]	$A_{\|\|}$ [G]	$g_{\|\|}$
(1)	3	142.85	2.3228
	5	157.14	2.3174
(2)	3	149.99	2.3118
	5	155.71	2.3229

Table 2. EPR parameters corresponding to the resolved perpendicular band of the spectra

System	x [mol %]	$A_{\perp}$ [G]	$g_{\perp}$
(1)	0.3	25.15	2.0605
	0.5	23.21	2.0652
	1.0	23.21	2.0626
	3.0	23.49	2.0637
	5.0	23.21	2.0648
(2)	0.3	25.45	2.0613
	0.5	25.45	2.0632
	1.0	24.29	2.0640
	3.0	21.78	2.0626
	5.0	21.24	2.0623

From structural point of view the two systems have an similar evolution when adding CuO in their matrices, but the resonance line intensity changes differently when increasing concentration. The hfs resolution also differs for the two systems, hfs being better resolved on spectra corresponding to samples of system (2) than those corresponding to system (1). The absorption signal intensity, $\Im$, estimated as the absorption line integrate, is proportional with the number of spins involved in the resonance phenomenon, that is the paramagnetic ions concentration. We plotted in Fig. 4 the variation $\Im = f(x)$ for the two systems. One notes higher values of $\Im$ for samples of system (2) compared to those corresponding to system (1) and quite different evolution of these as increasing concentration. The values of $\Im$ characteristic to system (1) increase up to 15 mol % CuO, then, the increase is practically stopped. For samples of system (2) the values of $\Im$ increase almost within the entire concentration range with a slight change of slope of the variation curve at about 10 mol % CuO. There is a change in the $\Im = f(x)$ evolution with concentration for both systems, i.e. in the progressive accumulation of Cu^{2+} ions during the doping process. $\Im$ does not follow linearly the doping

level of the sample for x > 10 mol % CuO, suggesting some other valence state of copper ions, different from Cu^{2+}, which now do not contribute to the EPR absorption. These new ions balance the paramagnetic Cu^{2+} ionic species so that for samples of system (1) the addition of CuO no more change the EPR line intensity. The Cu^{+} ionic species simultaneously present with the Cu^{2+} ones are the most probable, their apparition when preparing samples being favoured in the melt of system (1) more rich in oxygen that the melt corresponding to system (2). By replacing SrO by SrF_2 in the vitreous matrix the (2+) valence state of copper was favoured. Consequently for samples of system (2) the Cu^{2+} ions concentration is higher than in samples of system (1), the EPR absorption lines are intenser and their hfs better resolved. Optical measurements data agree very well with these assumptions [12].

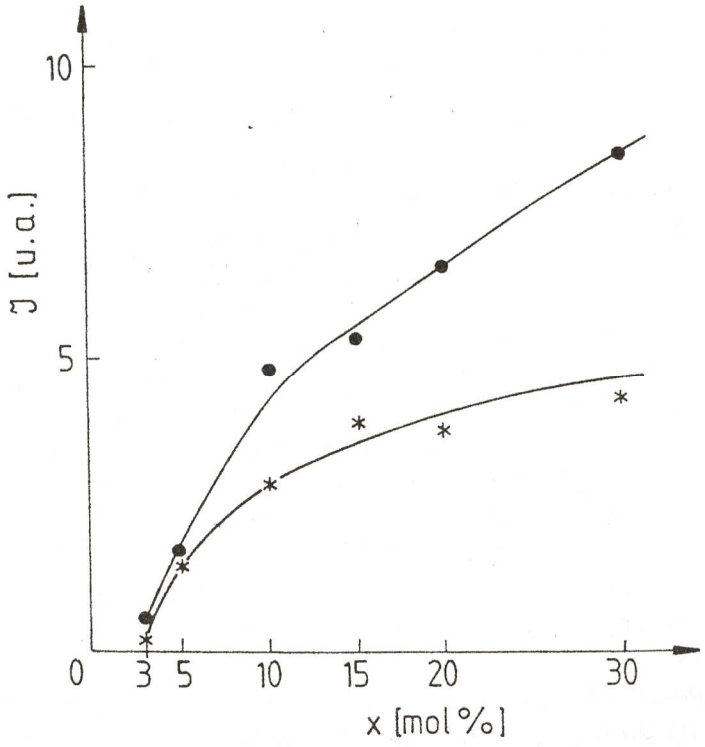

Fig. 4. Concentration dependence of the EPR line intensity corresponding to $xCuO(100-x)[2B_2O_3{\cdot}SrO]$...(*) and $xCuO(100-x)[2B_2O_3{\cdot}SrF_2]$...(.) glasses.

Conclusions

Homogeneous glasses corresponding to $[2B_2O_3 \cdot SrO]$ and $[2B_2O_3 \cdot SrF_2]$ glass matrices containing CuO within a broad concentration range (0.1 - 30 mol %) were obtained.

For all samples EPR absorption spectra due to Cu^{2+} ions were recorded. Up to 5 mol % CuO isolated Cu^{2+} ions in axially distorted octahedral sites (octahedron elongated along one axis) were detected. None of systems did not show resonance lines due to clustered formations of ions. The hyperfine structure resolved in both parallel and perpendicular bands of the spectra, show structural stable matrices when adding Cu^{2+} ions, within a relatively broad concentration range.

The interactions in which Cu^{2+} paramagnetic ions are involved revealed as dipole-dipole ones. The chemical bonding are preponderant ionic. The capacity of vitreous matrix in accepting copper ions in the (2+) valence state differs considerably from one system to another, the $[2B_2O_3 \cdot SrF_2]$ one presenting itself much more available than the other. By changing the network-modifier (SrF_2 instead of SrO) the Cu^{2+} species concentration increases and consequently the intensity of the EPR absorption rises and spectrum's resolution improves. For concentrations greater than 10 mol % CuO the Cu^{+} ionic species simultaneously enter the matrix with the Cu^{2+} ions during samples preparation. They do not contribute to the EPR absorption.

REFERENCES

1. P. C. Taylor, Resonance Effects in Glasses, Acad. Press, New York, London (1977).
2. G. E. Jellinson, P. J. Bray, J. Non. Cryst. Solids 29, 187 (1978).
3. P. J. Bray, Borate Glasses, Plenum Publ. New York (1978).
4. S. Simon, Al. Nicula, Solid State Commun. 3, 1251 (1981).
5. H. Imagawa, Phys. Status Solidi 30, 469 (1968).
6. L. D. Bogomolova, J. Mag. Res. 15, 283 (1974).
7. H. Kawazoe, H. Hosono, H. Hokumai, J. Non-Cryst. Solids 40, 291 (1980).
8. I. Ardelean, Gh. Ilonca, M. Peteanu, J. Non-Cryst. Solids 51, 389 (1982).
9. I. Ardelean, O. Cozar, Gh. Ilonca, Solid State Commun. 43, 707 (1982).
10. M. Peteanu, I. Ardelean, S. Filip, F. Ciorcas, J. Mat. Sci. : Mat. in Electronics 7, 165 (1996).
11. I. Ardelean, M. Peteanu, E. Burzo, F. Ciorcas, Solid State Commun. 98, 351 (1996).
12. I. Bratu, I. Ardelean, R. Ciceo-Lucacel, Rom. Rep. Phys. (to be published).

STUDIA UNIVERSITATIS BABEŞ-BOLYAI, PHYSICA, XLIII, 2, 1998

MAGNETOSTRICTION OF THE AMORPHOUS $Tb_{0.27}Dy_{0.73}(Fe_{1-x}Co_x)_2$ THIN FILMS

S. SÁRKÖZI[1], J. BETZ[2], N. H. DUC[3], K. MACKAY[2]

ABSTRACT. A series of amorphous $Tb_{0.27}Dy_{0.73}(Fe_{1-x}Co_x)_2$. Thin films were prepared. Magnetic and magnetostrictive measurements were performed. The partial substitution of Fe atoms by Co enhance magnetostriction.

INTRODUCTION

Magnetostrictive thin films have been studied since at least 1976 [1]. There is presently a renewed interest in these materials because of their potential use in microsystem applications [2],[3],[4]. The magnetostriction of R-Fe based alloys originates from the coupling between the R (ions that have highly aspherical 4f orbital) and the Fe moments.

The aim of our research was to find materials with high magnetostriction at sufficiently low magnetic fields. In order to obtain this, it is necessary to have low macroscopic anisotropy. That was obtained earlier in the famous cubic compound $Tb_{0.27}Dy_{0.73}Fe_2$, by combining two types of rare-earth, with positive and negative 4^{th} order anisotropies [1]. An other way was to use amorphous materials [5].

In this paper there are presented magnetic and magnetostrictive properties of the $Tb_{0.27}Dy_{0.73}(Fe_{1-x}Co_x)_2$ thin film series. The role of the substitution of the Fe atoms by Co is discussed.

EXPERIMENTAL

A series of amorphous $Tb_{0.27}Dy_{0.73}(Fe_{1-x}Co_x)_2$ thin films were deposited on glass substrate (microscope cover-slips with a nominal thickness of 150μm), by RF magnetron sputtering [6]. The height of the films was measured by π-step with a precision of 5% and the typical film-thickness was 1.2μm. The final composition of the films was determined by Scanning Electron Microscopy (SEM). X-ray diffraction was used to verify that no crystalline phase occurred. The samples were annealed for 1 hour

[1] Babes - Bolyai University, 3400 Cluj - Napoca, str. Kogalniceanu nr.1., Romania
[2] CNRS - Laboratoire Louis Neel, 25 Avenue des Martyrs, Grenoble, France
[3] Cryogenic Laboratory, University of Hanoi, Vietnam

under a magnetic field of 2.2T in order to induce an in-plane anisotropy. Heat treatments were made at 150^0C and 250^0C.

Magnetic and magnetostrictive measurements were performed. The magnetisation was measured using Vibrating Sample Magnetometer (VSM) in fields up to 8T from 4.2K to 300K.

Magnetostriction was determined using an optical deflectometer (cantilever method) [7], [8],[9]. This allows the magnetoelastic coupling energy *b* of the film to be determined [10]:

$$b = \frac{\alpha}{L}\frac{h_s^2}{h_f}\frac{E_s}{6(1+\nu_s)},$$

where α - the angle of the deflection of the sample as a function of the applied field.

L - the length of the sample (in the order of 10 mm)

h_S - the thickness of the substrate

h_f - the thickness of the film

E_S - Young's modulus of the substrate (it was taken to be 72GPa)

ν_S - Poisson's ratio of the substrate (0.21).

For comparison, magnetostriction (λ) values were calculated, using:

$$\lambda = \frac{b\,(1+\nu_f)}{E_f},$$

where E_f and ν_f are the Young's modulus and Poisson's ratio of the film, taken to be 80GPa and 0.31, respectively.

We measured two coefficients at saturation, $b_{//}$ and $b_{\perp}$, which correspond to the applied field direction parallel and perpendicular to the sample length and always in the film plane. In addition, the perpendicular direction corresponds to the easy-axis. The intrinsic properties of the material depend on the parameter $b^{\gamma,2}$ (or $\lambda^{\gamma,2}$) which is just the difference $b_{//} - b_{\perp}$ (or $\lambda_{//}-\lambda_{\perp}$).

RESULTS AND DISCUSSION

Table 1. presents the concentration and the thickness of each prepared $Tb_{0.27}Dy_{0.73}(Fe_{1-x}Co_x)_2$ film.

Sample	x_{Co}	h_f (μm)
1	0.00	1.45
2	0.12	1.25
3	0.31	1.55
4	0.47	1.10
5	0.65	1.55
6	0.83	1.55
7	1.00	1.50

Fig. 1. shows the hysteresis-loops for the sample 4 before (curve a) and after annealing (curve b). One can see that the annealed sample reaches saturation of magnetisation in lower magnetic field, which means that the effect of annealing was to reduce the internal stress of the sample.

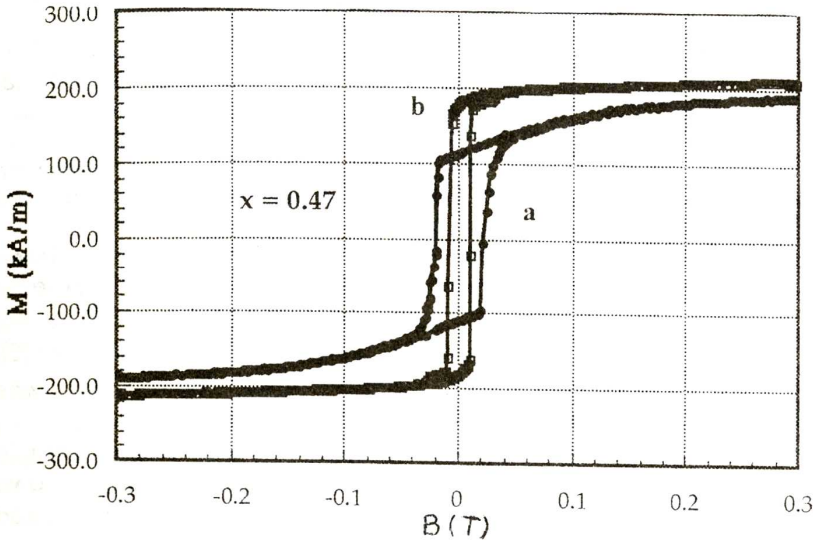

Fig. 1. Hysteresis-loops in case of sample 4

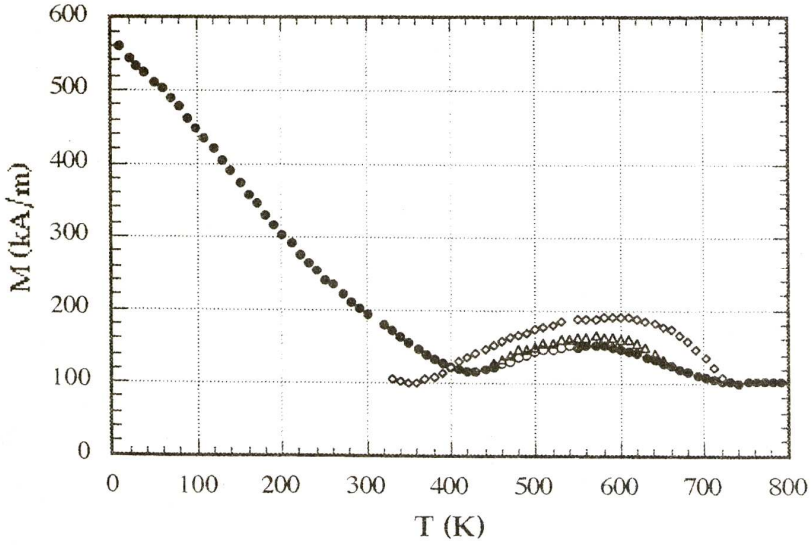

Fig. 2. Magnetisation for several cycles of heating and cooling in case of the oxidation-protected film

In order to verify the conservation of amorphous state, we measured the magnetisation for an oxidation-protected, supplementary sample in several cycles of heating and cooling (Fig. 2.). The protection against the oxidation was insured by a Ta layer (non magnetic) deposited on top of the film. The composition of this film was x_{Co} = 0.55. The following thermal cycles were performed: 340-450K, 340-560K, 340-660K, 340-720K. Above 560K, the magnetisation process is no longer reversible, so at greater temperatures than this, the crystallisation process appears. In case of this sample we found the compensation temperature to be at 420K. The Curie-point could not determined because of the crystallisation of the sample. This is in agreement with values measured by K.Lee and N.Heiman [11].

In Fig. 3. and Fig. 4. we show the variation of the magnetostriction as a function of the applied magnetic field, for the two extreme compositions of the series. Before annealing, $Tb_{0.27}Dy_{0.73}Co_2$ presented a typical easy-plane anisotropy, characterised by $\lambda_{//} = -\lambda_{\perp}$[5]. After annealing an enhancement from 1 to 10 of the $|\lambda_{//}/\lambda_{\perp}|$ ratio was observed. One can see that the effect of annealing was in this case also the creation of an easy-axis of magnetisation. In case of the sample $Tb_{0.27}Dy_{0.73}Fe_2$ the measurement indicate that the sample's own internal stresses (due to the deposition) before annealing were relaxed after. The installation of an easy-axis didn't appear.

We present in Fig. 5. the curves of magnetostriction for all the annealed samples that were measured. As it is shown, the presence of both Fe and Co atoms can give rise to greater magnetostriction values than those obtained in case of $Tb_{0.27}Dy_{0.73}Co_2$ or $Tb_{0.27}Dy_{0.73}Fe_2$ films. The very best performances are obtained in case of the $Tb_{0.27}Dy_{0.73}(Fe_{0.53}Co_{0.47})_2$. That is to say that this sample presents the greatest magnetostriction value at saturation and also in very low magnetic fields. For this property the x_{Co}= 0.47 compound could be useful in microactuator-applications. The phenomena of enhancement of the magnetostriction by partly substituting Fe atoms by Co, could be explained, based on [12]. The amorphous Co sublattice is a well ordered ferromagnet whereas for an amorphous Fe sublattice, the opposing Fe-Fe exchange interactions lead to a sperimagnetic structure with a low Curie temperature. However, the Fe moment being larger than the Co one, the R-Fe exchange energy is larger that the R-Co one. The substitution of Fe for Co thus increases the overall R-T exchange energy. However, when more Fe is added, a sperimagnetic sublattice starts to form thus reducing it effectiveness.

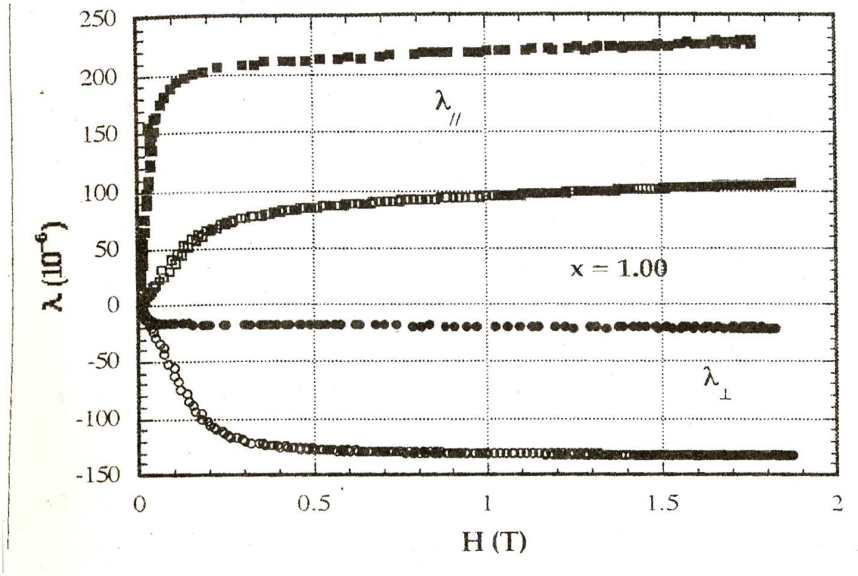

Fig. 3. Magnetostriction before (the empty character) and after the thermal treatment in case of sample 7

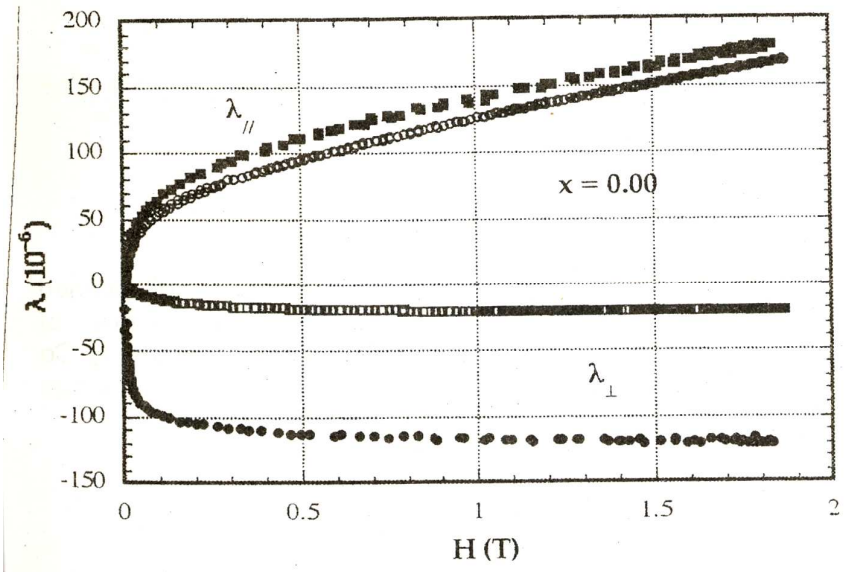

Fig. 4. Magnetostriction before (the empty characters) and after the thermal treatment in case of sample 1

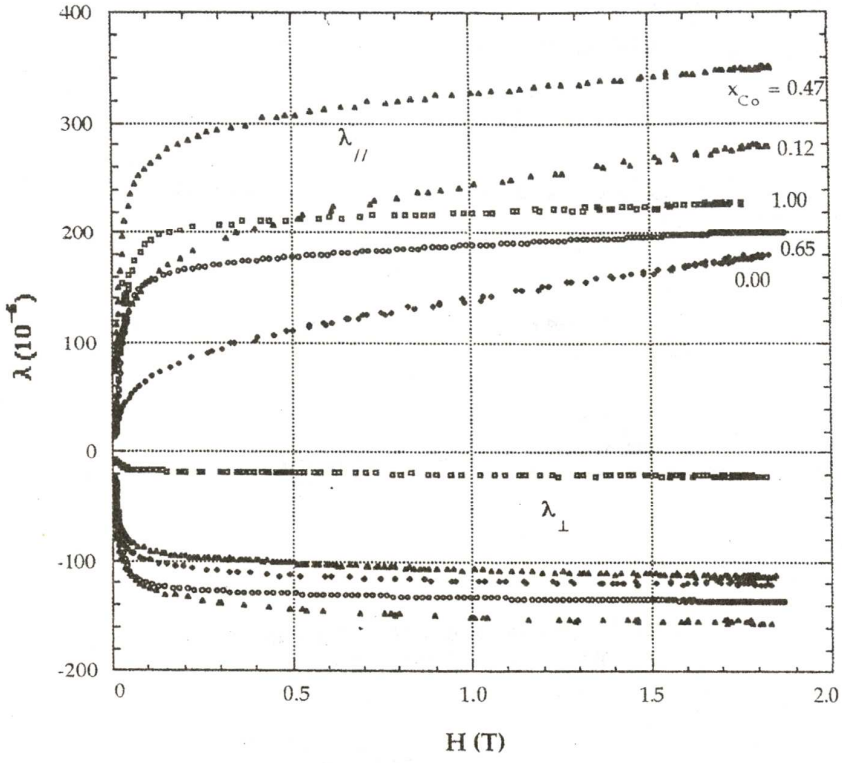

Fig. 5. Magnetostriction curves

CONCLUSIONS

We would like to point out that the creation of a well defined uniaxial anisotropy is advantageous for the enhancement of magnetostriction. The role of the partial substitution of Fe atoms by Co was to enhance magnetostriction, probably by strengthening the exchange interaction energy leading to better oriented rare-earth moments.

REFERENCES

1. A.E.Clark, "Magnetostrictive Rare Earth-Fe_2 Compounds", in "Ferromagnetic Materials", vol.1, ed. E. P. Wolfarth, North-Holland Publishing Company, (1980).
2. T.Honda, K.I. Arai, and M.Y.Yamaguchi, J.Appl.Phys., 76 (1994) 6994.
3. E.Quandt, J. Appl. Phys., 75 (1994) 5653.
4. K.Mackay, J.C.Peuzin, Ecole franco-roumaine "Magnetisme des systemes nanoscopiques", Oradea, Romania.
5. F.Sshatz et al., J. Appl. Phys., 76 (1994) 5380.
6. L. I. Maissel and R.Glang, "Handbook of thin film technology", (1970).
7. [E. du Tremolet de Lacheisserie, J.Peuzin, J. Magn. Magn. Mat., 136, (1994) 189.
8. E.Klockholm, IEEE Trans. Mag., vol. MAG-12, No6 (1976) 819.
9. A.C.Tam, H.Schroeder, IEEE Trans. Mag., vol.25 No3 (1989) 2629.
10. E. du Tremolet de Lacheisserie, "Magnetostriction", CRC Press, (1993).
11. K.Lee and N.Heiman, AIP Conf. Proc. 18 (1973) 108.
12. J.P.Gavigan, D.Givord, H.S.Li and J.Voiron, Physica B149 (1988) 345.

STUDIA UNIVERSITATIS BABEŞ-BOLYAI, PHYSICA, XLIII, 2, 1998

NMR AND EPR EVALUATION OF THE CORRELATION TIME OF LOCAL DYNAMICS IN POLYISOPRENE SOLUTIONS

**M. TODICA, V. SIMON, I. ARDELEAN,
E. MATEI, C. COSMA, D. STANILA**

ABSTRACT. The correlation time of the local dynamics of polymeric segments is evaluated from the temperature dependence of the spin-lattice relaxation time. The mathematical function for fitting the experimental data is based on the energy activation model of segmental reorientation. The values of the correlation time obtained from NMR are compared with the values of correlation time of nitroxide molecules introduced in the polymeric solutions.

INTRODUCTION

The dynamics of polymeric chain is a complex process, which occur in a large spatial and temporary scale. This dynamics lie from the elementary motion of the C – H bonds inside the monomeric unit, to the diffusion of the entire chain along the reptation tube, [1, 2].

To understanding this complex mechanism, an important step is the knowledge of the elementary motions which appears inside the monomeric units or the dynamics of few neighboring monomers. Direct observation of these motions is difficult task and request special techniques for labeling different part of the polymeric chain. However important information can be obtained by studying the influence of this kinds of motions on the different interactions which appears between the atoms of the chain, like the nuclear magnetic dipolar interaction. Also, the study of the dynamics of labeled molecules introduced in the vicinity of the chain is a reach source of information concerning the local dynamics of the chain.

The aim of our work is to estimate the correlation time of the elementary motions of the polymeric chain, by analyzing the spin-lattice relaxation time of the protons attached to the chain and the EPR spectra of some labeled molecules placed in the vicinity of the chain.

EXPERIMENTAL

We studied some polyisoprene-CCl_4 solutions with the polymeric concentration Φ=94% Φ=77% and Φ=59%, in the temperature range of 234K to 350K. The isomeric conformation of the polyisoprene sample was 92% cis-1,4, the glass transition temperature Tg=201±4K and the thermal expansion coefficient α=6.7 10^{-4} K^{-1}. The samples were enclosed in NMR tubes and sealed under a primary vacuum. Spin-lattice relaxation time of the protons was measured using the inversion-recovery sequence (π-τ-π/2), [3]. All the measurements were performed at 45 MHz, using a CXP Bruker spectrometer.

EPR measurements were made using a JEOL-JES spectrometer in X band, at room temperature.

RESULTS AND DISCUSSION

The dominant mechanism which govern the spin-lattice relaxation of the protons attached to the polymeric chain is the dipolar interaction between the nuclear spins located within one given chain segments, [4]. This interaction depends on the relative orientation of the spins and decreases rapidly with the distance between the spins so that only the neighboring spins the are taken into account.

The relative orientation of spins is affected by the local dynamics of the chain, and is described by the auto-correlation function G(τ).

$$G(\tau) = \frac{1}{2}\langle 3(\vec{e}(0).\vec{e}(\tau))^2 - 1\rangle \qquad (1)$$

were the $\vec{e}(\tau)$ is the unit vector in the spin-spin direction at time τ, [5].

In a qualitative sense the auto-correlation function G(τ) describes the persistence of dynamical property of the molecular system before being averaged out by the molecular motion. This persistence depends on the frequency of the local reorientation of the spins. For a complex system the local reorientation of the spins can not be characterized by a single frequency. The distribution of motional frequencies and their intensities is described by the spectral density function J(ω), [5]. This function is the Fourier inverse of the auto-correlation function G(τ) and

$$J(\omega) = \int_{\infty}^{-\infty} G(\tau) e^{-i\omega\tau} d\tau \qquad (2)$$

represents a transformation from the time to frequency domain.

Assuming a purely spin-spin relaxation mechanism, the expression for spin-lattice relaxation time T_1, for identical spins is given by equation (3), where *r* is the distance between two spins, ω is the Larmor frequency of the spins, and γ is the gyromagnetic ratio:

$$\frac{1}{T_1} = \frac{3}{20}\frac{\gamma^2 \mathrm{h}^2}{r^6}\left[J(\omega) + 4J(2\omega)\right] \tag{3}$$

To describe the local local dynamics it is necessarily to know the spectral density function J(ω). Estimation of the function J(ω) requires a description of the time decay of G(τ). The correlation function is derived on the basis of specific models for polymer motion. For neat liquids and solutions, the decay process is assumed to be exponential, with a characteristic time constant τ_c, [6]:

$$G(\tau) = \langle e^2(0)\rangle . \exp\left(-\frac{\tau}{\tau_c}\right) \tag{4}$$

Under these assumption the spectral density function is, [7]:

$$J(\omega) = 2\langle e^2(0)\rangle \frac{\tau_c}{1 + \omega^2 \tau_c^2} \tag{5}$$

From the relations (3) and (5) we obtained for the spin-lattice relaxation rate the relation:

$$\frac{1}{T_1} = K\left[\frac{\tau_c}{1+\omega^2\tau_c^2} + \frac{4\tau_c}{1+4\omega^2\tau_c^2}\right] \tag{6}$$

The constant K depends on the distance between the interacting spins

$$K \propto \frac{1}{r^6} \tag{7}$$

The spin-lattice relaxation rate is temperature dependent and reach its maximum where the condition $\omega\tau_c \approx 0.616$ is fulfilled. In our experiments the minimum of the spin-lattice relaxation time was observed for each sample for a characteristic temperature θ(ϕ). Using the above relation we can calculate the correlation time of segmental motion of the polymeric chain, corresponding to these temperatures. We found the value τ_c (Φ(ϕ)) ≈10^{-9}s. But we are interested to know the correlation time to any temperature. To do this we must know the temperature dependence of the correlation time.

One of the most used frame-work for quantitatively estimations of the correlation time of, the molecular dynamics in solutions is based on the Kramer and Helfands theory, [8], [9]. This theory is based on the passage of a particle over a potential energy barrier. Two different stable conformations of the polymeric chain are separated by a barrier potential energy of height E_a. The energy required for conformational translation is provided by the thermal activation. The solvent is treated as a random frictional force opposing passage across the barrier. Any spatial or temporal correlation in the solvent motion are neglected. Under these assumptions the temperature and viscosity dependence of the correlation time is:

$$\tau_c = A.\eta.\exp\left(\frac{E_a}{RT}\right) \tag{8}$$

The pre-factor *A* is a constant independent of temperature. The temperature dependence of the viscosity can be often described with an Arrhenius form:

$$\eta = \eta_0(\phi).\exp\left(\frac{E_\eta}{RT}\right) \tag{9}$$

Under these conditions:

$$\tau_c = B.\exp\left(\frac{E_a + E_\eta}{RT}\right) = B.\exp\left(\frac{E_{\exp}}{RT}\right) \tag{10}$$

where *B* is a constant and. $E_{\exp} = E_a + E_\eta$ is the experimental activation energy (apparent activation energy). It is clear that in the case of the pure polymer, the viscosity of the solvent can be replaced by a constant, and the apparent activation energy contines only the contribution of the polymer.

The relation (8) became

$$\tau_c = B.\exp\left(\frac{E_a}{RT}\right) \tag{11}$$

Using the expression (10) or (11) in equation (6) we obtained the temperature dependence of the spin-lattice relaxation rate for the molten polymer and the solutions. Many parameters are unknown in this equation: the activation energy *Eexp*, the pre-exponential factor *B* and the constant *K*. The activation energy can be calculated from the Arrhenius plot of the experimental data of T_1 versus the inverse of the temperature. When the

extreme narrowing condition $\omega\tau_c \ll 1$ is fulfilled, then the equation (6) simplify to

$$\frac{1}{T_1} = 5K\tau_c \propto \exp\left(\frac{E_{\exp}}{RT}\right) \tag{12}$$

Eexp is calculated from the best fit slope of the plot *ln* (T_1) versus *(1/T)* over the temperature range of interest (Fig. 1).

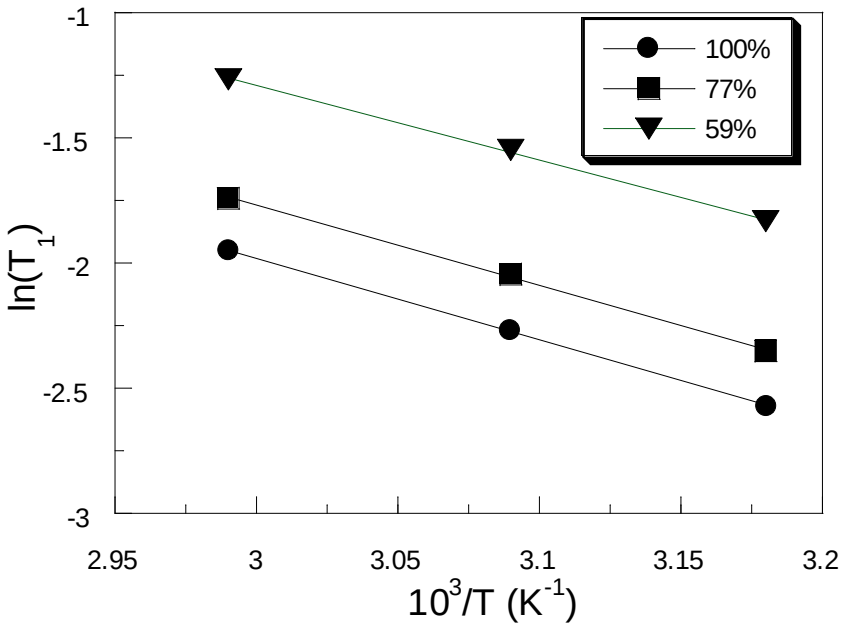

Fig.1. Arrhenius plot of the experimental T_1 data for the molten polymer and solutions.

The activation energy depends on the concentration of the polymer. It decrease when the solvent concentration increase. This fact indicates an increasing of the mobility of the polymer in the solutions when the solvent concentration increases (Fig. 2). The values of the activation energy were utilized to fit the experimental data of T_1. *B* and *K* were treated as adjustable parameters. *K* depends only on the characteristic of the polymer (distance between the neighboring protons, gyromagnetic ration of the proton, Planck constant) so that its value is the same for the molten polymer and for the solutions.

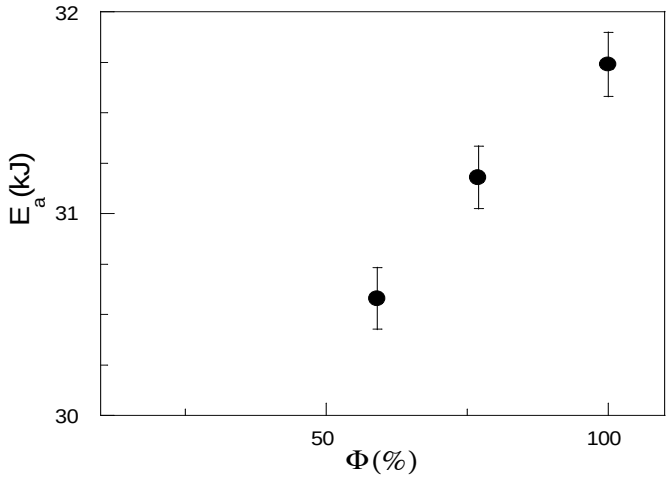

Fig. 2. The concentration dependence of the experimental activation energy obtained for the polyisoprene –CCl_4 solutions.

There are many pairs of parameters *K* and *B* which can fit our data. From the minimum condition of T_1, $\omega\tau_c \approx 0.616$ we known the value of the correlation time corresponding of the temperature $\theta(\phi)$. We selected only the pairs of parameters K and B, which provided the same value of τc when they are introduced in equation (6).The best values of the parameter B are listed in the table 1.

Table 1.

B	θ(%)
0.303 0.389 0.408	59% 77% 100%

The fit of experimental data of $T_1(T)$, using these parameters, is satisfactory (Fig. 3).

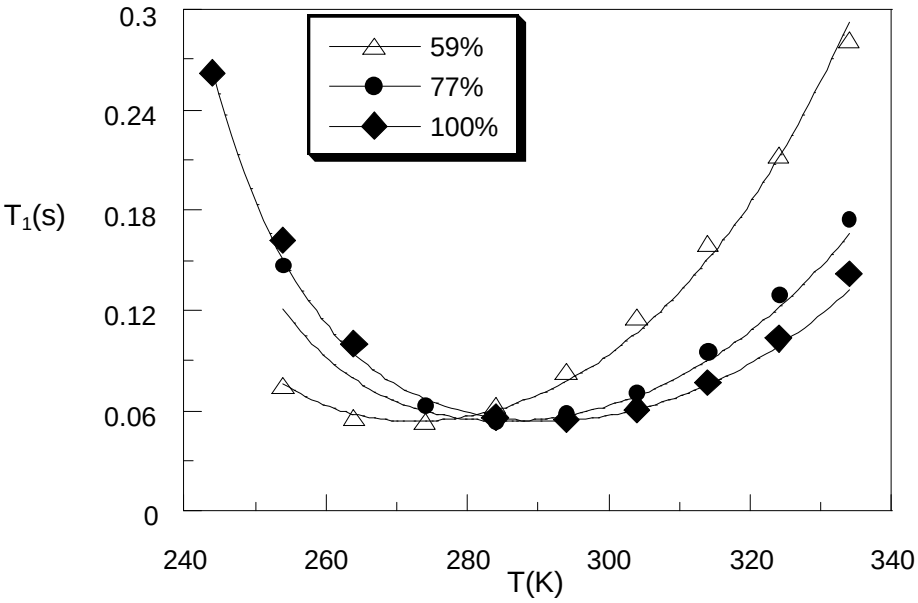

Fig. 3. The fit of the experimental data $T_1(T)$ using the equation 6

We can consider that the equations (6) and (10) can describe in the first order of approximation the temperature dependence of $T_1(T)$. We can calculate now the value of the correlation time for each solution at any temperature. Particularly we are interested for these values at room temperature, in order to compare the values of τc obtained by NMR method with those obtained by EPR method. These values are represented in Fig. 6.

EPR technique is based on the observation of the behavior of the unpaired electronic spins attached to the chain or attached to solvent molecules situated in the local environment of the chain. Indirect information about the dynamics of the chain can be obtained from labeled molecules introduced in the vicinity of the polymeric chain by means of different solvents. In our study we utilized free nitroxide radicals as labeled molecules, 2,2,6,6, tetramethyl piperidin-l-yloxyl (Tempo).

Different polymeric concentrations are obtained by evaporation of the solvent. Two situations are of interest:

a) High concentration of the solvent (CCl_4) so that the labeled molecules be insulated from the polymer.

b) Low concentration of the solvent, so that labeled molecules can interact directly with the polymeric segments.

The interaction is analyzed observing the modifications of the ESR spectrum of the labeled molecules. Each spectrum consists on three lines due to the hyperfine coupling of the unpaired spin with the nitrogen nucleus of the labeled molecules. An isotropic spectrum is obtained when the labeled molecules are completely free to move or in the case when these molecules are placed into isotropic medium. This situation is characteristic for the polymeric solution with high solvent concentration (Fig. 4). We can assume that only the labeled molecules are surrounded by the solvent molecules and do not interact with the polymeric links. The vicinity of the labeled molecules is isotropic, so that all the directions are equivalent.

The spectrum became anisotropic when the labeled molecules are not completely free to move. This situation is characteristic for the concentrated solutions (Fig. 5). It is possible in this case that the labeled molecules interact directly with the polymeric segments and then theirs motions are not isotropic.

Fig. 4. The EPR spectrum of the polyisoprene-CCl_4 solution with the concentration Φ=59%.

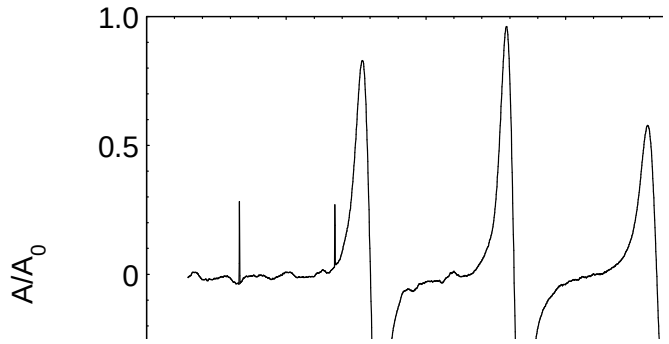

Fig. 5. The EPR spectrum of the polyisoprene-CCl_4 solutions with the concentration Φ=98%.

The correlation time of the rotation of the labeled molecules is calculated from the amplitude of the resonance lines using the relation [10]:

$$\tau_c = \frac{1}{3}\left(\tau_z + 2\tau_{xy}\right) \tag{13}$$

where:

$$\tau_{xy} = 6.5 * 10^{-10}\,\Delta H_0 \left| \sqrt{\frac{I_{+1}}{I_0}} - \sqrt{\frac{I_{-1}}{I_0}} \right|;$$

$$\tau_z = 6.5 * 10^{-10}\,\Delta H_0 \left| \sqrt{\frac{I_{+1}}{I_0}} + \sqrt{\frac{I_{-1}}{I_0}} - 2 \right| \tag{14}$$

For a given temperature, the correlation time increases with the polymeric concentration (Fig.6).

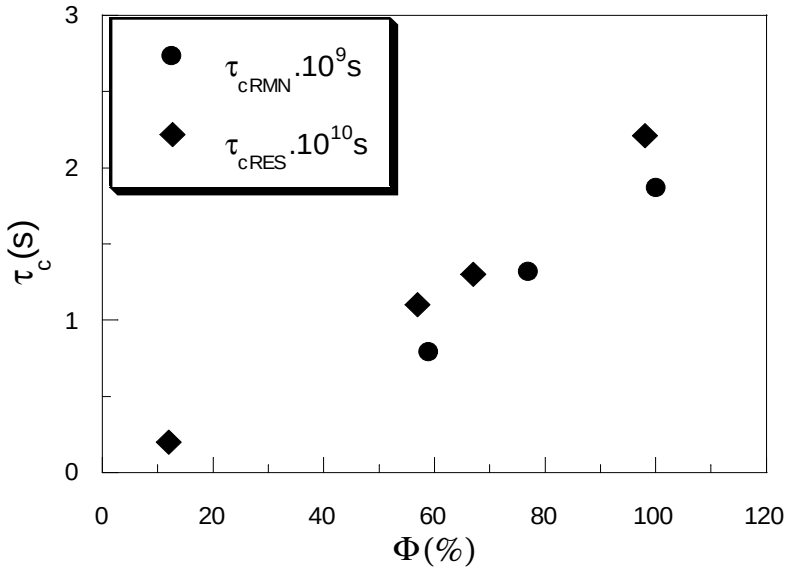

Fig. 6. Concentration dependence of the correlation time τc of the nitroxide molecules disolved in the polyisoprene-CCl_4 solutions (EPR and NMR measurements).

However the values of the correlation time of the labeled molecules is much smaller than those of the local motion of the polymeric segments obtained from NMR measurements. The motion of the nitroxide molecules is faster than the local motion of the polymeric segments. This fact indicates only a weak interaction between the labeled molecules and the polymeric links.

CONCLUSION

The model of polymeric local dynamics based on the Kramer's theory of the passage of a particle over a barrier potential energy, provide, in the first order of approximation, good values for the activation energy of the polymer conformational transformation.

This model, in addition with assumption of the exponential decay of the correlation function of the spin dynamics leads to a good description of the temperature dependence of the experimental spin-lattice relaxation

data and allow the evaluation of the correlation time of the polymeric local dynamics at any temperature.

The values of the τ_c obtained by EPR measurements, are smaller that those obtained by NMR measurements which indicate only a weak interaction between the labeled molecules and the polymeric segments. However EPR measurements provide additional information which allows to estimate the correlation time of the local dynamics of the polymeric segments.

REFERENCES

1. P.G. de Gennes, Scaling Concepts in Polymer Physics, Cornell University Press, Ithaca, London, (1979).
2. J. P. Cohen-Addad, "Physical Properties of Polymeric Gels", John Wiley and Sons, Chichester, New-York, Toronto, (1996).
3. H. Y. Carr, E. R. Purcell, Phys. Rev., 94, 630, (1954).
4. J. P. Cohen Addad, NMR and fractal properties of polymer liquids and gels, Pergaman Press, London (1992).
5. A. Abragam, "Principles of Nuclear Magnetism", Oxford University Press, London, (1961).
6. L. Morton and C. Morton, Methdos of Experimental Physics, Academic Press, New York, London, Toronto (1980).
7. C.P. Slichter, Principles of Magnetic Resonance, Harper, New York, 1963.
8. H. A. Kramers, J. Chem. Physica, 1940, 7, 284.
9. E. Helfand, J. Chem. Phys., 1971, 54, 4651.
10. S. Schreiver, C.F. Polnaszek, I.C. Smith, Biochim. Biophys. Acta, 515, 359, 197.

STUDIA UNIVERSITATIS BABEŞ-BOLYAI, PHYSICA, XLIII, 2, 1998

OXIDATION OF SOME TERPENES IN 13X ZEOLITE

I. BARBUR*, L. DAVID*, I. BATIU*, O. STAN, C. CRACIUN***

ABSTRACT. The behavior of three terpenes (verbenone, carvone and citral) in 13X activated zeolite was investigated by EPR. Owing to the thermal treatment of the zeolite, the organic terpenes can accept a H^+ ion which confers theirs radicalic character. All three species give the same EPR spectrum of one single gaussian line close to g_0=2. 0023 value for the free electron. There are some differences in the intensities and shapes of these spectra because of the steric effects and partial recombination (in the citral case).

INTRODUCTION

In order to understand the catalytic processes, the EPR investigation of radical and radical cations generated to zeolites is of great interest. As catalysts, zeolites are used in the synthesis of fine chemicals and in the petrochemical industry [1]. A great deal of research has been carried out on the structures and properties of zeolites, but very little is known about the mechanisms of the organic reactions which take place in them. EPR has proved to be a useful tool in investigating these reactions and possible transformations induced by zeolites [2].

Thermal treatment of several zeolites leads to defects in the zeolite structure, which can accept an electron from an organic molecule with a sufficiently low ionization potential (below 11 eV) [3]. The observed radical cation is usually persistent without important recombination effects and the EPR spectrum can be measured over a wide range of temperature.

In our previous paper [4] we have reported the EPR investigation of gamma-irradiation effect on some hydrazine derivatives and the new compounds resulting from the condensation of the hydrazine derivatives with some terpenoides (verbenone, carvone and citral) (Fig. 1). This class of compounds is present in some natural products and the investigation of theirs radiolysis products is important for radiation processing and sterilization in food and drug production.

* "Babes-Bolyai" University, Faculty of Physics, Cluj-Napoca, Romania

** "Babes-Bolyai" University, Faculty of Chemistry and Chemical Engineering, Cluj-Napoca, Romania

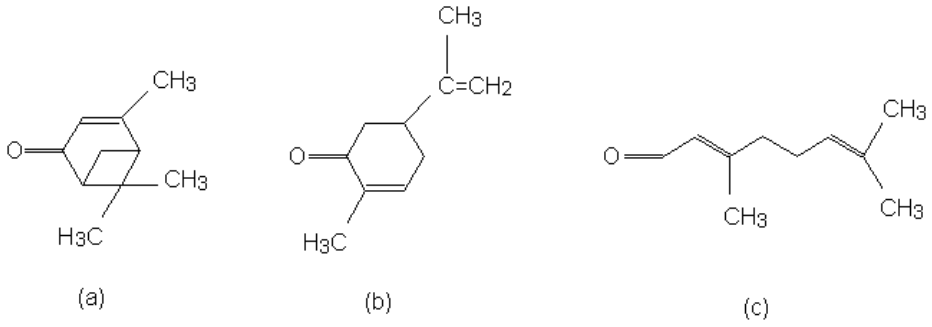

Fig. 1. Molecular structures of three terpenes verbenone (a), carvone (b) and citral (c)

In this paper we present EPR investigation of the radicals resulted from the reaction between these terpenes and the 13X zeolite.

EXPERIMENTAL

All three terpenes (verbenone, carvone and citral) in the highest available purity were used in liquid form. The 13X zeolite of high purity was used in powder form. The 13X zeolite was activated by heating in air to 380 K and than left at this temperature for 4 hours. The terpenes were adsorbed onto the zeolite at 380 K.

ESR spectra were recorded using a JOEL-JES-3B modified X-band spectrometer. The instrument settings are: microwave frequency 9. 5 GHz, modulation frequency 100 KHz, cavity TE_{102} sensitivity $3x10^{11}$ spins/Gauss and microwave power 10 mW.

The calibration of magnetic field for g factor was performed by using NMR proton signal from one magnetometer of MJ 100 R type.

RESULTS AND DISCUSSION

The three terpenes (verbenone, carvone and citral) were adsorbed onto inactivated and activated 13X zeolite. No EPR signal was obtained for terpenes adsorbed onto the inactivate zeolite. Fig. 2 presents the EPR spectra obtained for the three terpenes adsorbed onto the activate 13X. Each spectrum consists of one simple gaussian line. The g factor values (g=2**.**0020 for verbenone, g=2.0025 for carvone and g=2**.**0019 for citral) are very close given the g_0=2**.**0023 value of the free electron. It is the indication that all the EPR spectra from the terpenes adsorbed in 13X zeolite are assigned to the radical cations of corresponding terpenes. These radicals are formed as a consequence of the heat treatment of 13X zeolite, which

leads to defects in the structure. These defects can accept an electron from one organic molecule (or equivalent can yield one proton).

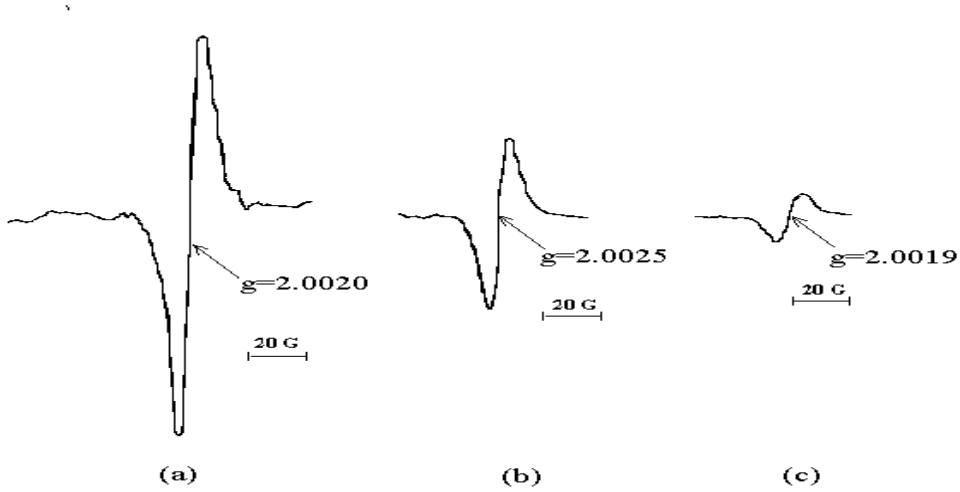

Fig. 2. ESR spectra ofthree terpene adsorbed on to 13X activated zeolite
(a) verbenone, (b) carvone, (c) citral

There are two mechanisms, which can appear by heating the zeolite. The nature of mechanisms and the concentration of the organic molecules adsorbed onto the activate zeolite too influence directly the reactions' character.

1. The Bronsted acid site of the zeolite [6] is characterized by the fact that one hydrogen atom coordinate the bonding oxygen atom between two cationic atoms of the zeolite. This site can initiate a variety of reactions like polymerization and dehydrogenation. After a thermal treatment, one conversion of the Bronsted acid site to Lewis acid site occurs. This conversion is responsible for the spontaneous generation of radical cations (being induced a Bronsted acid catalysis process).

In this case, the small alkenes and the quasilinear structures have the great reactivity with the zeolite. The cyclic compounds were found to take part in dimerisation reaction [5,7]. In this case, EPR spectra for structures with S=1 are expected.

2. The zeolites, by heating, can lose hydrogen atoms (terminal hydrogen atoms or the protons resulted through the decomposition of water molecules from the zeolites' canals) like in γ-radiolysis process [6]. The hydrogen atoms can coordinate the oxygen and carbon atoms of the organic molecules, resulting the radical cations with S=1/2 spin. The EPR spectrum is formed by one single signal at $g \cong 2.0$. The paramagnetic hole is delocalised over the organic molecule, especially for the cyclic molecules.

The reaction between the organic molecule and the proton (H^+) can be reaction proceed via intermediate (par example a carbonium ion) or via transition state [5,9].

The carbonium ion can be instable and one recombination process appears. In this situation, the amplitude of the signal is small, only some molecules being in radicalic state.

The fact that the obtained spectra have no hyperfine structure show that the paramagnetic hole is not localized to any hydrogen atom, being delocalised over the molecule.

The EPR spectra obtained from the three samples are identical to each other. We can suppose that the process nature is the same for the three terpenes. Like for the other terpenes [5], the most probable effect is that of the protonation of double bond C=C (situation 2) [8]. The steric effects upon protonation of organic molecules may be very important too [10].

In the citral case, the small EPR intensity of the ligand appears because of a double possibility of the reaction citral-zeolite. One reaction lead to a radical without one double bond, EPR active. Another way of reaction consists of the protonation of citral molecule in the first time and then her deprotonation. In this case the molecule is EPR inactive.

The difference of the intensity of the spectra for verbenone and carvone may be because of steric effects. The little differences in theirs shapes are determined by the geometric implications and the distortions of the molecular rings [7].

CONCLUSIONS

Three terpenes (verbenone, carvone and citral) were adsorbed onto 13X zeolite. The verbenone and carvone are cyclic compounds and citral is quasilinear. The zeolite was treated thermal at 380 K, eliminating H^+ ions. These ions react with the organic molecules, resulting the radicalic compounds EPR actives by the protonation of double bond C=C.

The obtained EPR spectra consist of one single line. No hyperfine splitting due to the interaction of the paramagnetic hole with hydrogen nuclei of terpenes was observed. This indicates his electrons'delocalisation on the molecule, in each case. The differences of the intensity and shape of the spectra result from steric effects and recombination process.

REFERENCES

1. M. S. Rigutto, Stud. Surf. Sci. Catal. 58, 727 (1991).
2. E. Popovici, Studii spectroscopice RMN şi RES pe materiale zeolitice, Ed. Zecasin, Bucureşti, 1996.
3. S. Shih, J. Catal. , 36, 238 (1975).
4. I. Barbur, I. Batiu, V. Simon, J. Radioanol. Nucl. Chem. 196, 135 (1995).
5. R. Crockett, E. Roduner, J. Chem. Soc. , Perkin. Trans. 2, 347 (1994).
6. R. A. van Santen, G. J. Kramel, Chem. Rev. 95, 637 (1995).
7. R. Crockett, E. Roduner, J. Chem. Soc. , Perkin. Trans. 2, 1503 (1993).
8. P. J. Borker, A. G. Davies, Acc. Chem. Res. , 20, 90 (1987).
9. J. M. Coxon, P. J. Steel, Terpene Chemistry, Mc Graw-Hill, New Delhi, 119 (1982).
10. M. Czjzek, H. Jobic, A. Fitch, T. Vogt, J. Phys. Chem. , 96, 1535 (1992).

STUDIA UNIVERSITATIS BABEŞ-BOLYAI, PHYSICA, XLIII, 2, 1998

THE METAL-LIGAND BONDING IN SOME CU(II)-COMPLEXES WITH LIGANDS OF BIOLOGICAL RELEVANCE. PART I: CU(II)-ANTIINFLAMMATORY DRUGS

C. CRACIUN*, C. BALAN*, C. AGUT, D. RISTOIU*, O. COZAR*, L. DAVID***

ABSTRACT. The ESR and optical spectra of Cu(II)-complexes with some anti-inflammatory drugs (aspirinate and indomethacin) in different solvents (pyridine, dimethylformamide) and adsorbed on NaY zeolite have been used to investigate the solute-solvent interaction, spin-Hamiltonian constants of the complexes, metal-ligand bond parameters and the environment around the metal ion. The molecular coefficients were calculated using the LCAO-MO method. The character of σ and π-bondings and the local symmetry around the Cu(II) ion are sensitive to the solvent and ligand nature.

INTRODUCTION

The copper (II) complexes of active medical ligands have been shown to be more active than the ligands themselves [1]. The magnetical and optical properties of Cu(II)-complexes with some medical drugs have been investigated by ESR and UV-VIS spectroscopies in order to elucidate the structure and nature of the bonding between the metal ion and the ligand atoms. We used as ligands the molecular systems with biological relevance: aspirinate and indomethacin–antiinflammatory agents (Part I); diazepam, oxazepam and nitrazepam-tranquilizing sedative-hypnotic and myorelaxant agents (Part II).

The antiinflammatory drugs indomethacin (ind) and aspirinate (asp) (Fig.1) have been used for the preparation of $[Cu_2(Ind)_4](H_2O)_2$ and $[Cu_2(Asp)_4](H_2O)_2$ complexes respectively. The pyridine (Py) and dimethylformamide (DMF) solutions of these complexes and the solutions adsorbed on NaY zeolite have been investigated in order to determine the local structure around the copper (II) ion.

* "Babeş-Bolyai" University, Faculty of Physics, Cluj-Napoca, Romania

** University of Oradea, Departament of Physics, Romania

EXPERIMENTAL

The $[Cu_2(Ind)_4](H_2O)_2$ and $[Cu_2(Asp)_4](H_2O)_2$ complexes were prepared as previously reported [2,3]. The Py, Py-DMF and DMF solutions having a concentration of 20 mg/cm^3 were then prepared. The powder NaY zeolite was impregnated in the respective solution for one hour. The excess of the solution was decanted and the powder was dried in air. ESR measurements were performed at 9.4 GHz (X-band) using a standard JEOL-JES-3B equipment at 295 K.

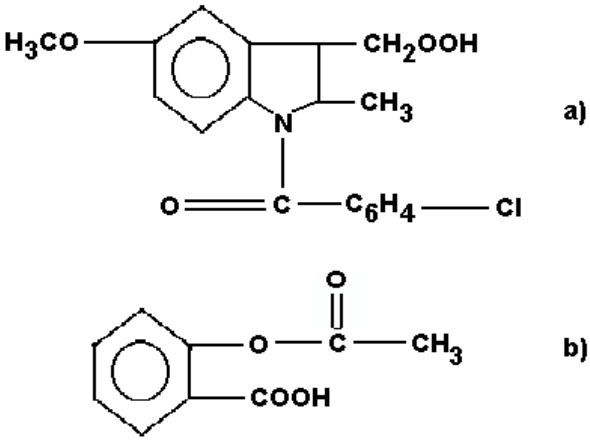

Fig. 1. *The molecular structure of indomethacin (a) and aspirinate (b)*

RESULTS AND DISCUSSION

The solution ESR spectra of studied compounds (Fig.2) suggest the presence of Cu(II) pseodotetrahedral monomeric species [4]. The characteristic isotropic parameters are $g_0 \approx 2.16$ and $A_0 \approx 62$ G. No resolved superhyperfine structure due to the interaction of the paramagnetic electron with nitrogen atoms of pyridine molecules was observed.

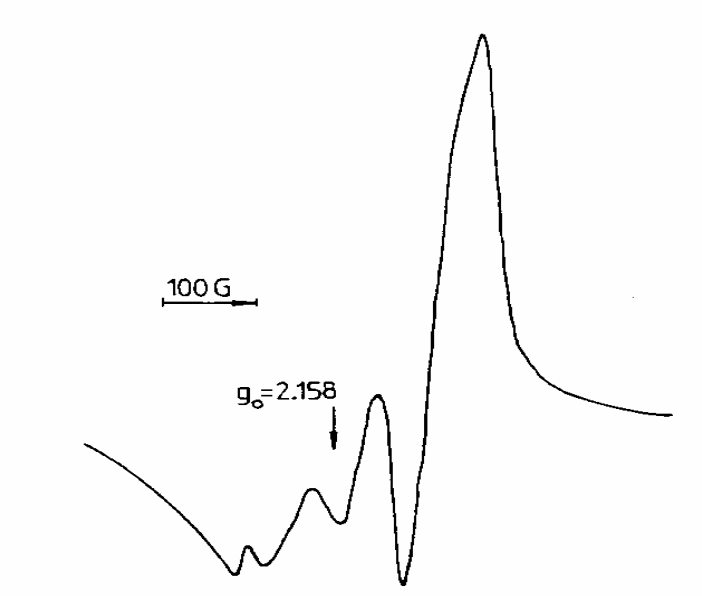

Fig.2. ESR spectrum of a 60% DMF +40% Py Cu(II)-aspirinate solution at 295 K

Anisotropic spectra with four hyperfine lines in the g_{II} region and a strong signal in the perpendicular band were obtained for the solutions of Cu(II) complexes adsorbed on NaY zeolite. They suggest that mononuclear Cu(II) species prevail in these samples.

The ESR spectrum of DMF Cu(II) aspirinate solution adsorbed on NaY zeolite show the presence of two magnetically nonequivalent monomeric species (Fig.3).

One of these which is characterized by g_{II}=2.370 and A_{II}=131.2 G may be of $Cu(DMF)_4$ cromophore with a planar-distorted tetrahedral (T_d) symmetry around the metallic ion. The other set of parameters corresponds to $Cu(Asp)_2(DMF)_2$ specie with an elongated tetrahedral-octahedral symmetry due to the coordination of solvent molecules at Cu^{2+} ion along the Oz axis [5].

The spectra of 40% Py +60% DMF Cu(II)-complexes solutions also show the presence of two different mononuclear species (Fig.4).

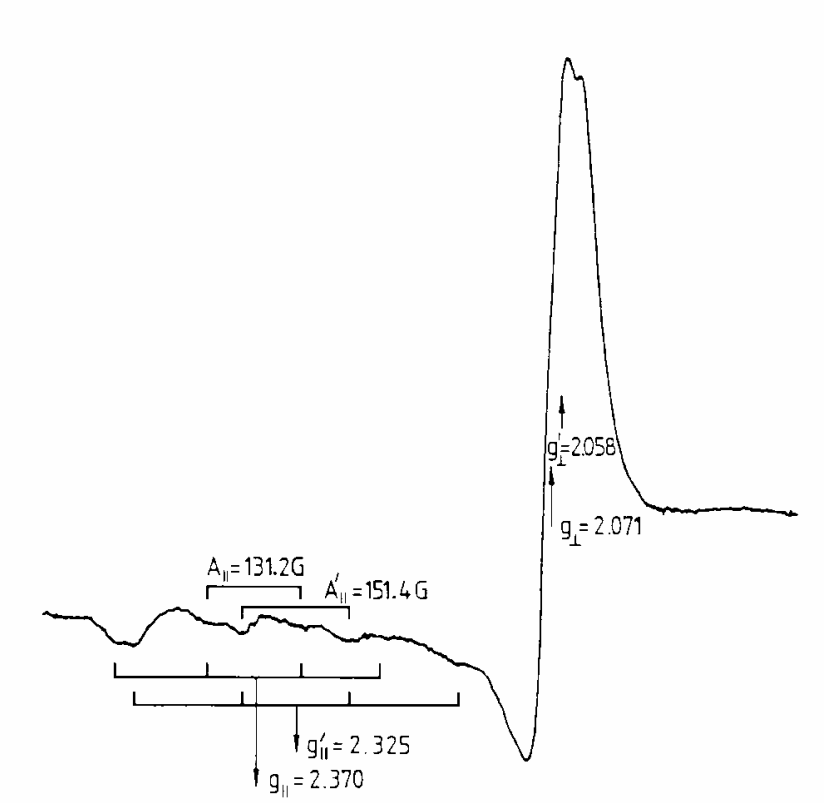

Fig. 3. ESR spectrum of a DMF Cu(II)-aspirinate solution adsorbed on NaY zeolite at 295 K

One of these (g_{II}=2.273, A_{II}=156 G) is $Cu(Asp)_2(DMF)_2$ or $Cu(Ind)_2(DMF)_2$ respectively, previously described. The other set of parameters show that in this case the copper(II) ion is bonded in a *trans* square-planar arrangement at the nitrogen atom of two pyridine molecules and to one carboxylate oxygen from each of two ligand anions [6].

The existence of CuN_2O_2 cromophore is confirmed by the appearance of nitrogen superhyperfine lines in the perpendicular band of the spectra ($g_{\perp}$ region)(Fig.4 b).

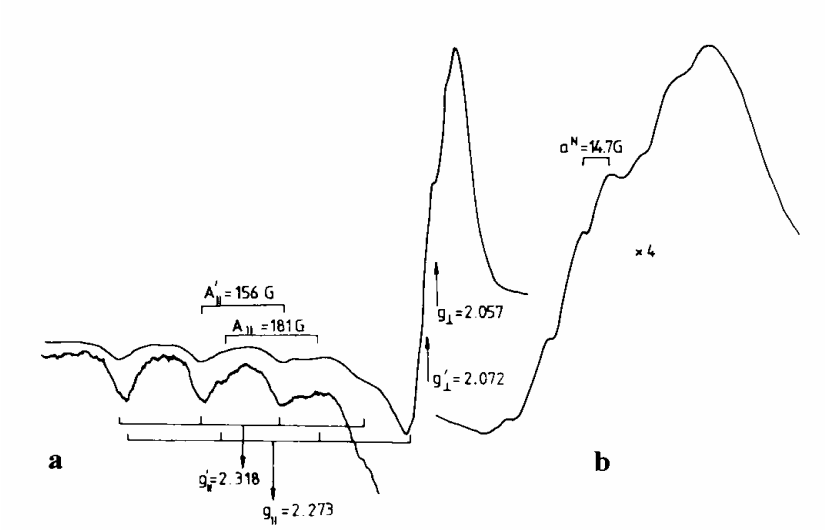

Fig.4. ESR spectrum of a 40%Py+60%DMF Cu(II)-Indomethacin solution adsorbed on NaY zeolite (**a**). Extended perpendicular absorbtion (**b**)

In Py Cu(II)-solutions only ones monomeric species occurs (Fig.5). The ligands molecules are completely substituted by solvent molecules [7]. The weak resolution of nitrogen superhyperfine lines are due to the dipole-dipole interactions between the copper (II) ion and the neighboring pyridine molecules.

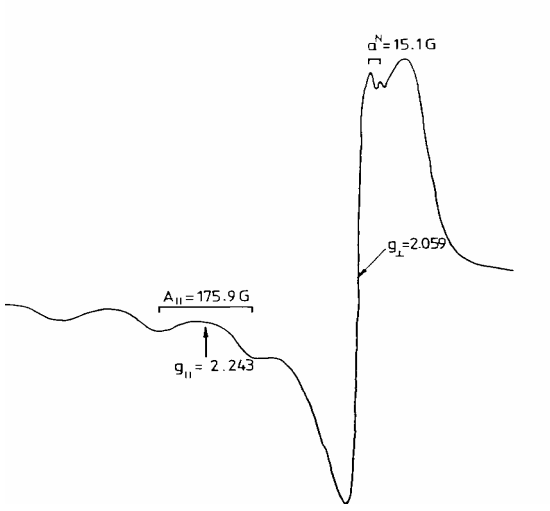

Fig.5. ESR spectrum of a pyridine Cu(II)-aspirinate solution adsorbed on NaY zeolite at 295K

The characteristic ESR parameters of all monomeric species are given in Table1 and Table 2.

Table 1. ESR and covalency parameters of mononuclear species obtained in Cu (II)-Aspirinate solutions adsorbed on NaY zeolite

Solvent	100% DMF		40% Py + 60% DMF		100% Py
Monomeric Species	$Cu(DMF)_4$	$Cu(Asp)_2(DMF)_2$	$Cu(Asp)_2(DMF)_2$	$Cu(Asp)_2(Py)_2$	$Cu(Py)_4$
g_{II}	2.370	2.325	2.324	2.285	2.243
$g_{\perp}$	2.071	2.058	2.059	2.052	2.059
A_{II} $(10^{+4}cm^{-1})$	144.4	163.2	161	184.9	183.6
a^N $(10^{+4}cm^{-1})$	-	-	-	14	14.5
α^2	0.88	0.88	0.87	0.89	0.84
α'^2	0.18	0.18	0.19	0.18	0.25
β^2	0.90	0.79	0.79	0.68	0.62
δ^2	1.12	0.91	0.94	0.80	0.97
Cromophore and symmetry	$CuO_4 \rightarrow T_d$	$CuO_4 \rightarrow O_h$	$CuO_4 \rightarrow O_h$	$CuO_2N_2 \rightarrow D_{2h}$	$CuN_4 \rightarrow D_{4h}$

Table 2. ESR and covalency parameters of mononuclear species obtained in Cu(II)-Indomethacin solutions adsorbed on NaY zeolite

Solvent	20% Py + 80% DMF	40% Py + 60% DMF		100% Py
Monomeric Species	$Cu(Ind)_2(Py)_2$	$Cu(Ind)_2(DMF)_2$		$Cu(Py)_4$
g_{II}	2.287	2.318	2.273	2.248
$g_{\perp}$	2.073	2.073	2.057	2.049
A_{II} $(10^{+4}cm^{-1})$	189.3	168.1	183.9	190.2
a^n $(10^{+4}cm^{-1})$	14.5	-	14	14.1
α^2	0.91	0.89	0.87	0.86
α'^2	0.15	0.17	0.20	0.22
β^2	0.67	0.76	0.66	0.61
δ^2	1.11	1.14	0.90	0.78
Cromophore and symmetry	$CuN_2O_2 \rightarrow D_{2h}$	$CuO_4 \rightarrow T_d$	$CuN_2O_2 \rightarrow D_{2h}$	$CuN_4 \rightarrow D_{2h}$

With the experimental values determined by ESR (the principal values of the **g** tensor, hyperfine structure tensor **A** and hyperfine ligand tensor $\mathbf{a}^{Lig.}$) the LCAO-MO coefficients which give the information about the

nature and the strength of metal-ligand bonding ca be evaluated.The ground state and the first excited states for the paramagnetic hole in the D_{4h} symmetry are described by the following antibonding orbitals [8]:

$$\Psi_{B_{1g}} = \alpha d_{x^2-y^2} - \frac{\alpha'}{2}(-\sigma_x^{(1)} + \sigma_y^{(2)} + \sigma_x^{(3)} - \sigma_y^{(4)})$$

$$\Psi_{B_{2g}} = \beta d_{xy} - \frac{\beta'}{2}(p_y^{(1)} + p_x^{(2)} - p_y^{(3)} - p_x^{(4)})$$

$$\Psi_{A_{1g}} = \alpha_1 d_{z^2} - \frac{\alpha_1'}{2}(\sigma_x^{(1)} + \sigma_y^{(2)} - \sigma_x^{(3)} - \sigma_y^{(4)})$$

$$\Psi_{E_g} = \delta d_{xz} - \frac{\delta'}{\sqrt{2}}(p_z^{(1)} - p_z^{(3)})$$

$$\Psi_{E_g} = \delta d_{yz} - \frac{\delta'}{\sqrt{2}}(p_z^{(2)} - p_z^{(4)})$$

The B_{1g} state represents the in-plane σ-bonding, B_{2g} represents the in-plane π- bonding and the double degenerate E_g state corresponds to the out-of-plane π bonding. The A_{1g} state does not affect the magnetic parameters in the second order of the perturbation theory and so is not relevant to the present discussion. α, α_1, α' and α_1' are the σ-bonding parameters, and β, δ, β', and δ' are the π-bonding parameters. α, β and δ are the coefficients which point to the ionic character of the orbitals B_{1g}, B_{2g}, E_g. The squares of these coefficients are the messier of the covalent character of the corresponding orbitals.

The Hamiltonian for Cu^{2+} ion in a tetragonal crystal field is given by [9]:

$$H = \beta_0[g_{II}B_zS_z + g_\perp(B_xS_x + B_yS_y) + A_{II}S_zI_z + A_\perp(S_xI_x + S_yI_y)$$

where β_0 is the Bohr magneton and **B** is the applied magnetic field. When the ligand superfine structure is present the paramagnetic electron interacts with the neighbours of the metallic ion and an additional term of the general form $S\sum a_n I_n$ is necessary. Here **S** is the total spin operator, $\mathbf{a_n}$ is the superfine structure tensor for the n ligand atoms and I_n is the ligand atom nuclear spin.

Resolving the equation for the proper values of the spin-Hamiltonian in an axial symmetry the following relations between g and A ESR parameters and the molecular orbitals MO coefficients just described are obtained [9,10,13]:

$$g_{II} = g_e - \frac{4\lambda\alpha\beta}{\Delta E_{xy}}\left[2\alpha\beta - 2\alpha'\beta S - \frac{\alpha'\beta' T(n)}{2}\right]$$

$$g_{\perp} = g_e - \frac{2\lambda\alpha\delta}{\Delta E_{xz}}\left[\alpha\delta - \alpha'\delta S - \frac{\alpha'\delta' T(n)}{\sqrt{2}}\right]$$

$$A_{II} = P\left[-\alpha^2(\frac{4}{7} + k_0) + (g_{II} - g_e) + \frac{3}{7}(g_{\perp} - g_e)\right] -$$

$$- P\left[\frac{8\lambda\alpha\beta}{\Delta E_{xy}}\{\alpha'\beta S + \frac{\alpha'\beta' T(n)}{2}\} + \frac{6\lambda\alpha\delta}{7\Delta E_{xz}}\{\alpha'\delta S + \frac{\alpha'\delta' T(n)}{\sqrt{2}}\}\right]$$

$$A_{\perp} = P\left[\alpha^2(\frac{2}{7} - k_0) + \frac{11}{14}(g_{II} - g_e)\right] - P\left[\frac{22\lambda\alpha\delta}{14\Delta E_{xz}}\{\alpha'\delta S + \frac{\alpha'\delta' T(n)}{\sqrt{2}}\}\right]$$

where g_e=2.0023 is the giromagnetic factor for the free electron, λ is the spin-orbit coupling constant (for copper(II) ion λ=-828 cm^{-1}), k_0=0.43±0.02 is the Fermi contact term for the copper(II) ion, P=-0.036 cm^{-1}. ΔE_{xy} and ΔE_{xz} are the electron transition energies of $^2B_{2g} \leftarrow {}^2B_{1g}$ and $^2E_g \leftarrow {}^2B_{1g}$ respectively, whose values are ΔE_{xy}=14200 cm^{-1} and ΔE_{xz} = 23800 cm^{-1} , for both complexes.

The in-plane σ-covalency parameter α^2 was calculated following Kivelson and Neiman's simplified expression [9]:

$$\alpha^2 = \frac{|A_{II}|}{0.036} + (g_{II} - g_e) + \frac{3}{7}(g_{\perp} - g_e) + 0.04$$

The α^2 value accounts for the fraction of the unpaired electron density located on the copper (II) ion.

The squares of the in-plane and out-of-plane metal π-bonding coefficients β^2 and δ^2 respectively, are obtained from the following first order approximate equations [11]:

$$\alpha^2\delta^2 \cong \frac{(g_{\perp} - g_e)\Delta E_{xz}}{2\lambda}$$

$$\alpha^2\beta^2 \cong \frac{(g_{II} - g_e)\Delta E_{xy}}{8\lambda}$$

Table 1 gives the ESR parameters and MO coefficients of the monomeric species obtained in Cu(II)-Aspirinate solutions. The ionic character of bondings is stronger for the DMF solution due to the T_d

symmetry. The higher the pyridine percentage, the more covalent is the in-plane π-bonding, due to the strong interaction between the Cu(II) ion and the nitrogen atoms of the pyridine [12]. The values of β^2 coefficient are greater for the monomeric species containing 4 DMF molecules then for those with 2 DMF molecules, because of the different local symmetry around the metal center. There is a growth of the β^2 values and a decrease of the covalent character with the increase of the symmetry ($D_{4h} \rightarrow T_d$, O_h) [13].

The values of the ESR parameters and the MO coefficients of monomeric species obtained in Cu(II)-Indomethacin are given in Table 2. The values of α^2 coefficients for these complexes are among 0.86÷0.91 corresponding to weak ionic character of in-plane σ-bonding while the values of β^2 (0.61÷0.76) indicate a dominant covalent character of the in-plane π-bonding. This dominant covalent character appears as compensation to the ionic character of the in-plane σ-bonding. α'^2 values shows that the unpaired electron is less delocalised towards the ligand for the σ-bonding.

CONCLUSIONS

The ESR spectra of Cu(II)-Aspirinate and Cu(II)-Indomethacin complexes in various Py-DMF solutions suggest the presence of pseudotetrahedral monomeric species. The powder-like spectra of these solutions adsorbed on NaY zeolite suggest the appearance of different monomeric species due to the partial or total coordination of the solvent molecules at the metal ion. The local symmetry may be planar-distorted tetrahedral or elongated tetrahedral-octahedral for CuO_4 chromophore and square-planar for CuN_2O_2 and CuN_4 units. The values of the molecular orbital coefficients indicate an ionic environment for the in-plane σ–bonding. Also, in the case of the in-plane π-bonding , the unpaired electron is more localized toward ligands in the chromophore with great number of nitrogen atoms. The role of the ligand nature is detected in the out-of-plane π-bonding. The unpaired electron spends more time in the ligand orbitals of Cu(II)-Aspirinate compounds then in the case of Cu(II)-Indomethacin.

REFERENCES

1. J. R. J. Sorenson, in Metal Ions in Biological Systems (Siegel H., ed.), 77(1982).
2. L. David, O. Cozar, V. Chis, A. Negoiescu and I. Vlasin, Appl. Magn. Reson. 6, 521(1994).
3. O. Cozar, L. David, V. Chis, C. Cosma, V. Znamirovschi, G. Damian, I. Bratu and Gh. Bora, Appl. Magn. Reson. 8, 235(1995).
4. H. Yokoi, A. W. Adisson, Inorg. Chem. 16, 1341(1977).
5. C. D. Samara, P. D. Iannakoudakis, D. P. Kessissoglu, G. E. Manoussakis, D. Mentzafos, A. Tersis, J. Chem. Soc. Dalton Trans. 3259(1992).
6. L. Abuhijleh, C. Woods, E. Bogas, G. Gnennion, Inorg. Chim. Acta, 195, 67(1992).
7. M. F. Ottaviani, Colloids and Surfaces 12, 305(1984).
8. H. Maki, McGarvey, J. Chem. Phys. 29, 31(1958).
9. D. Kivelson, R. Neiman, J. Chem. Phys. 35, 146(1961).
10. F. A. Cotton, J. J. Wise, Inorg. Chem. 6, 915(1967).
11. D. E. Billing, B. J. Hathaway and Nicholls, J. Chem. Soc. A, 316 (1969).
12. R. K. Ray and G. B. Kauffman, Inorg. Chim. Acta 173, 207(1990).
13. R. K. Ray and G. B. Kauffman, Inorg. Chim. Acta 174, 237(1990).

STUDIA UNIVERSITATIS BABEŞ-BOLYAI, PHYSICA, XLIII, 2, 1998

THE METAL-LIGAND BONDING IN SOME Cu(II)-COMPLEXES WITH LIGANDS OF BIOLOGICAL RELEVANCE. PART II: Cu(II)-TRANQUILIZING SEDATIVE-HYPNOTIC AND MYORELAXANT AGENTS

C. BALAN*, C. CRACIUN*, D. RISTOIU*, O. COZAR*, L. DAVID*

ABSTRACT. The ESR and optical spectra of CuL_2X_2 (L-diazepam, oxazepam, nitrazepam; X-Cl, Br) complexes were measured both in Py, DMF, CH_3Cl solutions and in solutions adsorbed on NaY zeolite, in order to elucidate solute-solvent interaction, metal-ligand bond parameters and the environment around the metallic ion. The molecular coefficients were calculated by LCAO-MO method and then used for the evaluation of the covalency degree of σ- and π-bondings between the Cu(II) ion and the nitrogen and oxygen atoms of the ligands.

INTRODUCTION

Diazepam, oxazepam and nitrazepam (Fig.1) are three benzodiazepines used for their tranquilizing sedative-hypnotic and myorelaxant properties [1-5].

The copper(II) complexes of these medical ligands are more efficient as drugs because they annihilate some negative effects of the ligands themselves. Therefore, the CuL_2X_2 complexes (L = diazepam, oxazepam, nitrazepam; X = Cl, Br) were investigated by ESR and optical measurements. The aim of this work was the investigation of the compounds v structure and the character (ionic or covalent) of Cu(II)-ligand bondings. For this purpose, pyridine (Py), dimethylformamide (DMF) and clorophorm (CH_3Cl) solutions of these complexes and solutions adsorbed on NaY zeolite have been prepared.

The ESR parameters obtained from the spectra of these solutions helped us to evaluate the molecular coefficients using Kivelson and Neiman's simplified expression and to establish the degree of covalency for σ- and π- bondings for each investigated compound.

* "Babes-Bolyai" University, Faculty of Physics, Cluj-Napoca, Romania

EXPERIMENTAL

The CuL_2X_2 complexes were prepared as previously reported [1,5]. The solutions of CuL_2X_2 in DMF, DMF-Py, Py and CH_3Cl (concentration = 10 mg/cm^3) were prepared. Each obtained solution was adsorbed onto NaY zeolite, for one hour. The insoluble precipitates were filtered off and the solution was dried in air.

ESR spectra were recorded at room temperature using a JEOL-JES-3B X band spectrometer.

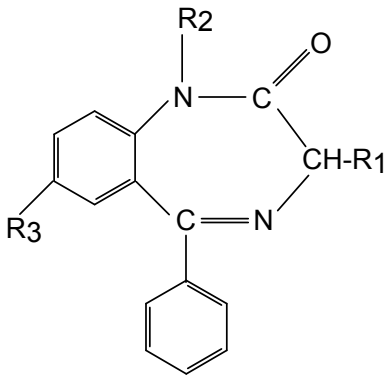

Fig.1. The molecular structure of diazepam (R_1=H; R_2=CH_3; R_3=Cl), oxazepam (R_1=H; R_2=H; R_3=NO_2), nitrazepam (R_1=OH; R_2=CH; R_3=Cl).

RESULTS AND DISCUSSION

The isotropic ESR spectra of the Cu(II)-diazepam compound in CH_3Cl solution and of Cu(II)-nitrazepam and Cu(II)-oxazepam compounds in Py and DMF solutions suggest the presence of pseudotetrahedral monomeric species [6] (Fig.2).

The four signals correspond to the isotropic hyperfine interaction between the paramagnetic electron and the Cu(II) nucleus.

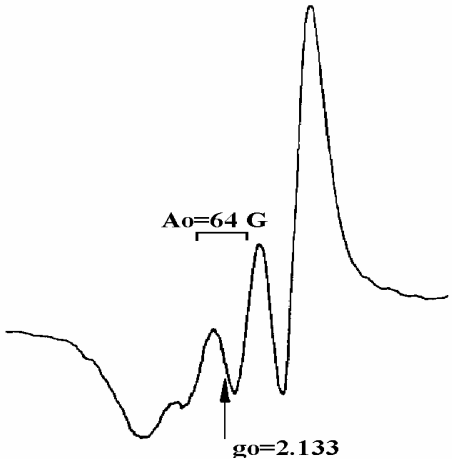

Fig.2. ESR spectrum of Py CuL_2Cl_2 (L-nitrazepam) solution at room temperature

The spectra of Cu(II)solutions adsorbed onto NaY zeolite are anisotropic with four hyperfine signals in the paralel band and a strong signal in $g_\perp$ region (Fig.3).

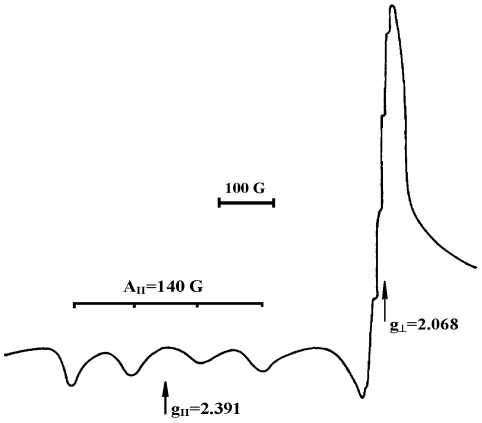

Fig.3. ESR spectrum of chloroform CuL_2Cl_2 (L-diazepam) solution adsorbed onto NaY zeolite.

The ESR parameters of Cu(II)-diazepam complexes (Table 1) and the appearance of five superhyperfine lines in the $g_\perp$ region, due to the interaction of the odd electron with two equivalent nitrogen nuclei (I_N=1, a_N=16G and 20G, respectively), confirm the existence of a CuN_2X_2 chromophore.

Table 1.

MO coefficients for Cu(II)-diazepam CH_3Cl solution adsorbed onto NaY zeolite

Compound	Solvent	$g_{\|\|}$	$g_{\perp}$	$A_{\|\|}$ (10^{+4} cm^{-1})	$A_{\perp}$ (10^{+4} cm^{-1})	α^2	β^2	δ^2	$\alpha^{'2}$
CuL_2Cl_2	CH_3Cl	2.391	2.068	155.6	15.4	0.94	0.84	0.65	0.13
CuL_2Br_2		2.374	2.062	163.4	19.2	0.94	0.80	0.59	0.13

The values of the ESR parameters for these compounds suggest a planar-tetrahedral distorted local symmetry at the Cu^{2+} site, with the paramagnetic electron in a $3d_{xy}+4p_z$ mixed ground state [7,8].

Information on the nature and the strength of metal-ligand bonding can be inferred from the evaluation of LCAO-MO coefficients (α^2, β^2, δ^2, $\alpha^{'2}$), which were calculated following the previously described method [4, Part.I] with ΔE_{xy}=13400 cm^{-1} ¿i ΔE_{xz}=15400 cm^{-1}.

In the case of Cu(II)-diazepam compound, the α^2, values correspond to a dominant ionic character of the σ-bonding. Smaller values of β^2 indicate a ionic character of the in-plane π bonding and δ^2 values indicate a strong covalent character of the out-of-plane π bonding.

The non-coplanarity of the copper ions with Cl and Br ligand atoms determines the ionic character of σ and in-plane π bondings, but the covalent character for the out-of-plane π bonding. The value of 0.13 for $\alpha^{'2}$ indicate the fact that the odd electron of Cu(II) spends 13% of the time in the donor states of the ligand.

The anisotropic spectrum of 100% Py CuL_2Cl_2 (L-oxazepam) solution adsorbed on NaY zeolite (Fig. 4) contains a hyperfine splitting in the $g_{\perp}$ region (a^N=18G), resulted from the interaction of the paramagnetic electron with the nitrogen nuclei. This fact and the ESR parameters of this spectrum suggest the presence of a CuN_4 chromophore, having a square-planar local symmetry. The halogen atoms were completely substituted by pyridine molecules [9].

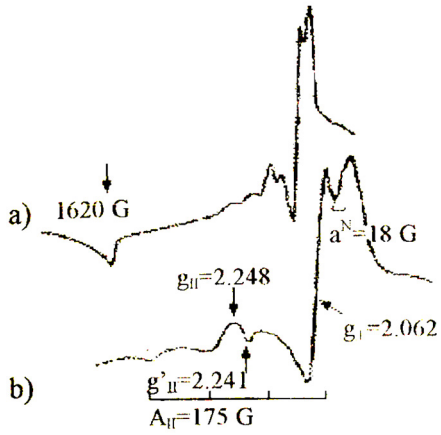

Fig. 4. ESR spectrum of 100%Py CuL_2Cl_2 (L-oxazepam) solution adsorbed onto NaY zeolite (a), the central part of the field (b)

This anisotropic spectrum contains a signal attributed to "forbidden" $\Delta M_S=\pm 2$ transitions at half-field, which suggests the presence of dimeric species, due to the coordination of Cu(II) ions at the same keto-oxygen from one oxazepam molecule.

The ESR spectrum of 60%Py+40%DMF CuL_2Br_2 (L-Oxazepam) solution adsorbed on NaY zeolite is presented in Fig.5.

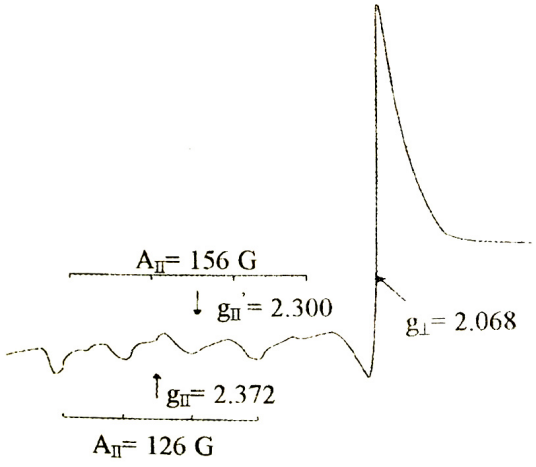

Fig. 5. **ESR** spectrum of 60%Py+40% DMF CuL_2Br_2 (L-oxazepam) solution adsorbed onto NaY zeolite

The analysis of hyperfine structure from the parallel band indicates the presence of two magnetically nonequivalent monomeric species, in the region g≈2.0. The characteristic ESR parameters of all identified monomeric species are given in Table 2.

Table 2. *ESR parameters of mononuclear species obtained in DMF and Py* Cu(II)-oxazepam solutions adsorbed on NaY zeolite, at room temperature

Compound	Solvent	$g_{\parallel}$	$g_{\perp}$	$A_{\parallel}$ (G)	α^2	β^2	δ^2	α'^2	Chromophore and symmetry
CuL_2Cl_2	100%DMF	2.384 2.368	2.087	125 155	0.843 0.916	0.916 0.808	0.934 0.860	0.223 0.143	$CuO_4 \rightarrow T_d$ $CuN_2O_2O_2^* \rightarrow O_h$
	60%DMF+40%Py	2.418 2.002	2.088 2.222	120 170	0.867 0.873	0.970 0.708	0.919 0.742	0.195 0.197	$CuO_4 \rightarrow T_d$ $CuN_2O_2N_2^* \rightarrow D_{4h}^*$
	100%Py	2.248	2.062	175	0.819	0.678	0.678	0.268	$CuN_4 \rightarrow D_{4h}$
CuL_2Br_2	100%DMF	2.397 2.332	2.088	123 165	0.852 0.903	0.935 0.882	0.935 0.882	0.212 0.158	$CuO_4 \rightarrow T_d$ $CuN_2O_2O_2^* \rightarrow O_h$
	60%DMF+40%Py	2.372 2.300	2.070	123 156	0.816 0.830	0.772 0.758	0.772 0.758	0.254 0.249	$CuO_4 \rightarrow T_d$ $CuN_2O_2N_2^* \rightarrow O_h$
	100%Py	2.363 2.309	2.065	126 178	0.812 0.904	0.718 0.645	0.718 0.645	0.276 0.168	$CuN_4 \rightarrow T_d$ $CuN_2N_4^* \rightarrow O_h$

The values between 0.81÷0.92 obtained for the molecular coefficient α^2 suggest a weak ionic character of the σ-bonding along the metal-ligand axis [10]. One may observe that the values of α^2, β^2, δ^2 parameters decrease with the decreasing of DMF percentage, the CuO_4 chromophore being changed into CuN_4 chromophore. The values of β^2 and δ^2 range from 0.6 to 0.9, indicating a weak to dominant covalent character of the in-plane and out-of-plane π-bondings, upon the DMF percentage. The α'^2 coefficient, which indicates the degree of delocalization of the paramagnetic electron towards the ligand atoms, it is seen to increase with the lowering of DMF percentage.

ESR spectrum of Py-Cu(II)-nitrazepam solution adsorbed onto NaY zeolite suggest also the presence of two magnetically nonequivalent monomeric species, as a result of partial or total substitution of the ligand atom by Py molecules (Fig.6). The existence of a CuN_4 unit is confirmed by the appearance of nine nitrogen superhyperfine lines (a^N=14G) in the $g_{\perp}$ region.

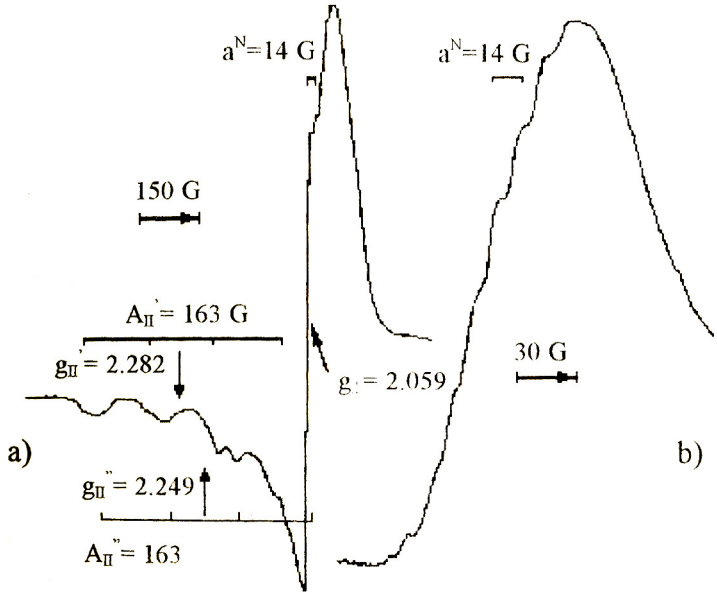

Fig.6. ESR spectrum of Py CuL_2Cl_2 (L-nitrazepam) solution adsorbed onto NaY zeolite a). Extended perpendicular absorption b).

Table 3 gives the characteristic ESR parameters and the proposed symmetry of all identified monomeric species. The spectra of DMF-Cu(II)-nitrazepam solutions adsorbed onto NaY zeolite show also the coexistence of two monomeric species. One of these species with the CuN_2O_2 chromophore is due to the coordination of solvent molecules at the Cu(II) ion. The other set of parameters confirms the existence of CuO_4 chromophore, with planar-tetrahedral (T_d) distorted symmetry [11]. The nitrazepam ligand molecules and the halogen atoms are completely substituted by DMF molecules.

Table 3.

ESR parameters of mononuclear species obtained in Cu(II)-nitrazepam solutions adsorbed onto NaY zeolite at room temperature

Compound	Sol-vent	$g_{\|\|}$	$g_{\perp}$	$A_{\|\|}$ (G)	α^2	β^2	δ^2	α'^2	Chromophore and symmetry
Cu L_2Cl_2	DMF	2.393	2.081	122	0.84	0.94	0.87	0.22	$CuO_4 \rightarrow T_d$
		2.353		170	0.94	0.75	0.78	0.11	$CuN_2O_2 \rightarrow D_{2d}$
Cu L_2Cl_2	Py	2.282	2.059	163	0.82	0.69	0.64	0.26	$CuN_2N_4^* \rightarrow O_h$
		2.249		178	0.83	0.60	0.64	0.26	$CuN_4 \rightarrow D_{4h}$
Cu L_2Br_2	DMF	2.383	2.083	125	0.84	0.92	0.89	0.23	$CuO_4 \rightarrow T_d$
		2.351		170	0.94	0.75	0.80	0.12	$CuN_2O_2 \rightarrow D_{2d}$
Cu L_2Br_2	Py	2.297	2.062	169	0.86	0.69	0.64	0.22	$CuN_2N_4^* \rightarrow O_h$
		2.251		174	0.82	0.61	0.68	0.27	$CuN_4 \rightarrow D_{4h}$

The values of about 0.8-0.9 for α^2 coefficient state for a weak ionic character of the σ-bonding. For the in-plane π-bonding, a dominant covalent character is suggested by the low values of β^2 coefficient (0.61÷0.75), while the larger values of β^2 (0.92-0.94) correspond to a ionic character. The out-of-plane π-bondings have a ionic character for the complexes in DMF-solutions and dominant covalent character for theirs Py-solutions [11].

CONCLUSIONS

The ESR parameters and the shape of the spectra obtained for the Cu(II)-diazepam in different solutions suggest a planar-tetrahedral distorted local symmetry at the Cu^{2+} site.

From the molecular coefficients obtained we conclude a dominant ionic character for σ-bonding and for the in-plane π-bonding, while the out-of-plane π-bonding was proved to have a strong ionic character. The ionic character of all σ- and π- bondings in these complexes can be explained by the non-coplanarity of the Cu ions with the Cl and Br ligand atoms.

The values obtained for the molecular coefficients in the case of Cu(II)-oxazepam compounds state for a weak ionic character of the σ-bonding. The weak or dominant covalent character of the in-plane and out-of-plane π-bondings was seen to depend on the DMF percentage of the solvent, the CuO_4 chromophore being changed into CuN_4 chromophore, accordingly.

The presence of the monomeric species, having a planar-tetrahedral distorted symmetry, was also confirmed in the spectra of Cu(II)-nitrazepam compounds. The values of α^2 coefficient indicate a weak ionic character of the σ-bonding, while the character of the in-plane and out-of-plane π-bondings depends of the solvent nature.

REFERENCES

1. C.Preti, G.Tosi, J. Coord. Chem., 6, 81 (1976).
2. C.Preti, G.Tosi, J. Coord. Chem., 8, 223 (1979).
3. O.Cozar, L.David, V.Chiş, E.Forizs, C.Cosma, G.Damian, Fresenius J. Anal. Chem., 355, 701 (1996).
4. G.Minghetti, M.L.Ganadu, C.Foddai, M.A.Cinellu, F.Demartin, M. Manassero, Inorg. Chim. Acta, 86, 93 (1984).
5. M.A.Cinellu, M.L.Ganadu, G.Minghetti, F.Cariati, F.Demartin, M.Manassero, Inorg.Chim.Acta, 143, 197 (1988).
6. H.Yokoi, A.W. Addison, Inorg. Chem., 31, 1575 (1992).
7. G.Batra, P.Mathur, Inorg.Chem., 31, 1575 (1992).
8. O.Cozar, I.Ardelean, J. Non-Crystalline Solids, 92, 278 (1987).
9. M.F. Ottaviani, Colloids and Surfaces, 12, 305 (1984).
10. O.Cozar, L.David, A.Hernanz, R.Navarro, E.Forizs, I.Bratu, M. de la Fuente, Spect. of Biol. Molec.:Modern Trends, 625 (1997).
11. O.Cozar, L.David, V.Chis, C.Cosma, V.Znamirovschi, G.Damian, I.Bratu, Gh.Bora, Appl. Magn. Reson., 8, 235 (1995).

STUDIA UNIVERSITATIS BABEŞ-BOLYAI, PHYSICA, XLIII, 2, 1998

MICROSTRUCTURE INFLUENCE OF THE LOCAL DYNAMICS IN MOLTEN POLYBUTADIENE

M. TODICA*

ABSTRACT. The spin-lattice relaxation time of the protons attached to the polymeric chain was measured by NMR method for some molten polybutadiene with different vinyl concentrations, in a large temperature range. The correlation time of the local motion of the polymeric segments calculated from the experimental T_1 data depends on the vinyl concentration.

INTRODUCTION

Some physical properties of the polymeric materials, like the viscoelasticity or mechanical rigidity are determined by the dynamic behavior of the polymeric chains, [1]. The molecular dynamics of the macromolecules is a complex process which includes many kinds of motions, going from the elementary motions inside the monomeric unit to the diffusion of the entire chain along the reptation tube [2].

The microscopic description of the elementary motions of the polymeric chain is based on the observation of the physical interactions between the neighboring atoms of the chain. Many techniques can be utilized to observe these interactions, but one of the most useful is the Nuclear Magnetic Resonance.

NMR is based on the observation of the interactions between the atomic nuclear spins of the chain and provides information in the microscopic range [3]. The characteristic environment of the nuclear spins due to the temperature or microstructure is reflected by the modification of NMR parameters. Our interest is to observe the dependence of the spin-lattice relaxation time in function of the microstructure of the polymer.

* "Babeş-Bolyai" University, Faculty of Physics, 3400 Cluj-Napoca, Romania

EXPERIMENTAL

We investigated some polybutadiene samples with different vinyl contents:

BR1200	1% vinyl	97% cis	110000 g/mol
PB1009	8% vinyl	38% cis	70000 g/mol
PB1507	40% vinyl	24% cis	190000 g/mol

The polymeric samples were supplied by the Manufacture Michelin, France. The samples were enclosed in NMR tubes (diameter 4mm) and sealed under a primary vacuum. All the measurements were performed using a CXP Bruker spectrometer working at 45 MHz, in the temperature range of 254 K to 344K. The spin-lattice relaxation time was measured using the inversion recovery method, [4]. The sample temperature was controlled within 1 K.

RESULTS AND DISCUSSION

The elementary motions which governs the dynamics of the entire chain are the rotations of the C-C and C-H links around the local symmetry axis. Every rotation modify the azimuthal angles of the links and the relative orientation of the nuclear spins within the segmental or monomeric units.

Now it is well-known that the dominant mechanism which governs the spin-lattice relaxation process of the protons attached to the polymeric chain is the dipolar interaction between the nuclear spins located within the given chain segment [5]. This interaction decreases rapidly with the distance between the spins, so that only the neighboring spins are taken into account [6]. For identical spins the spin-lattice relaxation time is given by:

$$\frac{1}{T_1} = K\left[\frac{\tau_c}{1+\omega^2\tau_c^2} + \frac{4\tau_c}{1+4\omega^2\tau_c^2}\right] \qquad (1)$$

The constant K depends on the distance between the interacting spins $K \propto \frac{1}{r^6}$ and ω is the resonance frequency of the protons, [6, 7]. τ_c represents the correlation time of the orientational motion of the nuclear spins and its mathematical expression is derived on the basis of specific model for the polymer motion. One of the most used model for quantitatively estimations of the correlation time is based on the Kramer's and Helfand theory concerning the passage of a particle over a potential

barrier energy [8, 9]. Two different stable conformations of the polymeric chain are separated by a barrier potential energy of height E_a. The energy required for conformational transition is provided by thermal activation. Under these assumptions the temperature dependence of the correlation time is:

$$\tau_c = B \exp\left(\frac{E_a}{RT}\right) \tag{2}$$

B is a constant depending on the nature of the polymer and E_a is the activation energy. Combining the relations (1) and (2) we can obtain the temperature dependence of the spin-lattice relaxation rate. This relation will contain some unknown parameters: the activation energy E_a, the constants B and K. One of the aims of this work is to determine these parameters from experimental data.

The activation energy can be calculated from the Arrhenius plot of the experimental data of T_1. When the extreme narrowing condition $\omega\tau_c<<1$ is fulfilled, then the equation (1) simplifies to:

$$\frac{1}{T_1} \propto \exp\left(\frac{E_a}{RT}\right) \tag{3}$$

E_a is calculated from the best fit slope of the plot $\ln(T_1)$ versus 1/T over the temperature range of interest. In the case of our samples the condition $\omega\cdot\tau_c<<1$ is fulfilled in the domain range of higher temperatures. We obtained linear dependencies of $\ln(T_1)$ versus 1/T for each sample (figure 1), which allows us to calculate the activation energies.

The values of the activation energies are listed in table 1:

Table 1

sample	vinyl contents	Ea (KJ/mol)
BR1220	1%	19.5±10%
PB1009	8%	17.8±10%
PB1507	40%	16.6±10%

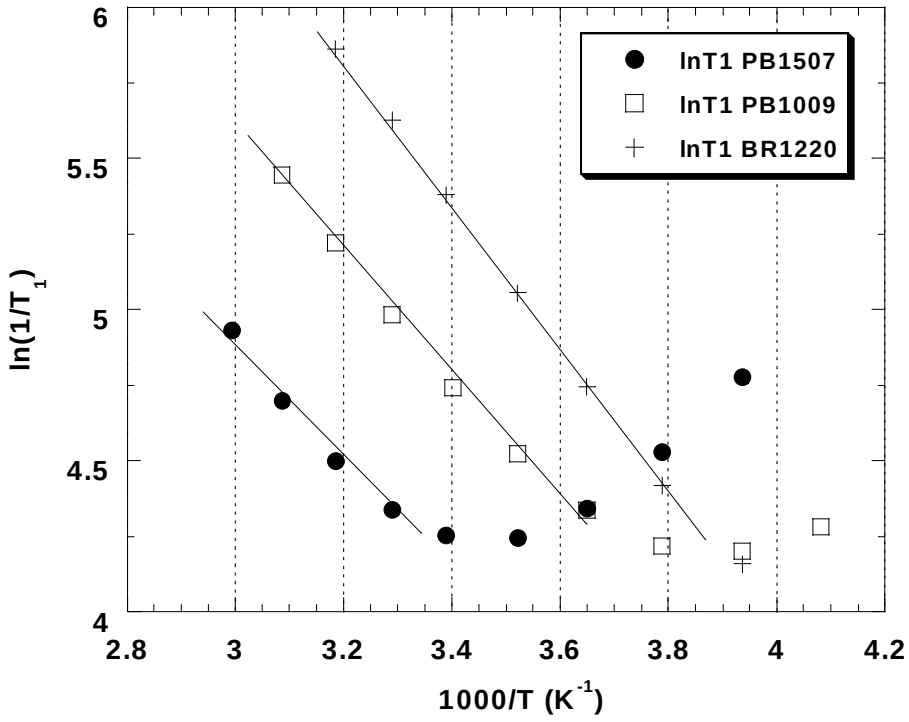

Fig. 1. Arrhenius plot of the experimental T1 data

We observed a little dependence of E_a on the vinyl concentration but the values obtained are very close to each other for these samples. This result is not surprising because all the samples have the same chemical composition of the monomeric unit and identical conformation in proportion of more than 50%. The difference is given only by the spatial orientation of the CH and CH_2 groups in the vinyl conformation. We can associate the lower values of E_a for the samples with high vinyl contents with the spatial orientation of CH and CH_2 bonds inside this group.

If the value of the activation energy is known, there would remain only two parameters unknown, K and B, in equation (1). The parameter K can be calculated from the minimum condition of the temperature dependence of the spin-lattice relaxation. From equation (1) results that T_1 reaches its minimum when the condition $\omega_0*\tau_c \cong 0.616$ is fulfilled. (ω is the Larmor frequency). In this case we obtain the simple relation

$$\frac{1}{T_1} = K * 5.035 * 10^{-9}\, s^{-1} \qquad (4)$$

This is a simple way to calculate the constant K.

For the samples PB1507 and PB1009 the minimum values of T_1 were observed at the temperatures θ=290K, respectively θ =258K, (see figure 2). The minimum value of T_1 is T_{1min}=65±3ms for both the samples. The correlation time corresponding to these temperatures is $\tau_c=2.1*10^{-12}$ s and the value of constant K obtained from relation (4) is $K \cong 2.9*10^9$ for both the samples. For the sample BR1220 the minimum of T_1 is not observed, but we can estimate its minimum value and the corresponding temperature θ by extrapolation. We estimate that T_{1min}=65±ms, like in the case of other two samples and θ =245±5K, (see also figure 2). So we can appreciate that the minimum value of T_1 is the same for all the samples. The physical support of this assumption is based on the fact that the constant K depends on the distance between the interacting spins. But the chemical structure of the monomeric units of our samples are very close to each other, so that we can characterize all the samples by the same average distance between the interacting spins. Using this value of K and the corresponding activation energies we have fitted the experimental data for each sample. From the best fit we have estimated the values of parameter B, which allows us to calculate the correlation time of the elementary motions for each temperature. The values calculated with equation (2) for the correlation time are shown in figure 3.

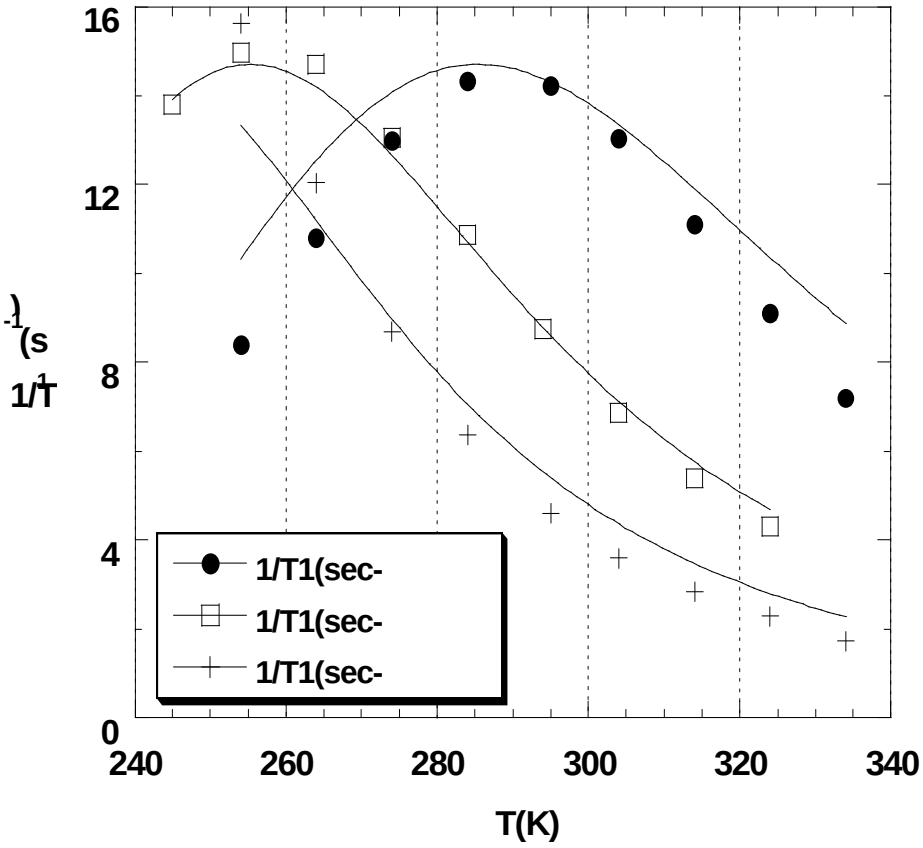

Fig. 2. The best fit of spin-lattice relaxation time
for molten polybutadienes with different vinyl contents, using equation (1).

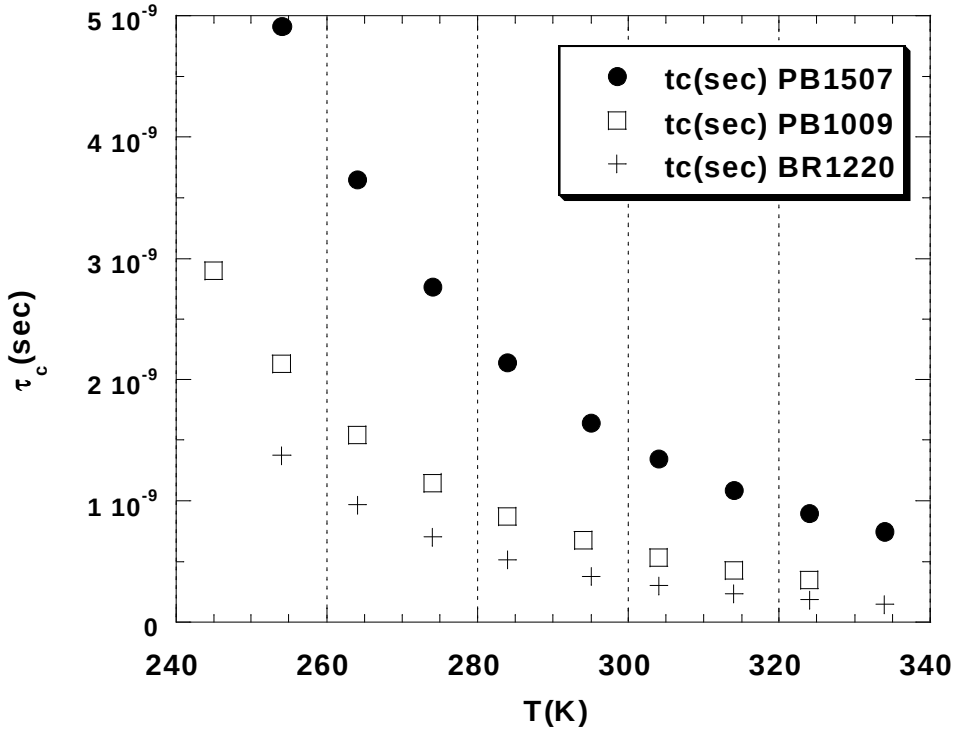

Fig. 3. The temperature dependence of the correlation time calculated with equation (2)

For a given temperature we observed that the correlation time increases with the vinyl contents of the sample. Polymeric samples with great vinyl contents are characterized by long correlation times. This means a weak mobility of the links. On the other hand, the correlation time decreases with the increasing of the temperature, which indicates an increase of the local mobility with the thermal activation. The molecular weight of macromolecules do not affect the local dynamics.

CONCLUSION

The local mobility of the polymeric links can be investigated by measuring the temperature dependence of the spin-lattice relaxation time. The correlation time of rotational motions of the links can be calculated in the first order of approximation using a model based on Kramer and Helfand`s theories. This correlation time decreases with the temperature, indicating an increasing of the local mobility.For a given temperature, the vinyl contents of the samples modify also the correlation time of these motions. This correlation time increase with the vinyl contents, indicating a lowering of the local mobility. We can conclude that the microstructure of the polymer is an important factor which affect the local mobility of the chain.

REFERENCES

1. J. Ferry, "Viscoelstic Properties of Polymers", John Wiley and Sons, New York, 1980.
2. P. G. De Gennes, Scaling Concepts in polymer Physics", Cornell University Press, Ithaca, New York, 1979.
3. 3. J. P. Cohen-Addad, "NMR and Fractal Properties of Polymers Liquids and Gels", Pergamon Press, London, 1992.
4. H. Y. Carr, E. R. Purcell, Phys. Rev., 1954, 94, 630.
5. 5. J. P. Cohen-Addad, "Physical Properties of Polymeric Gels", John Wiley and Sons, Chichester, New-York, Toronto, 1996.
6. 6. A. Abragam, The Principles of Nuclear Magnetism, Clarendon Press, Oxford, 1961.
7. 7. L. Morton and C. Morton, Methods of Experimental Physics, Academic Press Inc., 1980.
8. H. A. Kramers, Physica, 1940, 7, 284
9. E. Helfand, J. Chem. Phys., 1971, 54, 4651.

STUDIA UNIVERSITATIS BABEŞ-BOLYAI, PHYSICA, XLIII, 2, 1998

EVALUATION OF THE HIGHER-ORDER APPROXIMATIONS TO THE TRANSPORT PROPERTIES FROM MORSE-MORSE-SPLINE-VAN DER WAALS INTERMOLECULAR POTENTIAL

I. COROIU[1]

ABSTRACT. The Chapman-Cowling and Kihara higher approximations to the transport coefficients have been calculated from an improved intermolecular potential, Morse-Morse-Spline-van der Waals (MMSV) potential, proposed by R.A. Aziz *et al.* [J.Chem.Phys., 94(2), 1034 (1991)]. The results are tabulated over a large temperature range, kT/ε from 0.1 to 400. The treatment was completely classical and no corrections for quantum effects were made. These results would be employed to predict gaseous transport properties of different spherical and quasispherical molecules, especially for hexafluorides. The knowledge of transport coefficients has huge importance for the isotope separation technologies.

INTRODUCTION

The kinetic theory of gases can elucidate the macroscopic properties of gases in terms of the motion and interaction of molecules. The theory advanced by Enskog and Chapman [1] is able to show how the transport properties of gases, like as: viscosity, thermal conductivity, diffusions are connected to the properties of their molecules. The most significant feature of this theory is that if the intermolecular pair potential for the interaction of the molecules is known, it is possible to calculate the transport properties of a gas consisting of these molecules to any desired degree of accuracy at any temperature. Hence, each of the transport coefficients of the gas can be expressed in terms of well defined integrals over the intermolecular potential for each of the possible binaries encounters in the system. Leave out very simple and physically unrealistic potential forms, the calculations of collision integrals involve extensive numerical integration.

[1] Technical University, 3400 Cluj-Napoca

The inverse question [2] is also valid. Information concerning intermolecular forces may be achieved from the temperature variation of gaseous transport coefficients by means of Enskog and Chapman theory. Such information is helpful in correlating other properties of liquid and solid states [2], so that it is appear encouraging for future simulations of solids and liquids [3].

Numerous intermolecular potential forms have been proposed to date for the study of transport phenomena and bulk properties of diverse substances. These include: the Lennard Jonesn-mfunction [4], Kihara spherical core potential [5], Buckingham-Corner potential [6], modified Buckingham (Exp-Six) potential [7], Boys and Shavitt potential [9], Dymond-Rigby-Smith potential [10], Barker-Pompe potential [11], Barker-Bobetic-Maitland-Smith (BBMS) potential [12], Parson-Siska-Lee potential (a Morse Spline-van der Waals potential) [13], Smith-Thakkar potential [14], Morse-Hermite interpolation-Smith-Thakkar (MIST) potential [15], Hartree-Fock HFD potential [16], HFD-Aziz potential [17], spherical shell model (SSM) function [18], Simon-Parr - Finlan modified Dunham expansion function [19], n-6-4 potential function [20], etc.

Any one results accomplished for any potential function may be acceptable merely if it is reproduce the analogous experimental data with minimal errors.

Several effective isotropic pair potential functions [4-7, 12, 18] have been proposed to describe the bulk properties of quasispherical molecules and in particular the hexafluorides, lacking much success. Not long ago, R.A. Aziz *et al.* [21] have been constructed a Morse-Morse-Spline-van der Waals (MMSV) potential. The MMSV potential incorporates the determination of C_6 dispersion coefficient [22] and it satisfactorily correlates second virial and viscosity data of sulphur hexafluoride at the same time.

The purpose of this paper is to calculate for the first time the higher-order approximations to the transport properties from this more realistic potential form. The tabulated results over a large temperature range can be helpful for prediction the transport properties of any spherical and quasispherical molecules.

$$V(r) = \varepsilon V^*(x) \tag{1}$$

The Morse-Morse-Spline-van der Waals (MMSV) functional form is given by

where

$$V^*(x) = \exp\left[-2\beta_1(x-1) \right] - 2\exp\left[-\beta_1(x-1) \right], \quad 0 \le x \le 1$$

$$= \exp\left[-2\beta_2(x-1) \right] - 2\exp\left[-\beta_2(x-1) \right], \quad 1 \le x \le x_1$$

(2)

$$= a_1 + (x-x_1)\left\{ a_2 + (x-x_2)\left[a_3 + (x-x_1)a_4 \right] \right\}, \quad x_1 \le x \le x_2$$

$$= -\left(\frac{C_6}{x^6} + \frac{C_8}{x^8} + \frac{C_{10}}{x^{10}} \right), \quad x \ge x_2$$

and $x=r/r_m$.

The significance of the symbols in the above Equation is given in Reference [21].

GENERAL FORMULAE

The transport coefficients like as: diffusion, viscosity and thermal conductivity, quantify the difficulty of the transport of mass, momentum and energy respectively in a gas subjected to gradients of concentration, velocity or temperature. Because, in a gas, this transport is achieved by motion of molecules, the nature of the collisions that the molecules undergo influences the difficulty of transport. Further, because the form of the intermolecular potential determines the outcome of the binary collisions, these potential influences the transport coefficients in a complicated way.

Nevertheless, the fundamental kinetic theory for the transport coefficients can be formulated to involve only a set of well-defined *collision integrals* besides molecular mass (m), temperature (T) and pressure (p). These collision integrals represent variously weighted, energy-averaged cross sections for binary encounters between molecules of the gas and are defined [1-2, 23] by

$$\Omega^{(l,s)^*} = \left[(s+1)!\ T^{*s+2} \right]^{-1} \int_0^\infty Q^{(l)^*}(E^*)\ e^{-E^*/T^*} E^{*s+1} dE^* \quad (3)$$

where $T^*=KT/\varepsilon$ is the reduced temperature, k is the Boltzmann's constant, T is the absolute temperature, $E^*=E/\varepsilon$ is the reduced relative kinetic energy of the collision and $Q^{(l)*}(E^*)$ represents the reduced transport cross-sections. $Q^{(l)*}(E^*)$ are defined by equation

$$Q^{(l)*}(E^*) = 2\left[1 - \frac{1+(-1)^l}{2(1+l)}\right]^{-1} \int_0^\infty (1-\cos^l \chi) b^* db^* \tag{4}$$

where $b^*=b/\sigma$ is the reduced impact parameter and χ is the deflection angle in binary collision.

This angle is given by

$$\chi(E^*, b^*) = \pi - 2b^* \int_{r_o}^{\infty} \frac{dr^*/r^{*2}}{[1 - b^{*2}/r^{*2} - V(r^*)/E^*]^{1/2}} \tag{5}$$

where $r^*=r/\sigma$ is the reduced intermolecular separation, $r_o^*=r_o/\sigma$ is the reduced closest distance of approach, $V^*(r^*)=V(r)/\varepsilon$ is the intermolecular potential with parameters σ and ε.

It is useful to define some combinations of reduced collision integrals that occur in kinetic theory expressions for the transport coefficients [1-2, 23].

$$\begin{aligned}
A^* &= \Omega^{(2,2)*}/\Omega^{(1,1)*} \\
B^* &= \frac{5\Omega^{(1,2)*} - 4\Omega^{(1,3)*}}{\Omega^{(1,1)*}} \\
C^* &= \Omega^{(1,2)*}/\Omega^{(1,1)*} \\
E^* &= \Omega^{(2,3)*}/\Omega^{(2,2)*} \\
F^* &= \Omega^{(3,3)*}/\Omega^{(1,1)*} \\
G^* &= \Omega^{(1,4)*}/\Omega^{(1,1)*} \\
H^* &= \Omega^{(2,4)*}/\Omega^{(2,2)*} \\
I^* &= \Omega^{(1,5)*}/\Omega^{(1,1)*}
\end{aligned} \tag{6}$$

The values of the transport coefficients [1-2, 23] may be expressed as infinite series, and higher-order approximations to the coefficients are obtained the more terms of the series that are taken. Fortunately, the convergence is rapid, and very few terms are needed. Hence, any transport coefficient can be defined by the equation

$$[X]_n = [X]_1 f_x^n \tag{7}$$

where$X=\lambda, \eta, D$; n=1,2,..., and $f_x^{(n)}$ is the higher-order approximations.

These higher order approximations have been evaluated for two schemes. The first scheme is the Chapman-Cowling [1] method that implies a particular approximation way for obtaining solutions to an infinite set of simultaneous equations. The alternative method has been developed by Kihara [24]. In general the latter scheme leads to somewhat simpler formulae, which to an equal order of approximation are more accurate than the corresponding Chapman-Cowling expressions. However, the Kihara approximation is not available for all the transport properties of binary gas mixture.

The viscosity of a pure gas can be expressed in the following way:

a) for the first-order approximation

$$[\eta]_1 = \frac{5}{16}\left(\frac{mkT}{\pi}\right)^{1/2} \frac{1}{\sigma^2 \Omega^{(2,2)*}(T^*)} \tag{8}$$

b) for the second-order Chapman-Cowling approximation

$$[\eta]_2 = [\eta]_1 f_\eta^{(2)} \tag{9}$$

$$f_\eta^{(2)} = 1 + (H^{01})^2 / \left[H^{00} H^{11} - (H^{01})^2\right] \tag{10}$$

where

$$H^{00} = 1 / [\eta]_1$$

$$H^{01} = \frac{1}{[\eta]_1}\left[\frac{7}{4} - 2E^*\right]$$

$$H^{11} = \frac{1}{[\eta]_1}\left[\frac{301}{48} - 7E^* + 5H^*\right]$$

c) for the third Chapman-Cowling approximation

$$[\eta]_3 = [\eta]_1 f_\eta^{(3)} \tag{11}$$

$$f_\eta^{(3)} = f_\eta^{(2)} + H^{00}(H^{01}H^{12} - H^{11}H^{02})^2 / \{ \left[H^{00}H^{11} - (H^{01})^2\right] \times \left[H^{00}H^{11}H^{22} + 2H^{01}H^{02}H^{12} - H^{00}(H^{12})^2 - H^{11}(H^{02})^2 - H^{22}(H^{01})^2\right] \} \tag{12}$$

where, besides previously defined quantities,

$$H^{02} = \frac{1}{[\eta]_1}\left[\frac{63}{32} - \frac{9}{2}E^* + \frac{5}{2}H^*\right]$$

$$H^{12} = \frac{1}{[\eta]_1}\left[\frac{1365}{128} - \frac{321}{16}E^* + \frac{125}{8}H^* - \frac{15\Omega^{(2,5)*}}{2\Omega^{(2,2)*}}\right]$$

$$H^{22} = \frac{1}{[\eta]_1}\left[\frac{25137}{1024} - \frac{1755}{32}E^* + \frac{1905}{32}H^* - \frac{135}{4}\frac{\Omega^{(2,5)*}}{\Omega^{(2,2)*}} + \frac{105}{8}\frac{\Omega^{(2,6)*}}{\Omega^{(2,2)*}} + \frac{3\Omega^{(4,4)*}}{\Omega^{(2,2)*}}\right]$$

d) for the second-order Kihara approximation

$$[\eta]_2^K = [\eta]_1 f_\eta^{K(2)} \tag{13}$$

where

$$f_\eta^{K(2)} = 1 + \frac{3}{49}\left[4E^* - \frac{7}{2}\right]^2 \tag{14}$$

The thermal conductivity of a pure gas can be expressed in the following way:

a) for the first-order approximation

$$[\lambda]_1 = \frac{75}{64}\left(\frac{k^3 T}{m\pi}\right)^{1/2} \frac{1}{\sigma^2 \Omega^{(2,2)*}(T^*)} \tag{15}$$

b) for the second-order Chapman-Cowling approximation

$$[\lambda]_2 = [\lambda]_1 f_\lambda^{(2)} \tag{16}$$

where

$$f_\lambda^{(2)} = 1 + \frac{(L^{12})^2}{L^{11}L^{22} - (L^{12})^2} \tag{17}$$

and

$$L^{11} = \frac{1}{[\lambda]_1}$$

$$L^{12} = \frac{1}{[\lambda]_1}\left[\frac{7}{4} - 2E^*\right]$$

$$L^{22} = \frac{1}{[\lambda]_1}\left[\frac{77}{16} - E^* + 5H^*\right]$$

c) for the third-order Chapman-Cowling approximation

$$[\lambda]_3 = [\lambda]_1 f_\lambda^{(3)} \tag{18}$$

where

$$f_\lambda^{(3)} = f_\lambda^{(2)} + L^{11}(L^{12}L^{23} - L^{22}L^{13})^2 / \left\{ \left[L^{11}L^{22} - (L^{12})^2\right] \times \left[L^{11}L^{22}L^{33} + 2L^{12}L^{13}L^{23} - L^{11}(L^{23})^2 - L^{22}(L^{13})^2 - L^{33}(L^{12})^2\right] \right\} \tag{19}$$

and

$$L^{13} = \frac{1}{[\lambda]_1}\left[\frac{63}{32} - \frac{9}{2}E^* + \frac{5}{2}H^*\right]$$

$$L^{23} = \frac{1}{[\lambda]_1}\left[\frac{945}{128} - \frac{261}{16}E^* + \frac{125}{8}H^* - \frac{15\Omega^{(2,5)*}}{2\Omega^{(2,2)*}}\right]$$

$$L^{33} = \frac{1}{[\lambda]_1}\left[\frac{14553}{1024} - \frac{1215}{32}E^* + \frac{1565}{32}H^* - \frac{135\Omega^{(2,5)*}}{4\Omega^{(2,2)*}} + \frac{105\Omega^{(2,6)*}}{8\Omega^{(2,2)*}} + \frac{\Omega^{(4,4)*}}{\Omega^{(2,2)*}}\right]$$

d) for the second-order Kihara approximation

$$[\lambda]_2^K = [\lambda]_1 f_\lambda^{K(2)} \tag{20}$$

where

$$f_\lambda^{K(2)} = 1 + \frac{2}{21}\left[4E^* - \frac{7}{2}\right]^2 \tag{21}$$

The self-diffusion coefficient-of a pure gas can be expressed in the following way:

a) for the first-order approximation

$$[D]_1 = \frac{3}{8n}\left(\frac{kT}{\pi m}\right)^{1/2} \frac{1}{\sigma^2 \Omega^{(1,1)^*}(T^*)} \tag{22}$$

b) for the second-order Chapman-Cowling approximation

$$[D]_2 = [D]_1 f_D^{(2)} \tag{23}$$

where

$$f_D^{(2)} = \frac{1}{1-\Delta} \tag{24}$$

and

$$\Delta = \frac{\left(6C^* - 5\right)^2}{\left(55 - 12B^* + 16A^*\right)} \tag{25}$$

c) for the second order Kihara approximation

$$[D]_2 = [D]_1 f_D^{K(2)} \tag{26}$$

where

$$f_D^{K(2)} = 1 + \frac{\left(6C^* - 5\right)^2}{16A^* + 40} \tag{27}$$

RESULTS AND DISCUSSIONS

To estimate the higher-order approximations to the transport properties from Morse-Morse-Spline-van der Waals potential form, first it must to calculate different reduced collision integrals and some combination of these. For calculation of the reduced collision integrals we have chosen the programme catalogue number ACQN, authors H. O'Hara and F. J. Smith [25]. This programme was adapted to run in double precision on IBM computers by P.D. Neufeld and R.A. Aziz [26] and subsequent adapted by us to run on PC computers. The programme contains an efficacious calculation method with a high degree of simplicity and accuracy. This method advanced by Clenshow and Curtiss [27] computes the definite integrals through the integrant growth in a finite series of Cebishev polynomials and the integration of each term of series. The inherent computational error is estimated to be of the order of 0.1% except for very small T^*, where it may be larger.

Figures 1 and 2 show the behaviour of the most important reduced collision integrals $\Omega^{(2,2)*}$ and respectively, $\Omega^{(1,1)*}$, computed from Lennard Jones 12-6 potential [2], modified Buckingham (Exp-Six), (α=15), potential [2] and Morse-Morse-Spline-van der Waals potential, for T^* variation. These reduced collision integrals are involved in the first-order approximations of the viscosity, thermal conductivity and self-diffusion coefficient, respectively.

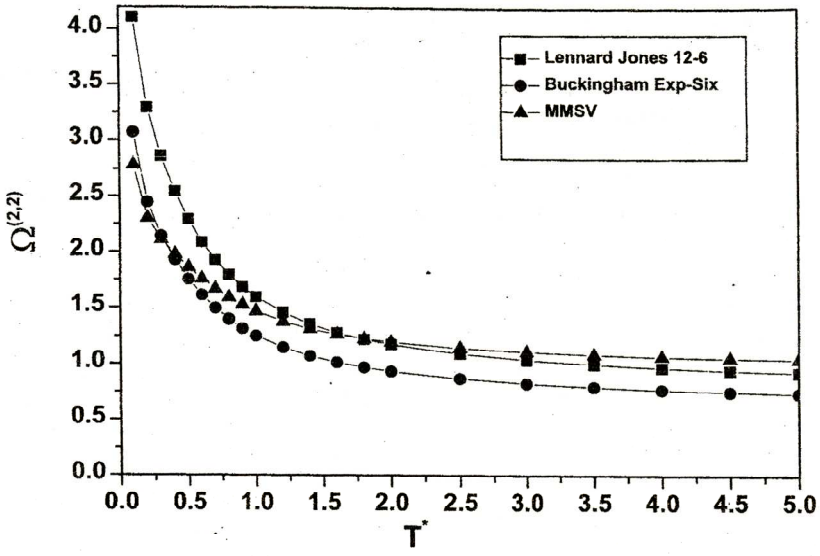

Fig. 1. Temperature variation of the $\Omega^{(2,2)^*}$ reduced collision integrals:
a) for Lennard-Jones 12-6 potential (¦);
b) for modified Buckingham (Exp-Six), (α=15), potential (●);
c) for MMSV potential (Δ).

It is observed that the most integrals lie near unity because of the reduction by their rigid-sphere values and they decrease monotonically with increasing temperature excepting the region from 0 to 0.5. This featureless behaviour contrast greatly with the form of the intermolecular potential function from which they were derived. The changes in the collision integrals are small by comparison with the changes in the potentials, a result that occurs because the collision integrals at a fixed temperature arise from the effects of the potential over the entire trajectories of many binary collisions, at many impact parameters and energies.

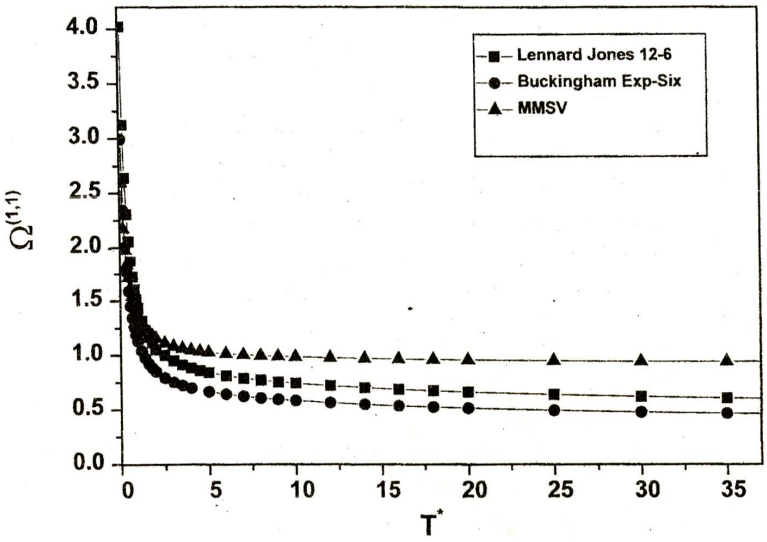

Fig. 2. Temperature variation of the $\Omega^{(1,1)^*}$ reduced collision integrals: a) for Lennard-Jones 12-6 potential (¦);b) for modified Buckingham (Exp-Six), (α=15), potential (●);c) for MMSV potential (Δ).

Some combinations of the reduced collision integrals calculated from MMSV potential that appear in the expressions of the higher-order approximations to the transport coefficients are tabulated for the reduced temperature ranging from 0.1 to 400 (see Table 1). The third-order Chapman-Cowling approximations to the viscosity and the thermal conductivity, and the second-order Chapman-Cowling approximation to the self-diffusion coefficient, calculated from MMSV potential are presented in Table 2, also for a large temperature kT/ε, ranges from 0.1 to 400. The second-order Kihara approximations to viscosity, thermal conductivity and self-diffusion coefficient calculated from MMSV potential for the same temperature domain are given in Table 3.

The higher-order correction factors to the transport properties $f_\eta^{(3)}$, $f_\lambda^{(3)}$, $f_D^{(2)}$, $f_\eta^{K(2)}$, $f_\lambda^{K(2)}$ and $f_D^{K(2)}$, differ from unity by only 1 or 2 per cent over a wide temperature range. For purpose of comparison we represented the higher-order correction factors $f_\eta^{(3)}$ calculated from Lennard-Jones 12-6 potential [2], modified Buckingham (Exp-Six), (α=15), potential [2] and MMSV potential in Figure 3. The depiction was made only in the domain over unity for more comprehensibility. It is seen that the change in the

correction from one potential to another is almost the same for Lennard Jones 12-6 potential [2] and modified Buckingham (Exp-Six), (α=15), potential [2], but it is greater for MMSV potential. An explanation would be that the MMSV potential is more sensitive to higher-order approximations than the others. It is also nonneglijibile the development of the computational technique in the last years.

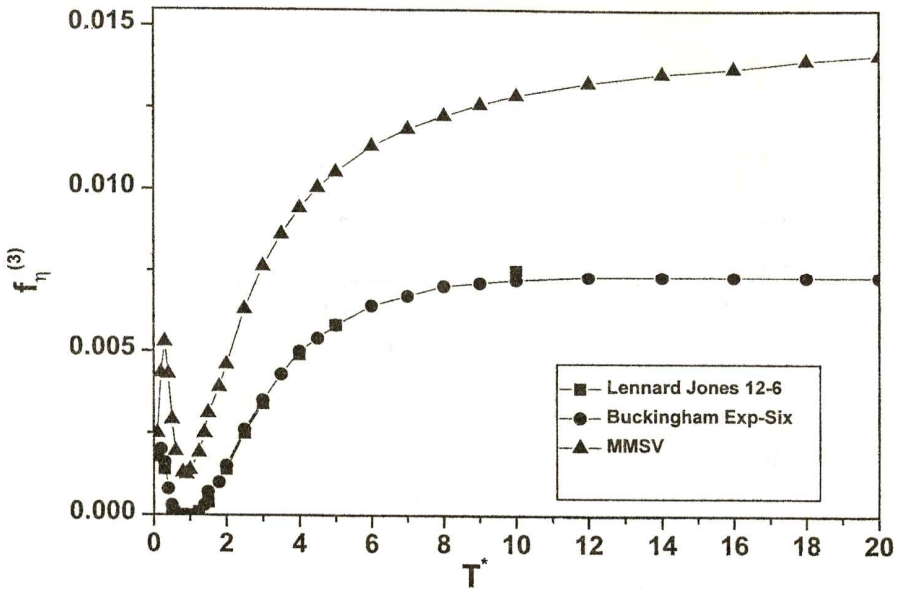

Fig. 3. Temperature variation of the Chapman-Cowling's higher-order correction factors $f_\eta^{(3)}$: a) for Lennard-Jones 12-6 potential (¦);b) for modified Buckingham (Exp- Six), (α=15), potential (●);c) for MMSV potential (Δ).

CONCLUSIONS

In conclusion, we present the calculation from MMSV potential and tabulation of some combinations of the reduced collision integrals and Chapman-Cowling's and Kihara's higher-order approximations to the transport coefficients over a large temperature range, kT/ε from 0.1 to 400. The higher-order correction factors both Chapman-Cowling and Kihara differ from unity only 1 or 2 per cent.

These accomplished results can be profitable for studies of the gaseous transport properties and bulk properties of spherical and quasispherical molecules and in particular the hexafluorides.

Table 1. Some combinations of the reduced collision integrals calculated from MMSV potential

T^*	A^*	B^*	C^*	E^*	H^*
0.10	1.071663	1.135208	0.906457	0.931146	0.970302
0.20	1.059806	1.129023	0.923175	0.955264	0.975226
0.30	1.067752	1.173676	0.918844	0.955532	0.966467
0.40	1.077611	1.202497	0.907747	0.938788	0.956793
0.50	1.082103	1.207642	0.898948	0.922626	0.949805
0.60	1.082411	1.193433	0.893419	0.910891	0.944387
0.70	1.078557	1.183412	0.892756	0.905589	0.941592
0.80	1.074043	1.167526	0.893508	0.903516	0.940510
0.90	1.069908	1.148904	0.896006	0.903964	0.941133
1.00	1.064346	1.131261	0.898676	0.906234	0.941717
1.20	1.054220	1.110269	0.906948	0.914061	0.944656
1.40	1.048306	1.094463	0.916123	0.921196	0.949553
1.60	1.042731	1.079065	0.923288	0.928211	0.953717
1.80	1.037583	1.066384	0.929371	0.934798	0.957185
2.00	1.034035	1.057632	0.935234	0.940393	0.960629
2.50	1.028312	1.045700	0.948084	0.951647	0.968661
3.00	1.024929	1.038995	0.957099	0.959007	0.974304
3.50	1.022178	1.033817	0.962920	0.963701	0.977615
4.00	1.020128	1.030048	0.967156	0.966975	0.980093
4.50	1.018598	1.027740	0.970504	0.969764	0.981952
5.00	1.017672	1.026280	0.973374	0.971689	0.983552
6.00	1.016168	1.023130	0.977421	0.974629	0.985999
7.00	1.015146	1.022312	0.980392	0.976809	0.987563
8.00	1.014318	1.021494	0.982460	0.978532	0.988657
9.00	1.013726	1.020435	0.984019	0.980008	0.989652
10.00	1.013085	1.019245	0.985036	0.981294	0.990299
12.00	1.012358	1.017829	0.986592	0.983284	0.991353
14.00	1.012102	1.016864	0.987819	0.984948	0.992397
16.00	1.011997	1.016060	0.988725	0.986391	0.993308
18.00	1.011978	1.015314	0.989398	0.987656	0.994111
20.00	1.012053	1.014667	0.989942	0.988775	0.994858
25.00	1.012494	1.013535	0.990972	0.991061	0.996516
30.00	1.013117	1.012789	0.991719	0.992841	0.997954
35.00	1.013745	1.012223	0.992247	0.994276	0.999163
40.00	1.014360	1.011790	0.992643	0.995458	1.000206
50.00	1.015517	1.011206	0.993212	0.997289	1.001932
60.00	1.016546	1.010850	0.993595	0.998634	1.003302
70.00	1.017447	1.010627	0.993866	0.999657	1.004413
80.00	1.018237	1.010486	0.994063	1.000454	1.005330
90.00	1.018932	1.010403	0.994211	1.001085	1.006099
100.00	1.019548	1.010358	0.994323	1.001590	1.006751
200.00	1.023139	1.010645	0.994660	1.003502	1.010026
300.00	1.024629	1.011161	0.994598	1.003506	1.011004
400.00	1.025330	1.011620	0.994471	1.003062	1.011258

Table 2. The Chapman-Cowling's higher-order approximations to the transport coefficients calculated from MMSV potential

T^*	$f_\eta^{(3)}$	$f_\lambda^{(3)}$	$f_D^{(2)}$
0.10	1.002486	1.003745	1.003300
0.20	1.004325	1.006520	1.005000
0.30	1.005276	1.007721	1.004559
0.40	1.004287	1.006048	1.003460
0.50	1.002907	1.004041	1.002688
0.60	1.001938	1.002721	1.002246
0.70	1.001565	1.002229	1.002194
0.80	1.001292	1.001912	1.002246
0.90	1.001232	1.001869	1.002430
1.00	1.001366	1.002087	1.002636
1.20	1.001899	1.002907	1.003343
1.40	1.002493	1.003812	1.004226
1.60	1.003173	1.004839	1.004984
1.80	1.003899	1.005928	1.005678
2.00	1.004591	1.006959	1.006392
2.50	1.006289	1.009442	1.008113
3.00	1.007631	1.011368	1.009446
3.50	1.008615	1.012769	1.010362
4.00	1.009428	1.013901	1.011055
4.50	1.010051	1.014775	1.011621
5.00	1.010528	1.015440	1.012118
6.00	1.011324	1.016534	1.012835
7.00	1.011850	1.017263	1.013378
8.00	1.012248	1.017815	1.013763
9.00	1.012592	1.018285	1.014055
10.00	1.012874	1.018670	1.014248
12.00	1.013258	1.019201	1.014544
14.00	1.013544	1.019596	1.014780
16.00	1.013771	1.019909	1.014954
18.00	1.013960	1.020168	1.015084
20.00	1.014116	1.020383	1.015188
25.00	1.014409	1.020779	1.015386
30.00	1.014608	1.021051	1.015530
35.00	1.014754	1.021250	1.015630
40.00	1.014863	1.021399	1.015706
50.00	1.015015	1.021605	1.015813
60.00	1.015112	1.021735	1.015884
70.00	1.015175	1.021820	1.015934
80.00	1.015217	1.021876	1.015970
90.00	1.015245	1.021913	1.015997
100.00	1.015264	1.021938	1.016016
200.00	1.015244	1.021905	1.016070
300.00	1.015152	1.021774	1.016052
400.00	1.015063	1.021649	1.016025

Table 3. The Kihara's higher-order approximations to the transport coefficients calculated from MMSV potential

T^*	$f_\eta^{K(2)}$	$f_\lambda^{K(2)}$	$f_D^{K(2)}$
0.01	1.002151	1.003346	1.002147
0.10	1.002456	1.003820	1.003368
0.20	1.004334	1.006742	1.005102
0.30	1.005035	1.007833	1.004611
0.40	1.003855	1.005997	1.003483
0.50	1.002554	1.003973	1.002704
0.60	1.001725	1.002683	1.002268
0.70	1.001419	1.002208	1.002220
0.80	1.001234	1.001919	1.002280
0.90	1.001220	1.001897	1.002476
1.00	1.001370	1.002131	1.002695
1.20	1.001923	1.002991	1.003431
1.40	1.002536	1.003945	1.004346
1.60	1.003233	1.005028	1.005139
1.80	1.003970	1.006175	1.005866
2.00	1.004667	1.007260	1.006611
2.50	1.006333	1.009851	1.008397
3.00	1.007617	1.011849	1.009778
3.50	1.008551	1.013302	1.010727
4.00	1.009296	1.014460	1.011447
4.50	1.009877	1.015364	1.012032
5.00	1.010317	1.016049	1.012544
6.00	1.011036	1.017167	1.013285
7.00	1.011520	1.017919	1.013843
8.00	1.011886	1.018489	1.014238
9.00	1.012196	1.018971	1.014540
10.00	1.012450	1.019366	1.014739
12.00	1.012803	1.019916	1.015046
14.00	1.013067	1.020326	1.015289
16.00	1.013276	1.020652	1.015470
18.00	1.013448	1.020920	1.015604
20.00	1.013591	1.021142	1.015713
25.00	1.013854	1.021551	1.015918
30.00	1.014035	1.021832	1.016067
35.00	1.014166	1.022037	1.016171
40.00	1.014265	1.022191	1.016249
50.00	1.014401	1.022402	1.016360
60.00	1.014486	1.022534	1.016433
70.00	1.014541	1.022620	1.016485
80.00	1.014578	1.022677	1.016522
90.00	1.014601	1.022713	1.016549
100.00	1.014616	1.022736	1.016569
200.00	1.014588	1.022692	1.016621
300.00	1.014496	1.022549	1.016602
400.00	1.014409	1.022415	1.016572

REFERENCES

1. S. Chapman, T.G. Cowling, *The Mathematical Theory of Non-Uniform Gases* (3rd ed) Cambridge University Press, London, 1970.
2. G. C. Maitland, M. Rigby, E. B. Smith, W. A. Wakeham, *Intermolecular Forces*, Clarendon Press, Oxford, 1981.
3. M. P. Allen, D. J. Tildesley, *Computer Simulation of Liquids*, Clarendon Press, Oxford, 1987.
4. J. E. Lennard-Jones, Proc. Roy. Soc., 106A, 463 (1924).
5. T. Kihara, Rev. Mod. Phys., 25, 83 (1953).
6. R. A. Buckingham, J. Corner, J. Proc. Roy. Soc., 189A, 118 (1947).
7. E. A. Manson, J. Chem. Phys., 22/2, 169 (1953).
8. D. D. Konowalow, J.O. Hirschfelder, Phys. Fluids, 4, 629 (1961).
9. S. F. Boys, I. Shavitt, Nature, 178, 1340 (1956).
10. R. J. J. Munn, J. Chem. Phys., 40, 1439 (1964).
11. H. Dymond, M. Rigby, E. B. Smith, J. Chem. Phys., 42, 2801 (1965).
12. J. A. Barker, A. Pompe, Aust. J. Chem., 21, 1683 (1968).
13. J. A. Barker, R. O. Watts, J. K. Lee, T. P. Schafer, Y. T. Lee, J. Chem. Phys., 61, 3081 (1974).
14. G. C. Maitland, E. B. Smith, Mol. Phys., 22, 861 (1971).
15. J. M. Parson, P. E. Siska, Y. T. Lee, J. Chem. Phys., 56, 1511 (1972).
16. V. H. Smith, A. J. Thakkar, Chem. Phys. Lett., 17 274 (1972).
17. J. Thakkar, V. H. Smith, Chem. Phys. Lett., 24, 157 91974).
18. R. Ahlrichs, R. Penco, G. Scoles, Chem. Phys., 19, 119 (1976).
19. R. A. Aziz, H. H. Chen, J. Chem. Phys., 67, 5719 (1977).
20. G. De Rocco, W. G. Hoover, J. Chem. Phys., 36, 916 (1962).
21. G. Simons, R. G. Parr, J. M. Finlan, J. Chem. Phys., 59, 3229 (1973).
22. R. W. Bickes, R. B. Bernstein, J. Chem. Phys., 66, 2408 (1977).
23. L. A. Viehland, E. A. Mason, W. F. Morrison, M. R. Flannery, Atomic Data and Nuclear Data Tables, 16, 495 (1975).
24. R. A. Aziz, M. J. Slaman, W. L. Taylor, J. J. Hurly, J. Chem. Phys., 94 (2), 1034 (1991).
25. Kumar, G. R. G. Fairley, W. J. Meath, J. Chem. Phys., 83, 70 (1985).
26. J. H. Ferziger, H. G. Kaper, *The Mathematical Theory of Transport Processes in Gases*, North-Holland, Amsterdam, 1972.
27. T. Kihara, *Imperfect Gases*, Asakusa Bookstore, Tokyo, 1949.
28. H. O'Hara, F. J. Smith, Comp. Phys. Commun., 2, 47 (1971).
29. P. P. Neufeld, R. A. Aziz, Comp. Phys. Commun., 3, 1269 (1972).
30. W. Clenshaw, A. R. Curtis, Nummm.Math., 2, 197 (1960).

STUDIA UNIVERSITATIS BABEŞ-BOLYAI, PHYSICA, XLIII, 2, 1998

TRANSPORT CROSS-SECTIONS ESTIMATED FROM MORSE-MORSE-SPLINE-VAN DER WAALS INTERMOLECULAR POTENTIAL

ILIOARA COROIU[1]

ABSTRACT. Transport cross - sections have been calculated from an improved intermolecular potential, Morse - Morse - Spline - van der Waals (MMSV) potential proposed, by R.A. Aziz *et al.* {J. Chem. Phys., 92(2), 1034 (1991)]. The results are tabulated over a large reduced kinetic energy range, from 0.01 to 500. The treatment was exhaustively classical and no corrections for quantum effects were made. From these results the comparable n-m Lennard - Jones potential was approximated. It was unearthed n = 46 and m = 7. The virial coefficients and viscosity data of uranium hexafluoride assessed by us from MMSV potential fit very well the related data evaluated from the 46 - 7 Lennard - Jones potential.

INTRODUCTION

The successful determination of the intermolecular potentials has proved a slow and tortuous process and even now these functions are not known quantitatively in all cases. Often the most reasonable and direct procedure is to build up the potential in a piece-wise manner by combining data from a variety of sources. Ample information about intermolecular forces can be obtained from thermally averaged properties such as second virial coefficients and dilute gas transport properties [1-9]. The molecular beam scattering [10-12] and spectroscopy of van der Waals dimers [14-17], can also provide detailed information about certain aspects of intermolecular potentials. In general, all the spectroscopic methods (UV, IR, NMR, Raman scattering, quadrupole relaxation) give information only about the well region of the intermolecular potential, although in the case of continuous spectra the short - range repulsive region is also probed. Because averaging over internuclear distance and over thermal energy distributions is involved for transport and equilibrium properties, significant

[1] Technical University, 3400 Cluj-Napoca

differences between the shapes of proposed potentials were observed, even between the potentials that gave a relative agreement with these properties. Therefore, the important requirement for any proposed potential, irrespective of its method of determination, is that it should fit all available data within experimental errors.

Several effective isotropic pair potential functions [2, 18-20] have been proposed to characterise the bulk properties of quasispherical molecules and in particular the hexafluorides, but none got a success. Unfortunately these potentials have steeper repulsive walls than those which describe the hexafluorides. That these intermolecular potentials are not quite adequate is shown by lack of complete agreement between theory and experiment even for the rare gases. Not long ago, R.A. Aziz *et al.* [21] have constructed a Morse- Morse-Spline-van der Waals (MMSV) potential. The MMSV potential incorporates the determination of C_6 dispersion coefficient [22] and it reasonable correlates second virial and viscosity data of sulphur hexafluoride at the same time. More, we were found [23] that the MMSV potential is able to predict simultaneously virial, viscosity, thermal conductivity and self diffusion data of the uranium hexafluoride.

The Morse-Morse-Spline-van der Waals (MMSV) functional form is given by

$$V(r) \;=\; \varepsilon\, V^{*}(x) \tag{1}$$

where

$$\begin{aligned} V^{*}(x) \;&=\; \exp\left[\; -2\beta_1(x-1)\;\right] - 2\exp\left[\; -\beta_1(x-1)\;\right], \quad 0 \le x \le 1 \\ &=\; \exp\left[\; -2\beta_2(x-1)\;\right] - 2\exp\left[\; -\beta_2(x-1)\;\right], \quad 1 \le x \le x_1 \\ &=\; a_1 + (x-x_1)\left\{\; a_2 + (x-x_2)\left[\; a_3 + (x-x_1)a_4 \;\right]\;\right\}, \quad x_1 \le x \le x_2 \\ &=\; -\left(\; \frac{C_6}{x^6} + \frac{C_8}{x^8} + \frac{C_{10}}{x^{10}} \;\right), \quad x \ge x_2 \end{aligned} \tag{2}$$

and $x=r/r_m$.

The significance of the symbols in the above Equation is given in Reference [21, 23].

The aim of the present paper is to count for the first time the transport cross-sections from this more realistic potential form. The results are tabulated over a large relative kinetic energy range and then these are used for approximation of the resembling n - m Lennard-Jones potential.

GENERAL FORMULAE

The simplest situation to examine theoretically is the elastic collision between a pair of particles that interact with a spherical symmetrical potential V(r). In practice, it is usually possible to make measurements at pressures where three - and higher body interactions are so rare that their effect on collision properties is either negligible or easily applied as a small correction [24]. We shall consider those gas densities which are high enough on the one hand so that a typical molecule undergoes many more collisions with other molecules than it does with the walls of the container, but which are low enough so that the majority of collisions involve only one other molecule. The first condition implies that the mean free path of the gas molecules is much smaller than the dimensions of the vessel, whereas the second requires that the thermodynamic state of the gas should be adequately described by a virial expansion up to and including the second virial coefficient.

In these conditions the transport cross-sections, $Q^{(l)}(E)$ are defined by

$$Q^{(1)}(E) = 2\left[\, 1 - \frac{1+(-1)^l}{2(1+l)} \,\right]^{-1} \int_0^{\infty} (1 - \cos^l\chi)\; b\; db \qquad (3)$$

where χ is the deflection angle in binary collision, E is the relative kinetic energy of the collision and b named impact parameter is the distance of closest approach in the absence of the potential V(r) and hence in the absence of any deflection.

The deflection angle χ has been related to the intermolecular potential energy function V(r) by the

$$\chi(E,b) = \pi - 2b \int_{r_o}^{\infty} \frac{dr \;/r^2}{\left[\; 1 - b^2/r^2 - V(r)/E \;\right]^{1/2}} \qquad (4)$$

where r is the vector that joints the centre of mass to the position of the particle of reduced mass of system μ and r_0 is the distance of the closest approach in a collision, so named turning point.

Collision with a large positive χ can be attributed to the repulsive portion of the potential acting at small impact parameters. As b increases, χ

decreases until at a value where the net force is zero and there is no deflection.. For higher value of b, χ passes through a minimum χ_r and soon afterward converges to zero as b tends towards infinity. The angle χ_r at which $d\chi/db$ is zero, is called the rainbow angle. As the relative velocity decreases (also the relative kinetic energy), the depth of minimum in χ increases and for small values of this velocity become infinite at the value $b=b_0$ named the orbiting value.

It is convenient to introduce the following reduced quantities:

$$r^* = \frac{r}{\sigma}, \quad b^* = \frac{b}{\sigma}, \quad V^* = \frac{V}{\varepsilon}, \quad E^* = \frac{E}{\varepsilon}, \quad (5)$$

where σ and ε represent the potential parameters.

By defining additional reduced variables Eqs. (3) and (4) become

$$Q^{(l)*}(E^*) = 2\left[1 - \frac{1+(-1)^l}{2(1+l)}\right]^{-1} \int_0^{\infty} (1 - \cos^l \chi)\, b^*\, db^* \quad (6)$$

and

$$\chi(E^*, b^*) = \pi - 2b^* \int_{r_o^*}^{\infty} \frac{dr^*/r^{*2}}{\left[1 - b^{*2}/r^{*2} - V^*(r^*)/E^*\right]^{1/2}} \quad (7)$$

RESULTS AND DISCUSSIONS

To calculate the transport cross-sections $Q^{(l)}(E)$ from Morse-Morse-Spline van der Waals potential form we used the programme catalogue number ACQN (authors O'Hara and Smith [25]) adapted to run in double precision on IBM computers by Neufeld and Aziz [26]. This programme, that involves a Clenshow and Curtiss method [27], was subsequently adapted by us to run on PC computers. The method of Clenshow and Curtiss implies the appraisal of definite integrals through the integrand growth in a finite series of Chebyshev polynomials and integration of each term of series.

If a certain integral, after different variable exchanges, yields the form

$$I = \int_{-1}^{+1} F(x)dx \quad (8)$$

the integrand may be expanded into finite Chebyshev series

$$F(x) = \sum_{r=0}^{N}{}'' a_r T_r(x) \quad (9)$$

The sign $''$ marks that the first and the last terms are halved in summation of Eq. (9). It must be emphasised that the function F(x) have to a good behaviour (no rapid oscillations) both inside of the interval and in -1 and +1 points. The term a_r is given by the relationship

$$a_r = \frac{2}{N} \sum_{s=0}^{N}{}'' \cos\frac{\pi rs}{N} F\left(\cos\frac{\pi s}{N}\right) \quad (10)$$

The Chebyshev series may be integrated term by term and the result will be the following quadrature

$$I_N = \sum_{s=0}^{N} h_s F\left(\cos\frac{s\pi}{N}\right) \tag{11}$$

where

$$h_s = (-1)^s \frac{2}{N^2-1} + \frac{4}{N}\sin\frac{\pi s}{N} \sum_{i=1}^{(1/2)N} \frac{\sin\left[(2i-1)\, s/N\right]}{2i-1} \tag{12}$$

and

$$h_0^N = h_N^N = \left(N^2-1\right)^{-1} \text{,for} \qquad 1 < s < N-1$$

Generally, the applied method for computation the deflection angle χ and cross-section $Q^{(l)}(E)$ integral consists in adequate variable exchanges for fulfilled -1 and +1 as integration limits, required to develop the integrand into finite Chebyshev series.

If for the repulsive part of intermolecular potential calculations are relative simples, some difficulties come into view for the minimum part of the internuclear potential where the orbiting phenomena must be taken into account. Mathematical difficulties occur in the integrand of Eqs. (4) or (7) from the singularity at orbiting value b_0. For the integrand of Eqs. (3) or (6), this involves an infinite number of oscillations in the $b=b_0$ vicinity. Despite, the orbitings turn up only at energies lower than a critical energy E_c, important oscillations of the integrand of Eqs. (3) or (6) may be exist in proximity of E_c energy, in the lack of the singularity. Consequently, three separate regions were considered: $E < E_c$, $E_c < E < 10E_c$ and $E > 10E_c$. For the $E_c < E < 10E_c$ region the deflection angle χ has a negative minimum (the rainbow angle) at b_r. In this point, the integrand $b(1-\cos^l\chi)$ can exhibit oscillatory behaviour. Using suitable variable exchanges all these problems were solved and the counts were accomplished at high accuracy. The inherent computational error is estimated to be of the order of 0.1% except for very small E^*, where it may be larger.

With MMSV potential, the values of the reduced cross-sections are given in Table 1 for E^* that range from 0.01 to 500.

Even though integral and differential cross-section measurements have been widely used to obtain information concerning intermolecular potential energy functions [10-12] we have not experimental data for hexafluorides at our disposal. Therefore, we endeavored to compare our calculated data with other experimental measurements. For this reason, we used the Bernstein's method [24, 28] that approximate from the slopes of log Q(E) vs. log E representation the corresponding n-m Lennard - Jones potential.

TABLE 1. The reduced cross-sections from MMSV potential

E^*	$Q^{(1)*}$	$Q^{(2)*}$	$Q^{(3)*}$	$Q^{(4)*}$	$Q^{(5)*}$	$Q^{(6)*}$
0.01	22.29910	17.39680	25.83220	22.53260	28.07160	25.41890
0.03	15.55300	12.27170	18.06040	15.84830	19.60720	17.90490
0.10	10.53570	8.45459	12.26420	10.83620	13.31830	12.2071
0.20	8.48592	6.82096	9.86089	8.73027	10.69140	9.82372
0.30	7.53895	6.01377	8.72260	7.70703	9.43170	8.67485
0.40	6.98148	5.50502	8.03156	7.06513	8.65834	7.95543
0.50	6.61812	5.14842	7.56363	6.61314	8.12939	7.44683
0.60	6.36925	4.88327	7.22726	6.27299	7.74554	7.06066
0.70	6.19520	4.67879	6.97670	6.00573	7.45694	6.75324
0.80	6.07365	4.51728	6.78610	5.78929	7.23525	6.50008
0.90	5.99091	4.38772	6.63954	5.61008	7.06298	6.28623
1.00	5.97000	4.27183	6.53926	5.46332	6.95700	6.20816
1.20	5.79318	4.25470	6.21615	5.37842	6.55466	6.02036
1.40	5.43183	4.27937	5.95629	5.33919	6.27346	5.86168
1.60	5.05972	4.22656	5.76022	5.25689	6.11208	5.75489
1.80	4.74546	4.10128	5.58091	5.13008	5.98301	5.65025
2.00	4.49785	3.93539	5.39985	4.97414	5.84453	5.52467
2.50	4.09478	3.50250	4.94937	4.54711	5.43120	5.12901
3.00	3.86325	3.16370	4.56439	4.16065	5.01506	4.71899
3.50	3.71052	2.93137	4.27444	3.85275	4.67368	4.37358
4.00	3.60021	2.77556	4.06699	3.62013	4.41702	4.10708
4.50	3.51794	2.66840	3.91919	3.44787	4.22825	3.90686
5.00	3.45648	2.59085	3.81105	3.32023	4.08710	3.75521
6.00	3.37590	2.48280	3.66146	3.14848	3.88790	3.54062
7.00	3.32497	2.40668	3.55634	3.03288	3.74510	3.38698
8.00	3.28282	2.34933	3.47516	2.93976	3.63248	3.26334
9.00	3.24547	2.30509	3.41117	2.86193	3.54212	3.16171
10.00	3.22091	2.27272	3.36483	2.80905	3.47676	3.08905
12.00	3.18424	2.22882	3.30163	2.73686	3.38859	2.99099
14.00	3.15628	2.19648	3.25505	2.68458	3.32476	2.92086
16.00	3.13411	2.17162	3.21923	2.64501	3.27645	2.86837
18.00	3.11600	2.15190	3.19080	2.61407	3.23867	2.82772
20.00	3.10087	2.13585	3.16767	2.58925	3.20837	2.79542
25.00	3.07184	2.10635	3.12512	2.54459	3.15387	2.73818
30.00	3.05083	2.08621	3.09606	2.51505	3.11784	2.70116
35.00	3.03473	2.07158	3.07494	2.49426	3.09249	2.67566
40.00	3.02189	2.06049	3.05890	2.47895	3.07383	2.65732
50.0	3.00242	2.04475	3.03614	2.45818	3.04853	2.63330
60.00	2.98810	2.03411	3.02072	2.44499	3.03247	2.61885
70.00	2.97695	2.02642	3.00954	2.43603	3.02156	2.60961
80.00	2.96789	2.02057	3.00102	2.42962	3.01376	2.60346
90.00	2.96030	2.01594	2.99426	2.42486	3.00796	2.59923
100.00	2.95379	2.01217	2.98874	2.42120	3.00350	2.59625
200.00	2.91544	1.99277	2.96005	2.40572	2.98452	2.58796
300.00	2.89470	1.98303	2.94543	2.39876	2.97584	2.58549
400.00	2.87999	1.97573	2.93442	2.39283	2.96839	2.58210
500.00	2.87331	1.97014	2.93138	2.39007	2.96199	2.58012

Thus from log Q(E) vs. log E plot (see Fig. 1) we have roughly estimated [24, 28] the equivalent n-m Lennard-Jones potential. The low - energy (velocity) limiting slope corresponds to the r^{-7} attractive potential. At high energy (velocity) the repulsive r^{-46} branch of the potential dominates the scattering and the mean slope of log Q(E) vs. log E approaches -2/46. We selected $Q^{1}(E)$ and $Q^{2}(E)$ because these cross - sections are predominantly used to characterise the transport properties. For checking, we also considered the cross - sections evaluated from 12-6 Lennard - Jones potential.

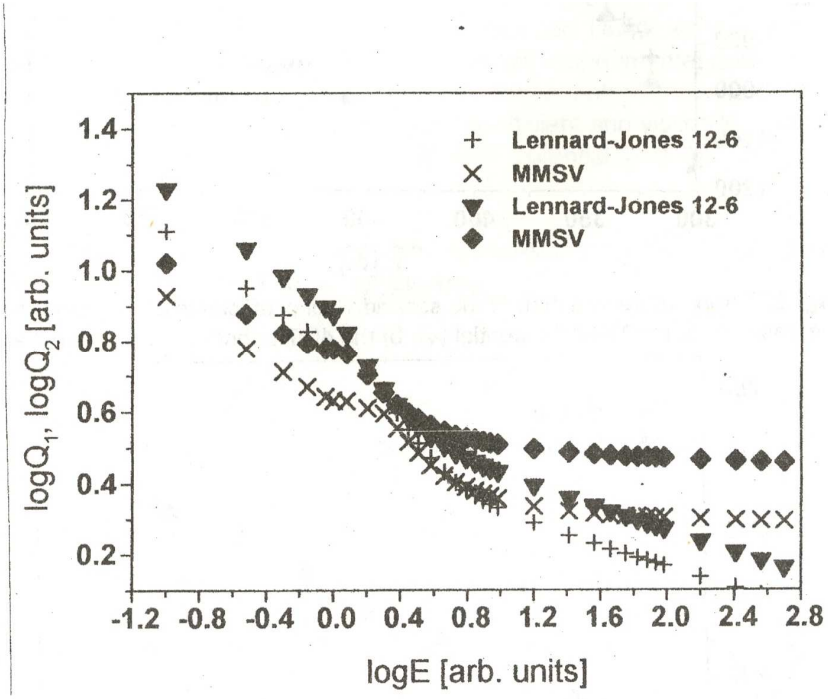

Fig. 1. $Q^{(1)}(E)$. and $Q^{(2)}(E)$ cross - sections as a function of relative kinetic energy: a) for MMSV potential (**x**) and (◆) b) for 12-6 Lennard-Jones potential (+) and (▼).

Afterwards, we were compared the second virial coefficient and viscosity data estimated by us from MMSV potential [23, 29] with that estimated from 46-7 Lennard-Jones [30] both for uranium hexafluoride (see Fig. 2 and Fig. 3). It is obvious that there is a good agreement between our data and that obtained from 46-7 Lennard-Jones [30]. The root mean square percentage deviations of virial coefficients predicted from MMSV potential [29]

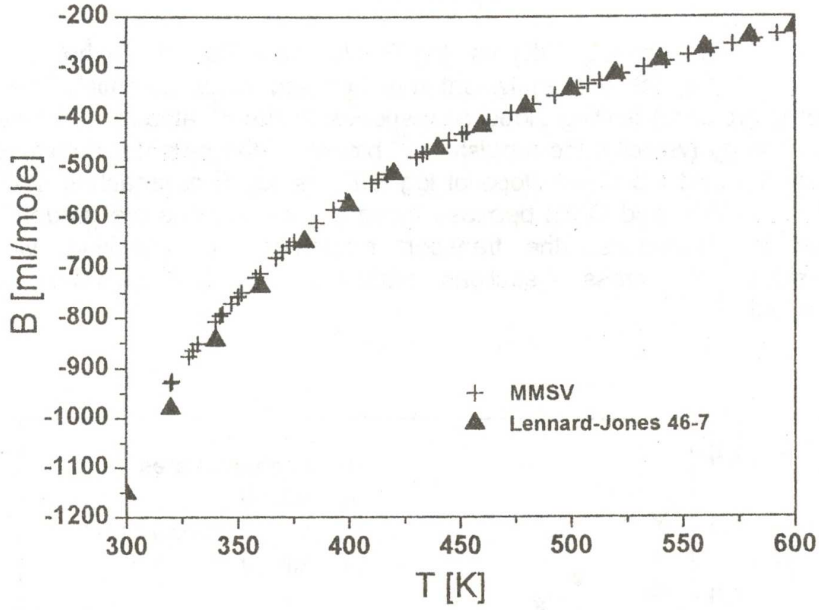

Fig. 2. Temperature variation of the second virial coefficients of UF_6 predicted on the basis of: a) the MMSV potential (+); b) the 46-7 Lennard- Jones potential (▲).

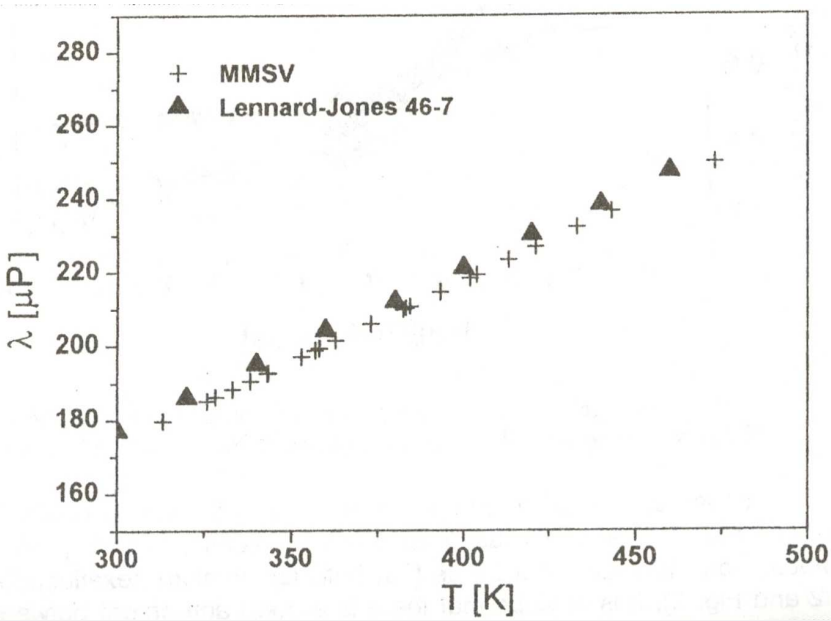

Fig. 3. Temperature variation of the viscosity of UF_6 predicted on the basis of: a) the MMSV potential (+); b) the 46-7 Lennard-Jones potential (▲).

amounts to 2%, underestimating by up to 6% the results obtained from 46-7 Lennard-Jones potential [30] in lower temperature range. For the viscosity data [23, 30] the root mean square percentage deviations alternate about 1.4%. The potential parameters of uranium hexafluoride are $\varepsilon/k = 764 \pm 2K$ and $r_m = 5.19Å$ for MMSV potential [23] and $\varepsilon/k = 835.8 \pm 2K$ and $r_m = 5.381Å$ for 46-7 Lennard-Jones potential [30].

CONCLUSIONS

In conclusion, we present the numerical values of the transport cross - sections for MMSV potential, over a large reduced kinetic energy range E^* from 0.01 to 500. For purpose of comparison with experimental data we were approximated the analogous n-m Lennard Jones potential. It was found a good agreement between the second virial coefficient and viscosity data of the uranium hexafluoride predicted from MMSV potential and 46-7 Lennard - Jones potential.

Acknowledgment. The author is indebted to Mr. T.Beu for the uranium hexafluoride data set at her disposal.

REFERENCES

1. J. E. Lennard-Jones, Proc. Roy. Soc., 106A, 463 (1924).
2. T. Kihara, Rev. Mod. Phys., 25, 83 (1953).
3. R. A. Buckingham, J. Corner, J. Proc. Roy. Soc., 189A, 118 (1947).
4. E. A. Manson, J. Chem. Phys., 22/2, 169 (1953).
5. G. C. Maitland, E. B. Smith, Mol. Phys., 22, 861 (1971).
6. A. J. Thakkar, V. H. Smith, Chem. Phys. Lett., 24, 157 91974).
7. R. Ahlrichs, R. Penco, G. Scoles, Chem. Phys., 19, 119 (1976).
8. R. A. Aziz, H. H. Chen, J. Chem. Phys., 67, 5719 (1977).
9. L. A. Viehland, E. A. Mason, W. F. Morrison, M. R. Flannery, Atomic Data and Nuclear Data Tables, 16, 495 (1975).
10. U. Buck, J. Chem. Phys., 54, 1923 (1971).
11. J. M. Parson, P.E. Siska, Y. T. Lee, J. Chem. Phys., 56, 1511 (1972).
12. R. W. Bickes, R. B. Bernstein, J. Chem. Phys., 66, 2408 (1977).
13. Y. Tanaka, K. Yoshino, D. E. Freeman, J. Chem. Phys., 59, 5160 (1973).

14. R. J. LeRoy, R. B. Bernstein, Chem.Phys. Lett., 5, 42 (1970); J. Chem. Phys., 52, 3869 (1970).
15. R. J. LeRoy, J. S. Carley, J. E. Granbenstetter, Faraday, Discuss. Chem. Soc., 62, 169 (1977).
16. H. B. Levine, J. Chem. Phys., 56, 2455 (1972).
17. T. A. Beu, J. One, K. Takeuchi, J. Chem. Phys., 106, 5910 (1997).
18. S. D. Hamann, J. A. Lambert, Austral. J. Chem., 7, 1 (1954).
19. A. G. De Rocco, W. G. Hoover, J. Chem. Phys., 36, 916 (1962).
20. R. A. Dawe, G. C. Maitland, M. Rigby, E. B. Smith, Trans. Faraday Soc., 66, 1955 (1970).
21. R.A. Aziz, M. J. Slaman, W. L. Taylor, J. J. Hurly, J. Chem. Phys., 94 (2)., 1034 (1991).
22. A. Kumar, G. R. G. Fairley, W. J. Meath, J. Chem. Phys., 83, 70 (1985).
23. I. Coroiu, D. E. Demco, Z. Naturforsch., 52a, 748 (1997).
24. G. C. Maitland, M. Rigby, E. B. Smith, W. A. Wakeham, Intermolecular Forces, Clarendon Press, Oxford, 1981.
25. H. O'Hara, F. J. Smith, Comp. Phys. Commun., 2, 47 (1971).
26. P. P. Neufeld, R. A. Aziz, Comp. Phys. Commun., 3, 1269 (1972).
27. C. W. Clenshaw, A. R. Curtis, Numm. Math., 2, 197 (1960).
28. R. B. Bernstein, J. Chem. Phys., 37, 1880 (1962).; 38, 2599 (1963).
29. I Coroiu, Rom. J. Phys., (in press).
30. R. A. Aziz and W. L. Taylor, Final Report: Intermolecular Potentials for Hexafluoride Gases, MLM-3611, Oct. 31, 1989, for the U. S. Department of Energy, Contract No. DE-AC04-88DP43495.

STUDIA UNIVERSITATIS BABEŞ-BOLYAI, PHYSICA, XLIII, 2, 1998

STORING STATIC AND TEMPORAL SEQUENCES OF PATTERNS IN ASSOCIATIVE MEMORIES WITH GRAY NEURONS

M. ANDRECUT[1]

ABSTRACT. A noniterative learning rule for storing static and temporal sequences of patterns in associative memories with *gray* neurons is presented. The learning and generalization rates (P_L and P_G) are expressed as functions of $\alpha = P/N$, where *P* is the number of learned patterns and *N* is the number of neurons in the network. The numerical simulations shows that the proposed learning rule is optimal, $P_L = 1$ and $P_G = 1$, for $0 < \alpha < 1$.

INTRODUCTION

After the famous paper of Hopfield [1], most of the investigations have concentrated on the ability of neural networks to function as associative memories which retrieve a complete stored pattern if a noisy or incomplete version of the associated pattern is presented to them as an input.

A possible way to realize an associative memory is to construct a dynamical system whose attractors in the configuration space coincide with the prototype patterns. Then every such a pattern has its basin of attraction. Any initial condition which represents one of the permitted patterns falls into a certain attraction basin. In the course of time, such an initial pattern is then transformed into the attractive pattern of this basin, *i.e.* into one of the memorized prototypes. In this sense, an associative memory also represents a special case of pattern recognition.

The “learning phase” in associative memories consists in setting the synaptic matrix, *W*, so that the relation

$$y^k = Wx^k . \tag{1}$$

is satisfied for all pairs (x^k, y^k), where $X = [x^k]$ and $Y = [y^k]$ $(k = 0, \ldots, \alpha N)$ are two sets of *N*-dimensional vectors (patterns) that one

[1] "Babes-Bolyai" University, Faculty of Physics, Cluj-Napoca, 3400, Romania

wanted to associate ($x^k = (x_1^k, \ldots, x_N^k)^T$ and $y^k = (y_1^k, \ldots, y_N^k)^T$). In case of bipolar neurons every component of these vectors takes the values $\{-1, +1\}$.

For example, the Hopfield-Little [2, 3] model with bipolar neurons, stores $P = 0.14N$ random patterns using the Hebbian learning rule

$$W = N^{-1} Y X^T . \tag{2}$$

The dynamics in the traditional Hopfield-Little model is governed by

$$x(t+1) = sign[Wx(t)], \tag{3}$$

where

$$sign(x) = \begin{cases} +1 & if \quad x \geq 0 \\ -1 & if \quad x < 0 \end{cases} \tag{4}$$

An optimal solution corresponds to the Moore-Penrose pseudo-inverse matrix [4], which can store up to *N* linearly independent *N*-bit patterns $(\alpha = 1)$. The pseudo-inverse solution minimizes the quadratic error

$$\varepsilon^2 = \|WX - Y\|^2 \tag{5}$$

and it is given by

$$W = YX^+, \tag{6}$$

where X^+ is the pseudo-inverse matrix of *X*:

$$X^+ = X^T (XX^T)^{-1} . \tag{7}$$

The maximum storage capacity of the network for random patterns is $\alpha = 2$ [5] and can be reached by using the perceptron algorithm [6-7]. Unfortunately, the iterative perceptron algorithm is proved by Krauth and Meyard [8] to diverge as $(2-\alpha)^{-1}$ for $\alpha \to 2$.

In these conditions the pseudo-inverse solution is very attractive for its simplicity and deterministic aspect. The major drawbacks of this solution are:

(i) The prototype patterns must be linearly independent [1, 4];
(ii) The bad generalization rate (due to overfitting) [9, 10];
(iii) In case of auto-associative memories, where the input vector is associated with itself $(X = Y)$, the pseudo-inverse solution become

trivial, because from (6-7) results immediately that $W = I_N$, where I_N is the $N \times N$ identity matrix.

In this paper we derive a simple learning rule which eliminates the drawbacks of the pseudo-inverse solution. Also, the learning rule is derived in the general case of *gray* (or multi-states) neurons.

THE LEARNING RULE

Let us to consider the case of associative memories with gray neurons. The prototype patterns, which have to be associated, are represented by formal *N*-dimensional vectors $X = [x^k]$, $Y = [y^k]$, $(k = 1, 2, \ldots, \alpha N)$. Every component of these vectors is an independent random variable that takes the following discrete values $\{-S, ..., -1, 1, ..., S\}$ $(S \geq 1)$ with equal probabilities. For $S = 1$ one obtain the case of bipolar neurons.

Let $\Gamma = [\gamma^k]$, $(k = 1, 2, \ldots, \alpha N)$ be the matrix of the corresponding noise in the space of input patterns. After applying the noise the input vectors are given by

$$r^k = x^k + \gamma^k, \quad (k = 1, 2, \ldots, \alpha N) \text{ or } R = X + \Gamma. \tag{8}$$

The output of the network is then given by:

$$\hat{x}^k = W r^k, \ (k = 1, 2, \ldots, M). \tag{9}$$

Because the patterns are random generated, in average we have

$$\langle x \rangle = \langle y \rangle = \langle \gamma \rangle = \langle r \rangle = 0. \tag{10}$$

Also, we consider that the patterns and the noise are uncorrelated, that is:

$$\langle x\gamma^T \rangle = \langle \gamma x^T \rangle = \langle y\gamma^T \rangle = \langle \gamma y^T \rangle = 0. \tag{11}$$

The quadratic error is then given by

$$\langle \varepsilon^2 \rangle = \left\langle \left\| Y - \hat{X} \right\|^2 \right\rangle = \left\langle (Y - \hat{X})^T (Y - \hat{X}) \right\rangle \tag{12}$$

and

$$\langle \varepsilon^2 \rangle = \langle R^T W^T W R \rangle - \langle R^T W^T Y \rangle - \langle Y^T R W \rangle + \left\langle \|Y\|^2 \right\rangle. \tag{13}$$

We choose *W* such that it minimizes the quadratic error (13). It results that

$$\nabla_W \langle \varepsilon^2 \rangle = 0. \tag{14}$$

The solution of equation (14) is straightforward [10]:

$$W = \left\langle YX^T \right\rangle \left(\left\langle XX^T \right\rangle + \left\langle \Gamma\Gamma^T \right\rangle \right)^{-1}. \quad (15)$$

Also, for white noise we have:

$$\left\langle \Gamma\Gamma^T \right\rangle = \sigma^2 I_N, \quad (16)$$

where σ^2 is the dispersion of the noise, and I_N is the $N \times N$ identity matrix.

It results that for a given pair of sets of prototype patterns, $X = [x^k]$, $Y = [y^k]$ the optimal learning rule in presence of noise is given by

$$W = YX^T (XX^T + \sigma^2 I)^{-1}. \quad (17)$$

It is important to observe that, for $\sigma > 0$, the inverse $(XX^T + \sigma^2 I)^{-1}$ always exist and can be easily calculated using any standard method.

Obviously, the Hopfield dynamics (3-4) must be adapted here for *gray* neurons. We propose the following dynamical equations:

$$s(t+1) = round(Ws(t)), \quad (18)$$

where the function $round(x)$, rounds the value of *x* to the nearest integer. The function $round(x)$ can be easily obtained using the function $floor(x)$ which gives the greatest integer smaller than *x*, and which is present in all computer languages: $round(x) = floor(x + 0.5)$.

STORING THE STATIC PATTERNS

In this section of the paper we refer to the case of auto-associative memories. As we have mentioned in the introduction, the major drawbacks of the pseudo-inverse solution (6) appear in the case of auto-associative memories, when $Y = X$.

In order to investigate the pattern recognition capability of the network we define two recognition rates:

i) the learning rate (P_L), which is the probability for a pattern to verify the equation:

$$x = round(Wx) \quad \text{if} \quad x \in X = [x^k]; \quad (19)$$

ii) the generalization rate (P_G), which is the probability for a pattern to verify the equation:

$$x \neq round(Wx) \quad \text{if} \quad x \notin X = [x^k]. \quad (20)$$

We have tested the recognition rates by numerical simulations for different values of *N*, *S*, α and σ^2. The simulations have been carried out

for $\sigma = 1$, $10^2 \le N \le 10^3$ and 10^3 runs with different inputs were averaged for each $\alpha \in [0, 2]$. We have found that the learning rate takes the maximum value:

$$P_L(\alpha) = 1 \quad if \quad 0 < \alpha \le 2\,, \tag{21}$$

and the generalization rate exhibits a steep transition at $\alpha = 1$:

$$P_G(\alpha) = \begin{cases} 1 & if \quad 0 < \alpha < 1 \\ 0 & if \quad \alpha \ge 1 \end{cases}. \tag{22}$$

The numerical simulation shows that these results do not depend on the value of the discrete variable $S \ge 1$.

STORING THE TEMPORAL SEQUENCES OF PATTERNS

Above we discussed the storing capacity of static patterns in associative memories. However, there are many tasks which require storage and associative recall of temporal sequences of patterns.

The human memory stores not only pictures, but also melodies and poems which can be retrieved by presentation of their short or distorted fragments. Another important function of the neural nets is generation of rhythmic motor patterns, which controls for instance, locomotion or heartbeats etc. Clearly, the same abilities are desirable in artificial systems of information processing.

Suppose we have an ordered set of orthogonal patterns: $X = [x^k]$, $\mathrm{x}^{\mathrm{k}} = (\mathrm{x}_1^{\mathrm{k}}, ..., \mathrm{x}_{\mathrm{N}}^{\mathrm{k}})^{\mathrm{T}}$, $(\mathrm{k} = 1, 2, ..., \mathrm{N})$ and $x^{i^T} x^j = \delta_{ij}$, where $\delta_{ij} = 1$ if $i = j$ and $\delta_{ij} = 0$ otherwise. We want to construct a neural network which will generate a periodic sequence of patterns:

$$\mathrm{x}^1, \mathrm{x}^2, ..., \mathrm{x}^{\mathrm{N}}, \mathrm{x}^1, \mathrm{x}^2, ... \tag{21}$$

For this particular case of orthogonal patterns, the storage problem can be easily solved by choosing the following asymmetric synaptic matrix

$$W = \sum_{k=1}^{N} x^{k+1} x^k\,, \tag{22}$$

where we assume $x^{N+1} = x^1$.

Suppose we start at $t = 1$ with the first pattern, then we find

$$W x^1 = \sum_{k=1}^{N} x^{k+1} x^k x^1 = \sum_{k=1}^{N} x^{k+1} \delta_{k1} = x^2\,. \tag{23}$$

At the next step this neural network will generate the third pattern, and so on until the *N*-th step after which it generates again the first pattern and the cycle is repeated.

It can be easily seen that for the learning rule (17) with the dynamical equation (18), the restriction to the particular case of orthogonal patterns is completely eliminated. For this learning rule, it is sufficiently to put:

$$y^1 = x^2,\ y^2 = x^3,\ \ldots,\ y^{\alpha N-1} = x^{\alpha N},\ y^{\alpha N} = x^1. \tag{24}$$

Also, the maximum number of *N*-dimensional patterns (vectors) is *N*, it results that using the learning rule (22), the maximum length of the sequence is *N*. In case of the learning rule (17) the length of the sequence is $\alpha N > N$.

CONCLUSION

In conclusion, we have derived an optimal learning rule for associative memories with *gray* neurons, which eliminates the drawbacks of the pseudo-inverse solution. The learning rule was deduced with respect to noise influence in the space of input patterns. The pattern recognition capability of the system was also discussed.

REFERENCES

1. T. Kohonen , *Self-organization and Associative Memory* (Springer-Verlag, 1988).
2. J. J. Hopfield, *Proc. Natl. Acad. Sc. USA*, **79**, 2554 (1982).
3. W. A. Little, *Math. Biosci.*, **19**, 101 (1974).
4. A. Albert, *Regression and the Moore-Penrose pseudo-inverse* (Acad. Press, 1972).
5. P. Baldi, S. Venkatesh, *Phys. Rev. Lett.*, **58**, 913 (1987).
6. M. Diederich, M. Opper, *Phys. Rev. Lett.*, **50**, 949 (1987).
7. G. Poppel, U. Krey, *Europhys. Lett.*, **4**, 979 (1987).
8. W. Krauth, M. Meyard, *J. Phys. A*, **20**, L745 (1987).
9. F. Vallet, J. Cailton, Ph. Refregier, *Europhys. Lett.*, **9**, 315 (1989).
10. M. Andrecut, *Int. J. Mod. Phys. B* (1998) in press.

STUDIA UNIVERSITATIS BABEŞ-BOLYAI, PHYSICA, XLIII, 2, 1998

INTERACTING POPULATIONS IN THE "GAME OF LIFE"

MIRCEA ANDRECUT*

ABSTRACT. The Conway's celebrated *game of life* deals with one population of cells. Here, we present a generalization of the Conway's *game of life* by considering a finite number of interacting populations. The computational study shows that the *game of life with interacting populations* generates an extremely complicated dynamics with a self-organization mechanism between the populations.

INTRODUCTION

Cellular automata (CA) are modeled by *cells* and *interaction rules*[1-3]. Intuitively, CA are indefinitely extended networks of trivially small, identical, uniformly interconnected, and synchronously clocked digital computers. From the mathematical point of view, CA are given by a tuple $\{C, N, Q, f\}$ where *C* is the cellular space (usually a regular lattice such as $Z, Z^2, ..., Z^n$), *N* is the neighborhood (which is usually the same for all the sites in the cellular space), *Q* is the finite set of states and *f* is the local transition function which associates a new state to each site, depending on the site state itself and the each state configuration in the neighborhood, i.e.

$$f : Q^{n+1} \to Q\,;\ \ (q_i, q_{i1}, \ldots, q_{in}) \in Q^{n+1} \to f(q_i, q_{i1}, \ldots, q_{in}) \in Q\,, \qquad (1)$$

where $(q_{i1}, \ldots, q_{in})$ is the state configuration of the neighborhood of the site *i*. The dynamics of the automaton is given by the synchronous application of the local function, *f*, to all the sites in the cellular space, i.e. for the site *i*,

$$q_i^{t+1} = f(q_i^t, q_{i1}^t, \ldots q_{in}^t)\,. \qquad (2)$$

In fact, CA provide explicit means for *parallel computation* on a *space-time* background. One can see that the CA paradigm is developed on basis of a few important principles:

* "Babes-Bolyai" University, Department of Physics, Cluj-Napoca, 3400, Romania

a) CA are *local* because each site is only affected by its finite neighborhood;
b) CA are *homogeneous*, or *translation invariant* because the neighborhood for each site in the system is defined in the same way, and each site updates according to the same rule;
c) CA are *deterministic* because the rules are so;
d) CA are *discrete in time* because the sites update at discrete times;
e) CA are *discrete in space* because their universe is a lattice;
f) CA are *dynamical systems* because the sites update at each time step;
g) CA are *parallel* because the sites update synchronously.

The numerous complex phenomena unified under these principles include: self organization and order-disorder transition, far from thermodynamic equilibrium, foundation of relativity, quantum computation, particle physics, artificial intelligence, artificial life etc. In fact, CA paradigm represents the expression of the profound similarities between the fundamental mathematical models, which are used to describe the cooperative behavior of active systems in physics, chemistry, biology and social sciences.

The generic models of cooperative behavior deal with systems made of simple elements. It is obvious that this assumption is not representative for biological, social or even physical systems where the elements have a very complicated structure. But, closer examination reveals that in cooperative interactions these elements act as simple units that can be described by a set of a few variables. Their internal complexity is not directly manifested in their interactions.

As was noted by Von Bertalanffy[4], Corning[5], Nicolis and Prigogine[6], living systems represent hierarchies of self-organized subsystems. At each level of hierarchy, we have a system of sufficiently autonomous units that interact in a simple manner one with another. Their interactions create a cooperative coherent behavior, which turn plays the role of an element of the next level.

Contrary to the living systems, the laws of statistical physics tell us that a physical system tends towards a state of equilibrium in which activity ceases. The only exception is observed in "open systems" that receive a flux of energy and dissipate is further into the environment. All living systems have such permanent input. These observations lead to the theory of self-organization in "open systems" which was largely developed by Prigogine and coworkers[6].

THE CONWAY'S "GAME OF LIFE"

The theory of self-organization and the results obtained via CA simulation have lead to the appearance of a new idea, the possibility of constructing *artificial living systems*. John Von Neumann used this idea to create a complex cellular automata (with 29 states) which was able to produce non-trivial self-reproducing patterns[7].

A particularly interesting approach to the *artificial life* is provided by the Conway's *game of life*[8]. More specifically, he defined the following criteria:

a) There should be no initial pattern for which there is a simple proof that the population can grow without limit;
b) There should be initial patterns that apparently do grow without limit;
c) There should be simple initial patterns that grow and change for a considerable period of time before coming to an end in three possible ways: fading away completely (from overcrowding or from becoming too sparse), settling into a stable configuration that remains unchanged thereafter, or entering an oscillating phase in which they repeat an endless cycle of two or more periods.

The game was first published in the Scientific American in October 1970, in Martin Gardner's "Mathematical Games" column[8]. Since then a great deal of work has been done for understanding the complex dynamics of the *game of life*.

Let us define the *game of life*. The universe is an infinite two-dimensional grid, or Z^2. At the each moment of time, t, the sites on the grid are occupied by a population of cells, $\{x_{ij}^t \mid i, j, t \in Z\}$. Each cell can be in one of two states 0 and 1, which we think as *dead* or *live*, respectively:

$$x_{ij}^t = \begin{cases} 1 & \text{if the cell is } \textit{live} \\ 0 & \text{if the cell is } \textit{dead} \end{cases}. \tag{3}$$

The neighborhood of each cell corresponds to the eight nearest neighbors. The sum over the neighborhood, at each moment t, is given by

$$n_{ij}^t = \sum_{n=-1}^{1} \sum_{m=-1}^{1} x_{i+n,j+m}^t - x_{ij}^t . \tag{4}$$

In a condensed form, the rule for the *game of life* is specified as follows:

$$x_{ij}^{t+1} = (x_{ij}^t \wedge (n_{ij}^t = 2)) \vee (n_{ij}^t = 3), \tag{5}$$

where $\wedge, \vee$ stands for the logical operators AND, respectively OR.

One can see that, the rule of the *game of life* is one-bit "semitotalistic". The rule is one-bit because it has only two possible states and choosing

between two states requires only one bit of information. The rule is "semitotalistic" because a cell's next state depends on the sum over the eight nearest neighbor states and the state of the cell itself. For a "totalistic" rule, a cell's next state depends only on the sum

$$\sum_{n=-1}^{1}\sum_{m=-1}^{1} x_{i+n,\,j+m}^{t} \,. \tag{6}$$

The *game of life* is characterized by an especially complex dynamics. It generates sophisticated sequences of patterns, which are extremely sensitive to the initial conditions. For example, one of the most famous patterns is the *glider*,

$$\begin{matrix} 0 & 0 & 1 \\ 1 & 0 & 1 \\ 0 & 1 & 1 \end{matrix}, \tag{7}$$

a pattern that moves across the cellular automaton array at a speed of one diagonal cell every four generations. If a CA rule uses nearest neighbors only, the fastest that a pattern can move is one cell per generation. This is sometimes called the *speed of light*, so one can say that *game of life's gliders* move at one-fourth the speed of light.

Another interesting pattern is the *R pentomino*

$$\begin{matrix} 0 & 1 & 1 \\ 1 & 1 & 0 \\ 0 & 1 & 0 \end{matrix}, \tag{8}$$

a five-cell start pattern which creates an amazing amount of activity. The pattern keeps growing and evolving through 1103 generations, at which time a 51 by 109 pixel rectangle of stable debris is left, as well as six receding gliders. Large collection of patterns, programs and documentation on the *game of life* can be obtained via Internet[9], so, we will not discuss here any other aspects of these problems, but we will refer shortly to different variants and generalizations of the Conway's *game of life*.

The question is. Why these patterns are interested ? Turing invented a machine which is an ideal computer (no computer of today can reach its capability). As is well known by now, the Conway's *game of life* has the infinite power of a universal Turing computer[10]. The proof of this is based on the glider gun patterns which can shoot out a stream of gliders. Using gliders streams to represent bits, all logic gates (AND, OR, NOT) can be produced. It results that these patterns could be used to construct the basic building blocks of a computer.

GENERALIZATIONS OF THE CONWAY'S GAME OF LIFE

One can see that the *game of life* rule (6) can be easily expressed by the following simple formula:

$$life = B3/S23, \tag{9}$$

where $B3$ means that a dead cell will come alive in the next generation if and only if exactly three of its eight neighbors are alive (the birth rule), and $S23$ means that a living cell will survive in the next generation if there are either two or three neighbors also alive (the survive rule); otherwise a living cell will die of over crowding or of exposure.

A simple idea to extend the game of life is to consider other formula for the birth and survive rule. We give here a short description of a few important rules (there are 2^{16} possible rules in a two-dimensional space !):

1) $B1357/S1357$ (Replicator)-(Exploding) In this remarkable universe every pattern is a replicator.
2) $B36/S23$ (High Life)-(Chaotic) This rule has a surprise replicator pattern. There is no known replicator in Conway's *game of life*.
3) $B34/S34$ (34-Life)-(Exploding) The First explored alternative to Conway's *life*. It creates an exploding universe with a very rich dynamics.
4) $B3678/S34678$ (Day & Night)-(Stable) So named because dead cells in fields of live cells act by the same rules as live cells in fields of dead cells. There are obviously other rules which have this symmetrical property, but this rule was chosen because it has some interesting high period of patterns.
5) $B345/S5$ (Long Life)-(Stable) This rule is called "Long life" because of the extremely high period patterns that can be produced in this universe.
6) $B35678/S5678$ (Diamoeba)-(Chaotic) Creates solid diamond-shaped "amoeba" patterns that are surprisingly unpredictable.

Another simple idea is to extend the game in a tree-dimensional space and to rescale the birth and survive conditions adequately. Note that in a tree-dimensional space, each cell has 26 nearest neighbors. Also, the number of possible rules, in a three-dimensional space, is enormous, 2^{52}.

Evans and Griffeat[11] have proposed a generalization of the Conway's game of life. *Larger than Life* (LtL) is a four-parameter family of two-state CA that generalize the *game of life* as follows:

- At each time, each site $x \in Z^d$ is either live or dead;
- The neighborhood of the origin is *N*, a finite subset of the *d*-dimensional space Z^d; The translation $x + N$ is the neighborhood of *x*;

- A dead cell at time *t*, become live at time $t+1$ if it sees between β_1 and β_2 live cells in its neighborhood;
- A live cell at time *t* survives to the time $t+1$ if it sees between δ_1 and δ_2 live cells in its neighborhood; otherwise it become dead.

LtL family of CA introduced a rich collection of new interesting patterns, called *bugs*, which have a similar behavior to *gliders*.

GAME OF LIFE WITH INTERACTING POPULATIONS

In this paper, we present a generalization of the Conway's *game of life* by considering a finite number of interacting populations $(P \geq 1)$. The *game of life with interacting populations* is defined as follows:

- The universe is Z^d;
- The populations are described by:

$$x_{ij}^t = \begin{cases} p & \text{if the site is occupied by a live cell from population } p \in \{1,2,...,P\} \\ 0 & \text{if the site is occupied by a dead cell} \end{cases}; \tag{10}$$

- The neighborhood of the origin is *N*, a finite subset of the *d*-dimensional space Z^d; The translation $x+N$ is the neighborhood of *x*;
- The following partial sums are defined at each moment *t*, over the neighborhood:

$$n_{ij}^t(p) = \sum_{n,m \in N} \delta(x_{i+n,j+m}^t, p) - \delta(x_{ij}^t, p), \quad p \in \{1,2,...,P\}, \tag{11}$$

where

$$\delta(x, p) = \begin{cases} 1 & \text{if} \quad x = p \\ 0 & \text{if} \quad x \neq p \end{cases}. \tag{12}$$

- The birth rule for the population *p* is given by:

$$x_{ij}^{t+1} = p \quad \text{if} \quad (x_{ij}^t = 0) \wedge [n_{ij}^t(p) \in \{\beta_1^p,...,\beta_2^p\}] \bigwedge_{\substack{q=1 \\ q \neq p}}^{P} [\neg(n_{ij}^t(q) \in \{\beta_1^q,...,\beta_2^q\})], \tag{13}$$

where $\neg$ is the logical operator NOT;

- The survive rule is given by:

$$x_{ij}^{t+1} = x_{ij}^t \quad \text{if} \quad (x_{ij}^t > 0) \wedge [\bigvee_{p=1}^{P} n_{ij}^t \in \{\delta_1^p,...,\delta_2^p\}]. \tag{14}$$

The game of life with interacting populations is a $2P$-parameter family of CA, and for $P=1$, is reducing to the four-parameter family of *Larger than Life* CA. In fact, for regions occupied by one kind of population, the dynamics of the *game of life with interacting populations* is governed by the *Larger than Life* CA. The differences appear when a neighborhood contains cells from different populations in competition for the central site.

The computational study of the *game of life with interacting populations* is very difficult for a large number of populations, but it is accessible for a small number of populations. We will consider the following particular case:

- The universe is Z^2;
- $P=2$, two populations:

$$x_{ij}^t = \begin{cases} 1 & \text{if the site is occupied by a live cell from population 1} \\ 2 & \text{if the site is occupied by a live cell from population 2;} \\ 0 & \text{if the site is occupied by a dead cell} \end{cases} \quad (15)$$

- The neighborhood of each cell corresponds to the eight nearest neighbors, as in the *game of life*. The partial sums over the neighborhood are given by

$$n_{ij}^t(p) = \sum_{n=-1}^{1}\sum_{m=-1}^{1} \delta(x_{i+n,j+m}^t, p) - \delta(x_{ij}^t, p), \quad p \in \{1,2\}; \quad (16)$$

- The birth and survive rules are given by (13) and respectively (14), but the parameters β and δ are those from the *game of life*, i.e. $\beta_1^p = \beta_2^p = 3$ and $\delta_1^p = 2$, $\delta_2^p = 3$. With these parameters the update rule is:

$$x_{ij}^{t+1} = \begin{cases} 1 & \text{if} \quad (x_{ij}^t = 0) \wedge (n_{ij}^t(1) = 3) \wedge [\neg(n_{ij}^t(2) = 3)] \\ 2 & \text{if} \quad (x_{ij}^t = 0) \wedge (n_{ij}^t(2) = 3) \wedge [\neg(n_{ij}^t(1) = 3)] \\ x_{ij}^t & \text{if} \quad (x_{ij}^t > 0) \wedge [n_{ij}^t(1) = 2 \vee n_{ij}^t(1) = 3 \vee n_{ij}^t(2) = 2 \vee n_{ij}^t(2) = 3] \\ 0 & \text{otherwise} \end{cases}. \quad (17)$$

One can see that in regions occupied by only one population, the dynamics is governed by the rules from the Conway's *game of life*. It results that the system will show a *game of life* like dynamics with an interaction between the two populations at the frontier.

We have simulated this system starting from a random initial configuration. If ξ_t denotes the state of the system at time *t* started from a

random initial configuration, then ξ_t can be thought of as a Markov process since the sites update independently from all preceding times except the current one. Also, the Markov process is degenerate since the transitions are deterministic.

Fig. 1 shows the evolution of the system starting from a random initial configuration. The populations are initialized in a small array (12×12), with equal probabilities $P(1)=P(2)=1/4$. It is interesting to see that the behavior of the system is different than of the *game of life*. In the *game of life*, the density of population decrease, but here the density remains almost constant. Also, a *self-organization mechanism* appears as a consequence of the interaction between the two populations. It seems like the populations cooperate in constructing a frontier which separate regions occupied by one type of population. In this regions the dynamics is governed by the rule of the *game of life*. The frontier increase continuously. The irregular shape of the frontier generates new patterns in both populations and play the role of a factory which generates patterns that can move and interact.

Now, we will change the rule $B3/S23$ with $B34/S34$, which is an interesting alternative for the *game of life*. The update rule in this case will be:

$$x_{ij}^{t+1}=\begin{cases}1 \quad \text{if} \quad (x_{ij}^t=0)\wedge[n_{ij}^t(1)=3\vee n_{ij}^t(1)=4]\wedge[\neg(n_{ij}^t(2)=3\vee n_{ij}^t(2)=4)]\\ 2 \quad \text{if} \quad (x_{ij}^t=0)\wedge[n_{ij}^t(2)=3\vee n_{ij}^t(2)=4]\wedge[\neg(n_{ij}^t(1)=3\vee n_{ij}^t(1)=4)]\\ x_{ij}^t \quad \text{if} \quad (x_{ij}^t>0)\wedge[n_{ij}^t(1)=3\vee n_{ij}^t(1)=4\vee n_{ij}^t(2)=3\vee n_{ij}^t(2)=3]\\ 0 \quad \text{otherwise}\end{cases} \quad . \quad (18)$$

In Fig. 2 we give the results of the numerical simulation. This time, the system has a completely different evolution. After a few time steps, the population are completely separated and forms two large random areas that resemble *amoebas* and that are in permanent contact. Internal to the random areas is chaos. The edge vascillates wildly, and patterns tend to grow. The more they grow, the more certain their survival. Also, the patterns move continuously in space.

Obviously, following the procedure described above, one can define many other rules, which describes the interaction of populations in the Conway's *game of life*. The given examples demonstrate that the *game of life with interacting populations* has a complex dynamics with interesting effects of self-organization.

Fig. 1. Temporal evolution of the *game of life with interacting populations*, rule (17).

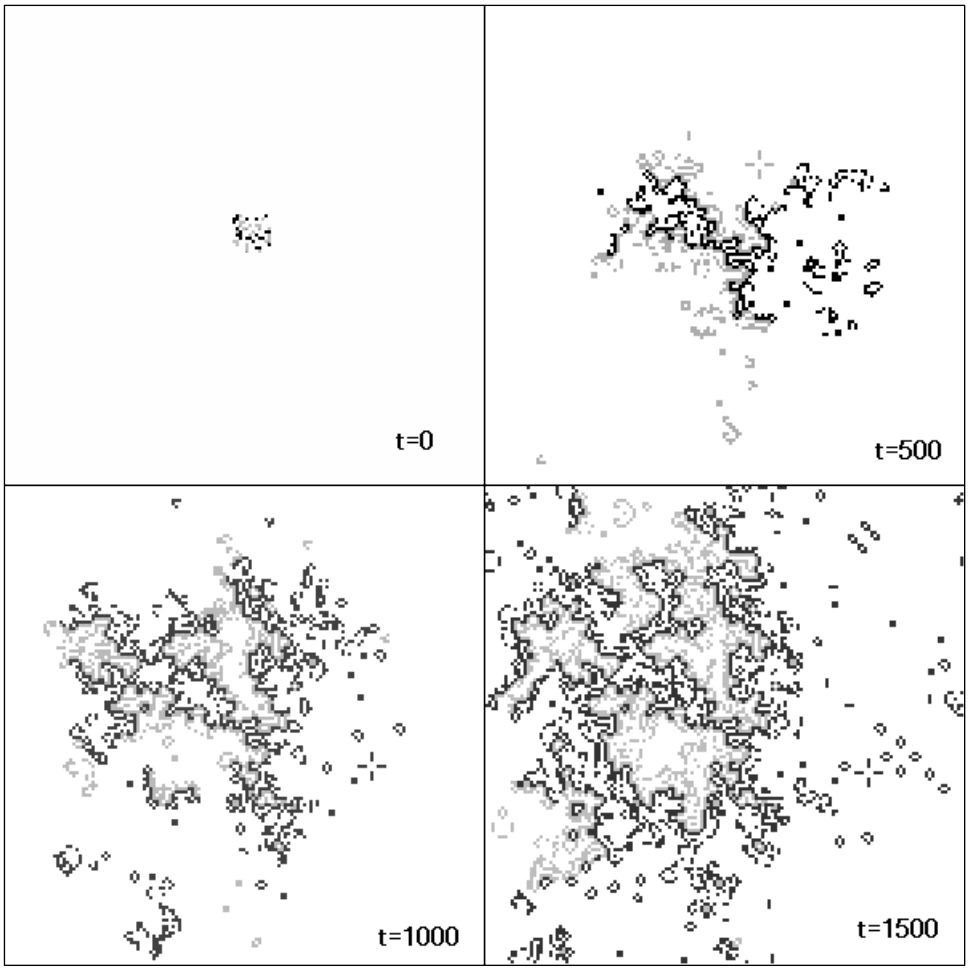

Fig. 2. Temporal evolution of the *game of life with interacting populations*, rule (17).

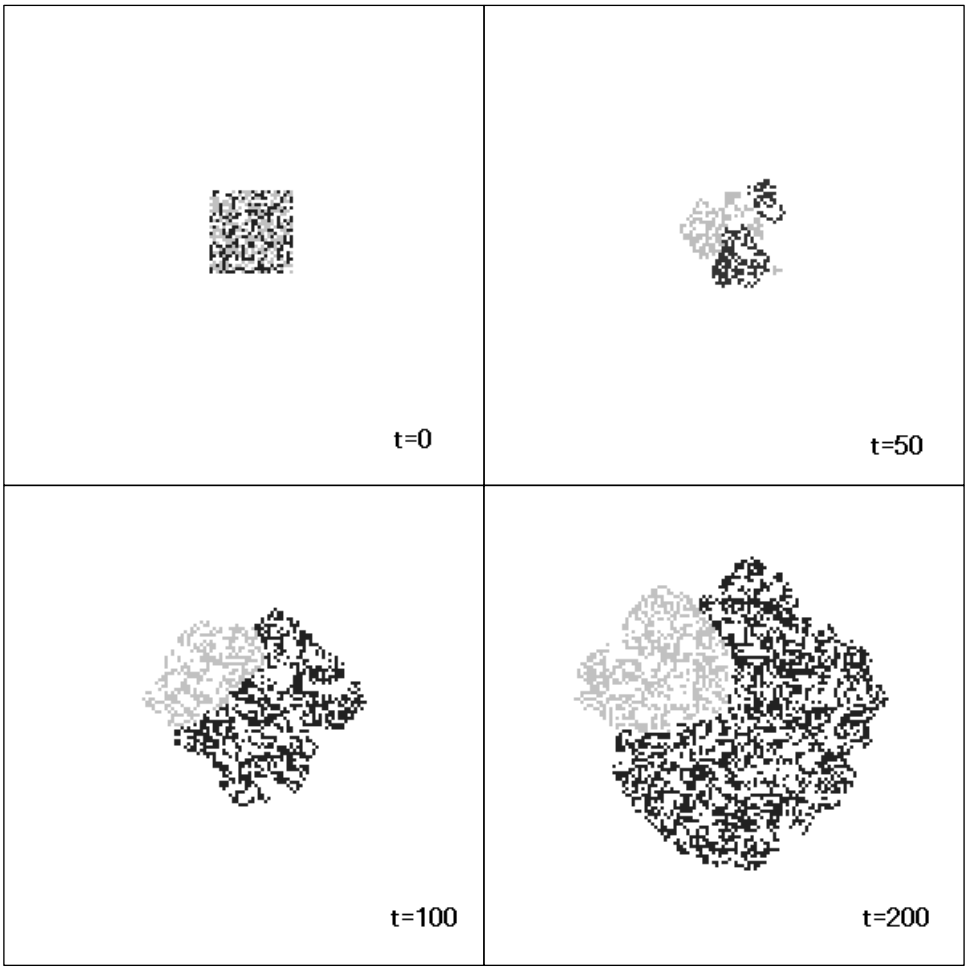

CONCLUSIONS

We have presented a generalization of the Conway's *game of life* by considering a finite number of interacting populations. The computational study shows that the *game of life with interacting populations* generates an extremely complicated dynamics with a self-organization mechanism. The quantitative analysis of the patterns emerged from this model, in large (multi-dimensional) systems, is a difficult task from the computational point of view. These difficulties can be avoided only by a parallel computational approach. New technology such as the Cellular Automata Machine (CAM)[12] could give greater empirical progress in understanding how such systems behave.

REFERENCES

1. S. Wolfram, *Cellular Automata and Complexity* (Addison-Wesley, 1994).
2. H. Gutowitz, *Cellular Automata: Theory and Experiment*, Physica D 45, Nos. 1-3 (1990).
3. L. O Chua, *CNN: A Paradigm for Complexity* (World Scientific, 1998).
4. L. Von Bertalanffy, *Problems of Life* (Watts, London, 1952).
5. P. A. Corning, *The Synergism Hypothesis* (McGraw-Hill, New-York, 1983).
6. G. Nicolis, I. Prigogine, *Self-Organization in Nonequilibrium Systems* (Wiley, New-York, 1977).
7. J. Von Neumann, *Theory of Self-Reproducing Automata*, (Univ. of Illinois Press, Urbana, 1966).
8. M. Gardner, *Mathematical Games-The Fantastic Combination of John Conway's New Solitaire Game, Life*, Scientific American, 120-123, (October 1970).
9. This is a short list of good starting places on the Internet:
   - http://www.cs.jhu.edu/~callahan/lifepage.html, World Wide Web, (Paul Callahan's page about Conway's Game of Life);
   - http://math.wisc.edu/~griffeat/sink.html, World Wide Web, (David Griffeat's page about artificial life);
   - http://www.tip.net.au/~dbell/, World Wide Web, (David Bell's page about Conway's Game of Life);
10. E. Berlekamp, J. Conway, R. Guy, *Winning Ways for Your Mathematical Plays*, Vol. 2 (Accademic Press, 1982).
11. K. M. Evans, D. Griffeat, *Larger than Life*, http://math.wisc.edu/~griffeat/sink.html, World Wide Web.
12. N. Margulos, *MIT-CAM 8 home page*, http://www.im.les.mit.edu/cam8, World Wide Web.